Programming DNA-based Reaction-Diffusion System

博 士 学 位 論 文
Doctoral Thesis

論文題目

Thesis Title

Programming DNA-based Reaction–Diffusion System

東北大学大学院工学研究科

Graduate School of Engineering,

TOHOKU UNIVERSITY

専攻/Department: Department of Robotics

学籍番号/ ID No: B9TD1401

氏名 / Ｎａｍｅ: Keita ABE

TOHOKU UNIVERSITY
Graduate School of Engineering

Programming DNA-based Reaction–Diffusion System
（DNAを利用した反応拡散システムのプログラミング）

A dissertation submitted for the degree of Doctor of Philosophy (Engineering)

Department of Robotics

by

Keita ABE

January 10，2023

Programming DNA-based Reaction–Diffusion System

Keita Abe

Abstract

Living organisms can build their bodies with complex shapes and functions. This process, called development, is remarkable because it achieves the desired shape and function in a programed manner without external help. Understanding and reconstructing this process will be useful to build complex artificial systems.

Biological development is interpreted as a combination of four phenomena: *pattern formation* that determines the shape, *morphogenesis* that changes shape, *cell differentiation* that functionalizes cells according to their location, and *growth* that increases size. Pattern formation, which plays a role in early developmental stage, proceeds through complex, simultaneous, and multi-step interactions among biomolecules. Although understanding the mechanism of development at molecular level is not easy, simulations of spatiotemporal concentration change due to molecular reaction and diffusion can reproduce the patterns. In other words, artificial pattern formation is possible if the actual chemical reactions and diffusion can be programed according to the desired purpose.

Synthetic DNA is beneficial for programing chemical reactions because DNA-DNA interaction can be defined by designing the base sequences. Various DNA reaction systems have been reported, and some have been applied to construct reaction–diffusion systems. However, diffusion programs have received almost no attention so far.

In this study, I aim to program both reaction and diffusion in a DNA chemical reaction system to realize cascaded pattern formation. I investigated a method to form a bisector pattern between sources by programming DNA.

First, I employed a DNA anchoring method and logic gate to construct a DNA reaction–diffusion system that forms a bisector pattern in a hydrogel. The AND gate forms a complex when two inputs from the sources coexist. The bisector pattern formation was observed by fluorescent modification for the inputs, and was well-reproduced by simulation.

Next, I introduced diffusion modulation to program the diffusion term. The diffusion of the inputs is suppressed by a trap DNA anchored to the hydrogel. The degree of suppression can be adjusted by changing the concentration of the competitor, which competes with the input. Using this method, I successfully changed the position of the bisector pattern.

However, there is a problem of low pattern resolution. To address this, I redesigned DNA reaction system to use the polymerization approach. In this approach, DNA is designed to hybridize each other alternately to form a polymer. As polymerization proceeds, the molecular size increases and diffusion decrease according to the Einstein–Stokes equation. When two DNAs diffuse from each source in a hydrogel, they react on the bisector between the sources and start forming a polymer and their diffusion stops after sufficient polymerization. This technique formed a four-fold sharper pattern using less DNA. In addition, I successfully shifted the bisector position by suppressing diffusion using adjuster DNA. The pattern formation was well-reproduced by numerical simulation.

For cascaded pattern formation, I prepared DNA pairs with orthogonal sequences to form multiple parallel bisector patterns. Using adjusters to parallelize the pattern formation, I achieved a cascaded pattern formation, where bisectors first appear on the left and right sides and an additional bisector forms between them. These pattern formation processes were also well-reproduced by simulations.

Cascaded pattern formation by DNA-based reaction–diffusion system is important for artificial systems that configure themselves like living organisms. Integration with other technologies, such as molecular motor control,

DNA hydrogel, and biosensing, will enable us to design artificial systems that change their shapes and functions. In future, it is expected to provide a new approach to realizing artifacts that develops by themselves.

Contents

1. Introduction

1.1 Pattern formation in nature

Living organisms autonomously construct their bodies, which have complex shapes and various functions. If we can understand and reconstruct the phenomena that realize the desired forms and functions during development, it will be possible to design self-organizing artifacts.

The process and principles of organismal development have been studied extensively. Wolpert *et al*. distinguished four processes in development as follows: pattern formation, morphogenesis, cell differentiation, and growth (Figure 1.1). Pattern formation is the process of determining body shape and function distribution, morphogenesis is the process of changing the shape, cell differentiation is the process of changing the cellular structure and function, and growth is the process of increasing body size [1, 2]. The first three processes are particularly important in achieving the desired shape and function.

In engineering, which can be regarded as an attempt to realize desired shapes and functions in an artificial system, morphogenesis and cell differentiation can be interpreted in terms of hardware and software. For example, mechanical analysis can be used to estimate the structural strength to obtain the desired shape, and informatic analysis uses the necessary algorithms to realize various functionalities. In other words, the self-organizing properties of natural organisms can be effectively used to achieve desired geometry and functionality in artificial systems.

Pattern formation is the process of translating the design into reality, and there is no equivalent specification- and blueprint-based ordinary fabrication process. Designing the pattern formation process is the central issue in an artificial system that self-organizes itself.

Multi-step gene expression causes pattern formation of natural organisms. Spatial gradients in the concentration of gene expression-produced proteins promote or inhibit gene expression and cause the spatial protein distribution. The patterns created by protein distribution become complex as these proteins influence the expression of other proteins.

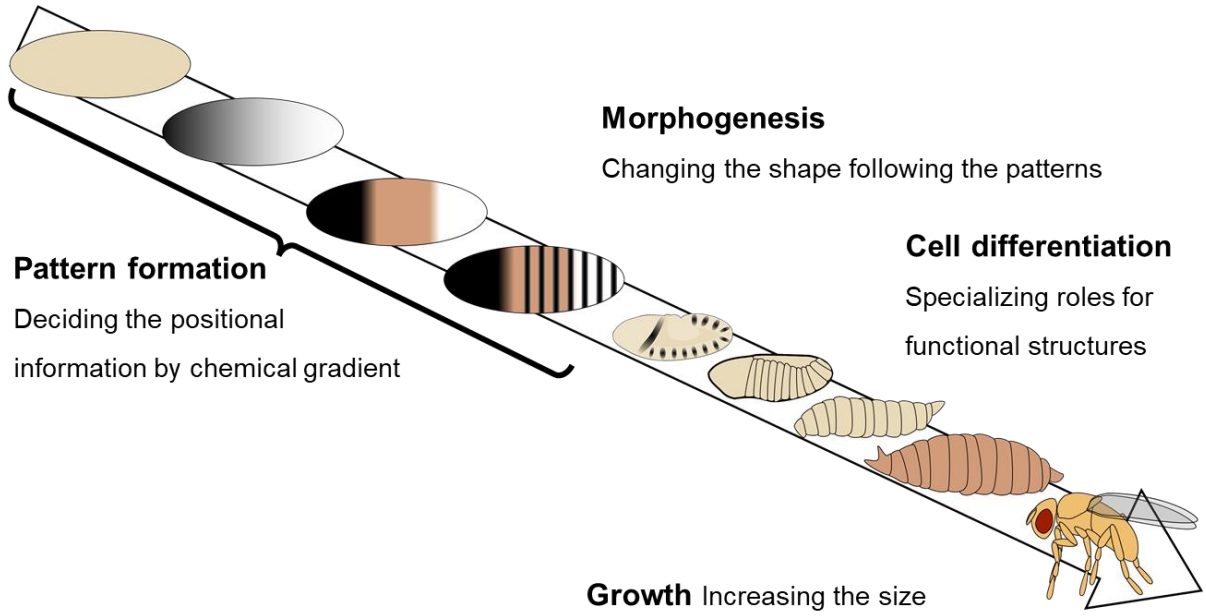

Figure 1.1 Schematics of biological development. A typical pattern formation in fly embryogenesis.

1.2 Reaction–diffusion system for pattern formation

Several studies have attempted to reproduce it in engineering systems by focusing on pattern dynamics instead of directly mimicking the principle of gene expression. The complex patterns seen on the body surface of living organisms are formed autonomously due to spatial differences in gene expression and proteins synthesized in each cell of the body surface [3,4]. Turing modeled the pattern formation by the interaction between molecular interaction (reaction) and molecular movement (diffusion) [5, 6]. The basic idea in the reaction–diffusion system is to express the spatiotemporal change in molecule concentration in a single partial differential equation. As an example, consider a situation where chemicals X and Y react to produce Z. The chemical reaction is described as follows:

$$X + Y \rightharpoonup Z,$$

where k is the rate constant for this reaction, and $D_X, D_Y,$ and D_Z are the X, Y, and Z diffusion coefficients, respectively. The spatiotemporal concentration change can be expressed by the following three partial differential equations:

$$\frac{\partial}{\partial t}[X] = D_X \Delta[X] - k[X][Y]$$

$$\frac{\partial}{\partial t}[Y] = D_Y \Delta[Y] - k[X][Y]$$

$$\frac{\partial}{\partial t}[Z] = D_Z \Delta[Z] + k[X][Y]$$

where [X], [Y], and [Z] are concentrations of each chemical and the left side is the time change of the concentration at a point. The first and second terms of the right side represent diffusion and reaction, respectively. Diffusion is proportional to the diffusion coefficient and spatial distribution gradient divergence. The Stokes–Einstein equation describes the diffusion coefficient as follows [7, 8]:

$$D = \frac{k_{\mathrm{B}} T}{6\pi\eta r}.$$

Here, k_{B} is the Boltzmann constant, T is the absolute temperature, η is the dynamic viscosity, and r is the radius of the spherical particle.

The reaction term explains the reaction that consumes one X and one Y to produce one Z, at k rate. Z production is proportional to k and X and Y concentration. The plus and minus signs are reversed in the equations of reactant and product. For a system consisting of three chemicals X, Y, and Z, the general reaction–diffusion equation can be described by summarizing the reaction term of X by $f_X([X], [Y], [Z])$ as follows:

$$\frac{\partial}{\partial t}[X] = D_X \Delta[X] + f_X([X], [Y], [Z])$$

$$\frac{\partial}{\partial t}[Y] = D_Y \Delta[Y] + f_Y([X], [Y], [Z])$$

$$\frac{\partial}{\partial t}[Z] = D_Z \Delta[Z] + f_Z([X], [Y], [Z])$$

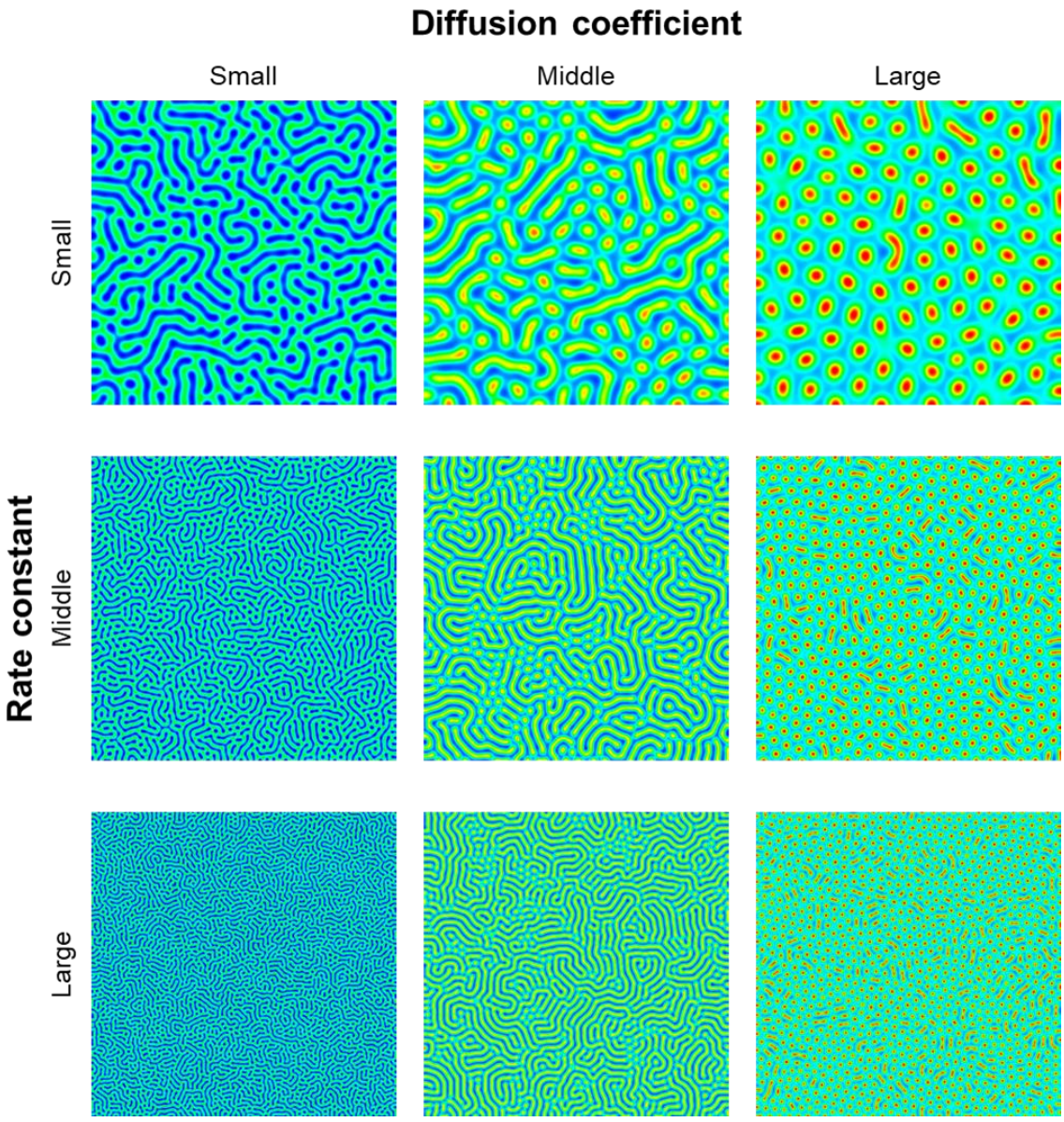

Figure 1.2 Turing pattern with several reaction rate and diffusion coefficients. Diffusion coefficient and rate constant increase in the rightward and downward directions, respectively.

When we have the chemical distribution of a system at a certain time step, the chemical distribution of the next timestep can be calculated based on the equations. The diffusion coefficient, the chemical equation, the rate constant of each reaction, and the initial spatial chemical distributions determine the behavior of the reaction–diffusion system.

Thus, we can realize a pattern formation in reaction–diffusion system by appropriately setting these conditions. Kondo *et al.* compared the pattern on fish skin and numerical simulation based

on the Turing model, which is one of a reaction–diffusion system, and reported that reaction–diffusion simulation can potentially predict such biological pattern formation [3,6].

Different rate constants and diffusion coefficients change the resultant pattern in the system with the same reaction equation. For example, in the Turing model, when the initial condition has a random noise for the concentration, a mazed-like pattern forms when the diffusion coefficient is small, while a dot pattern is obtained for a large diffusion coefficient. As the rate constant increases, the lines of the maze and the dots become fine (Figure 1.2).

A reaction–diffusion system with appropriate parameters, such as periodic oscillatory reaction called Belouzov–Zhabotinsky reaction, may be applied to the artificial pattern formation [9, 10]. In this reaction, the metal salts concentration ratio changes periodically by redox reaction, and the solution color changes, allowing us to observe the reaction dynamics. When the solution is prepared in a shallow dish, a spot-like pattern appears and then expands concentrically [11, 12].

Pattern formation using differences in metal compound solubility has also been reported [13]. Between two electrolytes that produce precipitates, one is spread throughout the system at a low concentration, while the other is dropped as a spot at a high concentration. In this situation, an area of lack of reactant surrounds the precipitate-producing area. When a high-concentration electrolyte solution is dropped on multiple points, these propagating areas contact each other, the reactant depletes, and the reaction stops. Accordingly, a Voronoi pattern referring to the drop locations forms.

Note that the pattern is composed of precipitates, so the resultant pattern remains as heterogeneous distribution of molecules.

Recently, a method to change the physical properties of the medium using the localization of molecules has been reported. Boekhoven *et al.* designed two molecules that form a polymer when they react with each other. They built a system where polymerization occurs in the central region by diffusing two molecules from the left and right sources [14-16]. In this system, polymer localization forms a bisector line between the two sources. Furthermore, since a polymer network forms, gelation occurs on the bisector. This means that by associating the reaction–diffusion system with the gel–sol phase transition, it is possible to create hydrogels with a shape of the formed pattern.

Various artificial reaction–diffusion systems based on chemical reactions have also been reported, and the effects of parameters have been well studied [17, 18]. However, constructing a new arbitrary reaction system is generally difficult because designing the materials interacting with each other in desired manner is difficult. Realizing the pattern formation seen in biological development may require a high level of programmability.

1.3 DNA-based reaction–diffusion system for artificial pattern formation

1.3.1. Synthetic DNA as a programmable material

Designing reaction–diffusion system requires materials that program their parameters for reaction and diffusion. Thus, synthetic DNA is particularly useful. While DNA carries genetic information, it is also programmable [19-22].

A DNA molecule is composed of three elements: a base, a sugar, and a phosphate. The base is attached to the sugar and the sugar and the phosphate are interlinked to form the backbone. These bases are one of four types: adenine (A), guanine (G), cytosine (C), and thymine (T). They specifically form base pairs when A–T or G–C face each other. This property is called complementarity, and complementary bases are called Watson–Crick base pairs [23]. This property determines the complementary sequence for an arbitrary DNA base sequence. The thermodynamic properties of base pair formation have been carefully investigated, and the structure composed of DNA sequences can be predicted presently [24-30]. In other words, appropriate base pair design enables us to construct various reaction systems and nanostructures using DNA.

Hybridization, the basis for implementing the desired reaction system, is base pairing between the complementary single-stranded DNA. When two DNAs X and Y with complementary sequences are in a solution, double-stranded DNA Z forms by hybridization.

$$X + Y \rightharpoonup Z,$$

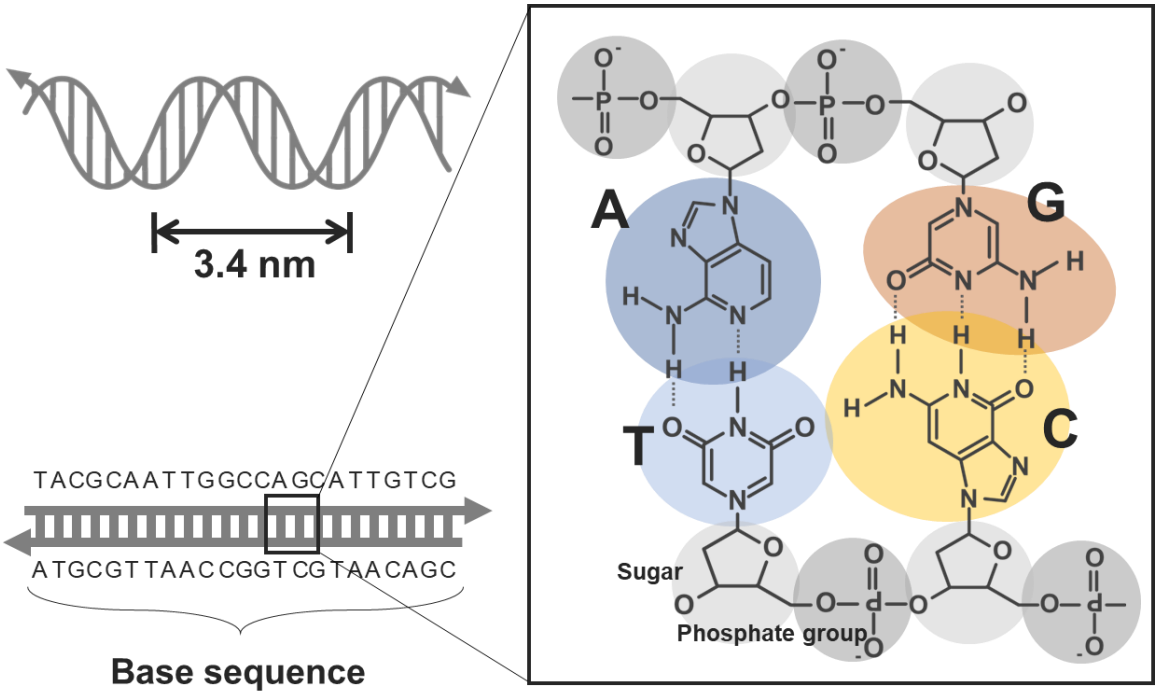

Figure 1.3 Shape of DNA. The DNAs are usually illustrated by the arrows (double-stranded DNA is indicated by a pair of anti-parallel two arrows.

Since the double-stranded DNA is less reactive, it is necessary to devise a way to denature it. For denaturing the double-stranded DNA, designing a single-stranded domain that serves as a toehold for the reaction and recombing it into a stable bond is useful [31, 32]. The reaction is called the toehold-mediated strand displacement reaction (or just strand displacement) based on the thermodynamical mechanism that a long complementary sequence stabilizes the double helix structure DNA *Y'*, which has more bases than *Y*, hybridizes with DNA *X*, DNA structure *Z'* with a single-stranded domain as a toehold. *Z'* and *X'*, which is fully complementary to *Y'*, react with each other to produce double-stranded DNA *Z"*, which comprises *X'* and *Y'*, and release the *X* as a single-stranded DNA. The reaction is described as a chemical equation as follows:

$$Z' + X' \rightharpoonup X + Z'',$$

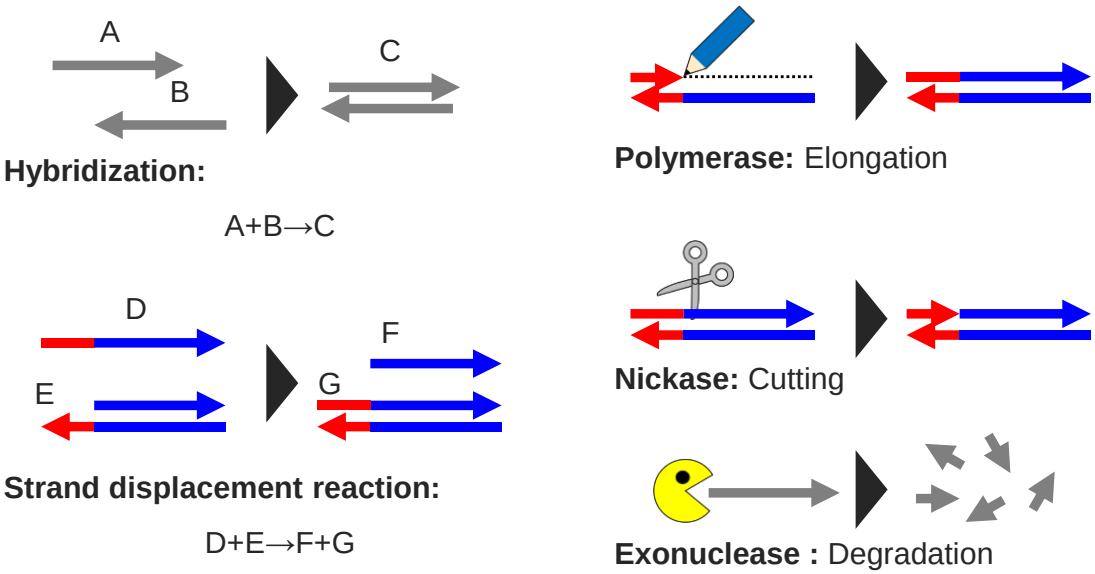

Fig. 1.4 Basic DNA reactions. Same color indicates a reaction domain with a complementary sequence.

Artificial reaction systems capable of information processing have been constructed by designing DNA sequences with the differences in stability due to complementary sequence domain and its arrangement [33-38]. The tools for sequence design, such as DINAMelt [39], NUPACK [40], and Visual DSD [41] are available online without installation. (However, as of 2022, we cannot access Visual DSD, which was a convenient tool for studying the time development of chain displacement reactions.)

Artificial reaction systems often utilize modified DNAs [42-44]. A typical example includes fluorescent modifications used to visualize specific DNA [45], and molecules that add reactivity to DNA such as functional peptides [46]. Other modifications that allow DNA manipulation, such as changing bonding between DNAs [47-49], and cleaving backbones in response to light [50] are also widely used. Developing artificial bases, which expands the possibilities of sequence design, is also progressing [51-53]. The application of functionalized DNA as a biocompatible molecule has also been well studied.

In the complementarity-based interaction, although the bond between DNAs changes, the primary structure of DNA molecules in solution does not change. Complex reaction systems are produced using DNA producing enzymes, such as polymerase, nickase, and exonuclease.

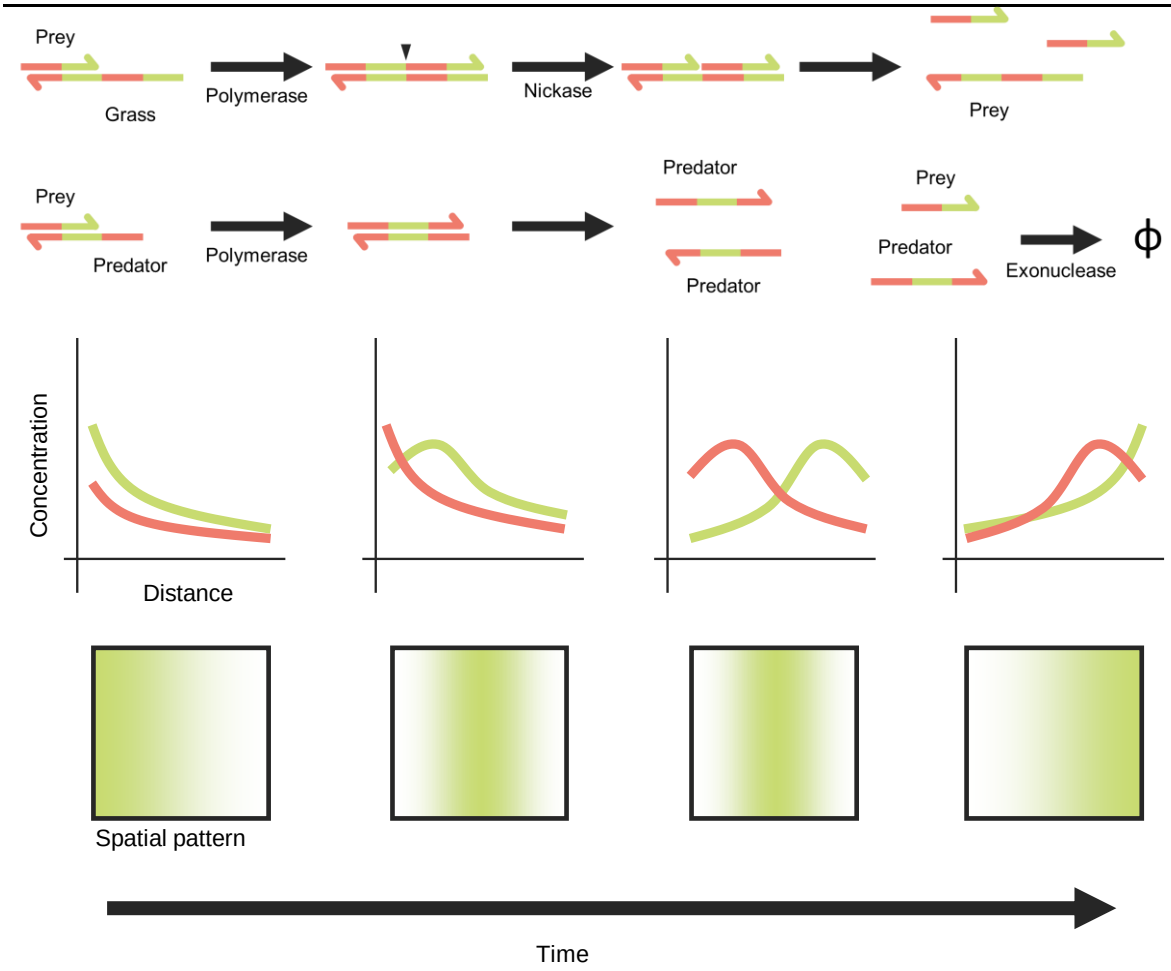

Figure 1.5 Wave pattern formation using enzymatic reactions. According to the reaction shown above, predator increases in the region of increased prey, and spatially propagates with highly prey concentration region followed by high predator concentration region. Adapted from [60].

Polymerase elongates DNA and synthesizes a complementary sequence to the template DNA. Nickase detects specific sequences in double-stranded DNA and cleaves the backbone, and the exonuclease degrades DNA molecules. A combination of these enzymes has been designed to control the DNA rection systems [54-56].

1.3.2. DNA-based reaction–diffusion system with enzymes

Recently, some studies have reported the application of DNA reactions to artificial reaction–diffusion systems. Enzymatic reactions that can produce or degrade DNA molecules in a system are particularly useful to design such reaction–diffusion systems.

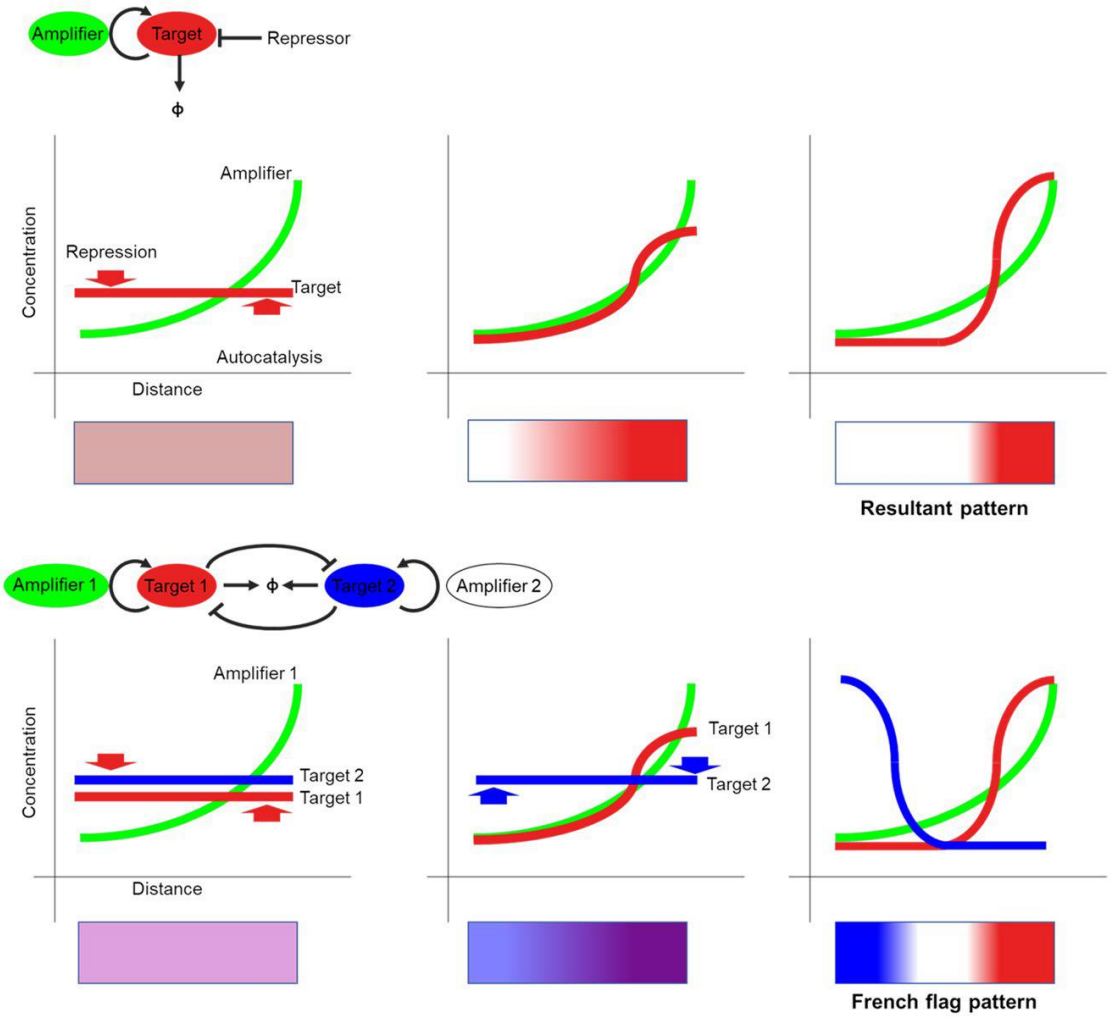

Figure 1.6 French flag pattern formation. As shown above, when there is a gradient in the amplifying factor concentration in a space where the target always degrades, the target is amplified in the high concentration region and degraded in the low concentration region, generating a steep concentration gradient. Furthermore, when target 1 repress the amplification of target 2, the target 2 is amplified on the opposite side of target 1, resulting in compartmentalization into three regions, including a region where the repression is balanced, and both do not increase. Adapted from [61].

Fujii *et al.* designed a DNA-based reaction referring to a predator-prey oscillator [57]. The oscillator consists of three chemicals: grass, prey, and predator. The grass works as a catalyst to increase the amount of the prey, the amount of predator increases by consuming the prey, and the prey and predator are degraded at a constant rate. Under an appropriate condition, an increase in the predator follows the increase in prey. Then, the predator decreases because of the lack of prey, and the prey increases again and the cycle goes on [58, 59].

Here, grass, prey, and predator are all represented by DNA strands, and they increase or decrease by enzymes. The grass strand has a repeated base sequence complementary to the prey strand sequence. When a prey strand hybridizes with a grass strand, a polymerase elongates the prey strand, a nickase cut it, and the number of prey strand increases to two. In contrast, the prey and predator strands hybridize and the prey strand transforms into a predator strand by polymerization. Thus, the grass strand increases the prey strand amount catalytically, and the predator strand increases by consuming the prey strand. Both prey and predator strands are degraded by exonuclease. The authors use these interactions among these DNA strands to realize wave propagation behavior [60].

Such a DNA reaction system using enzymes called “PEN DNA toolbox” is employed for several applications. Anton, *et al.* utilize the toolbox for a reaction–diffusion system that generates a French flag pattern [61] (Figure 1.6), which resembles fly development [62]. They use a reaction system similar to the previous oscillator to control the concentration of the prey strand as a target molecule, where the grass and predator strands are used as amplifier and repressor for the target, respectively. When the concentration of the amplifier has a gradient, the target increases only where the amplifier is rich. Furthermore, a reference DNA that works as an amplifier for target 1 and repressor for target 2 is introduced. Where the reference is rich, target 1 is amplified, but target 2 is repressed. However, where the reference concentration is low, target 2 is amplified and target 1 is degraded. Using such reactions, a French flag pattern in a 1D reaction–diffusion system is realized.

1.3.3. Enzyme-free DNA-based reaction–diffusion systems

The DNA reaction systems can be applied to program reaction–diffusion systems. A simulation study on designing the DNA reactions for programming desired patterns has constructed five reaction modules called SHARPEN, COPY, AND, NOT, and BLUR [63]. Reaction–diffusion systems that form some desired shapes were successfully programed by combining these modules.

Reaction and diffusion speeds should be considered while designing a reaction–diffusion system. If reaction and diffusion magnitudes are not in the same order, one term will dominate, and the influence of the other term will be suppressed. Many DNA computing systems are

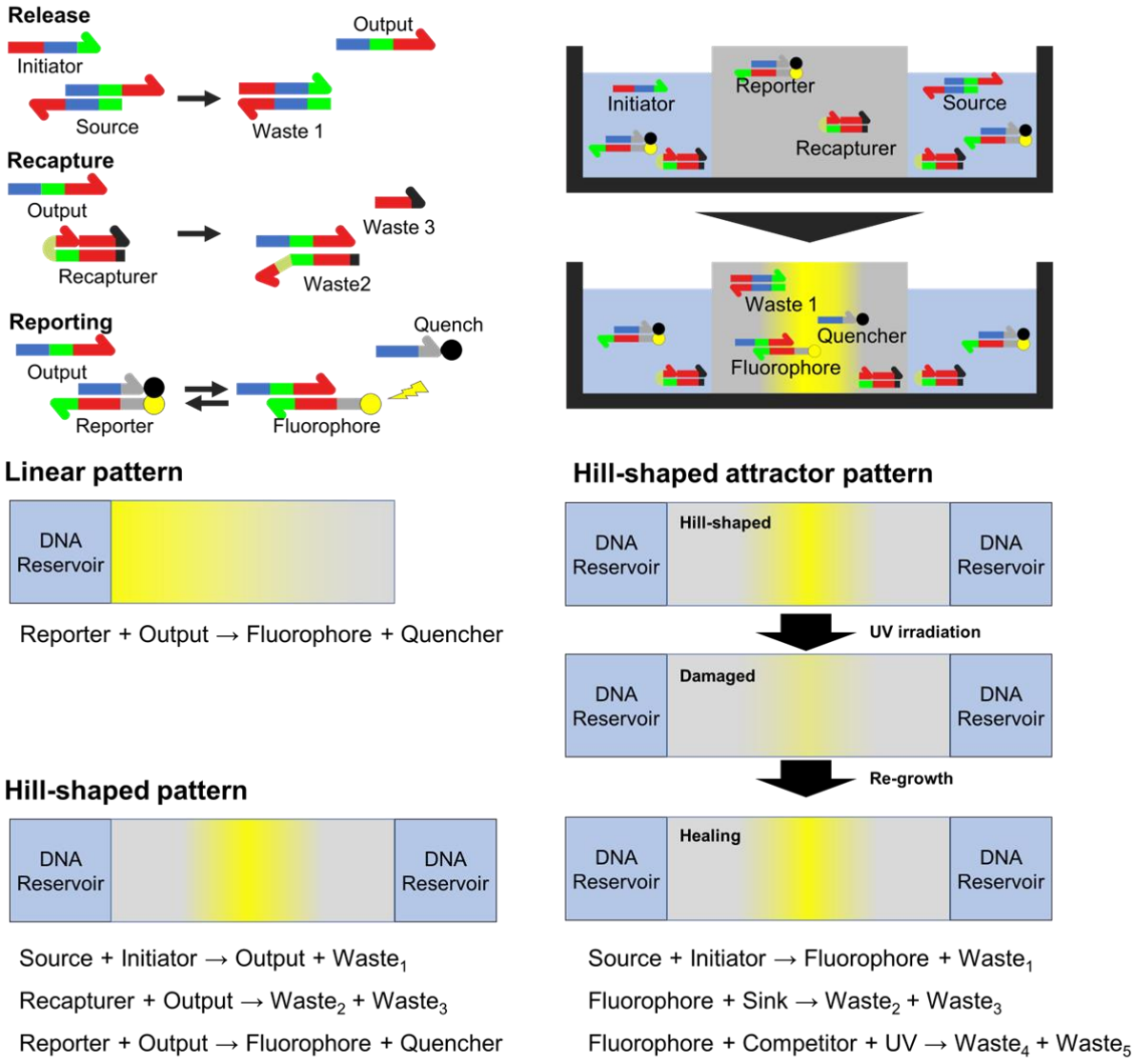

Figure. 1.7 Reaction–diffusion system using reservoirs. Based on the reaction system shown in the upper left, pattern formation can be realized by preparing DNA in the gel region (grey) and the solution region (light blue) as shown in the upper right. As shown in lower left, a linear or hill-shaped chemical gradient can forms by changing the DNA in the gel and solution, and a recovery behavior can be realized by continuously supplying DNA with a microfluidic device, as shown in the lower right. Adapted from [68, 69]

designed so that the reaction field is always homogeneous [64-66]. This is because the diffusion rate is larger than the DNA interaction rate in ordinary solution conditions. Thus, concentration changes due to the reaction are immediately homogenized by diffusion. For instance, the diffusion coefficient of 20 nt DNA is approximately 108.6 $\mu m^2/s$ [67]. On the contrary, when the DNA reacts with other DNA complex with strand displacement, is approximately 3×10^6 /M/s rate [31]. Thus spatial concentration gradient patterns are lost by diffusion. Constructing

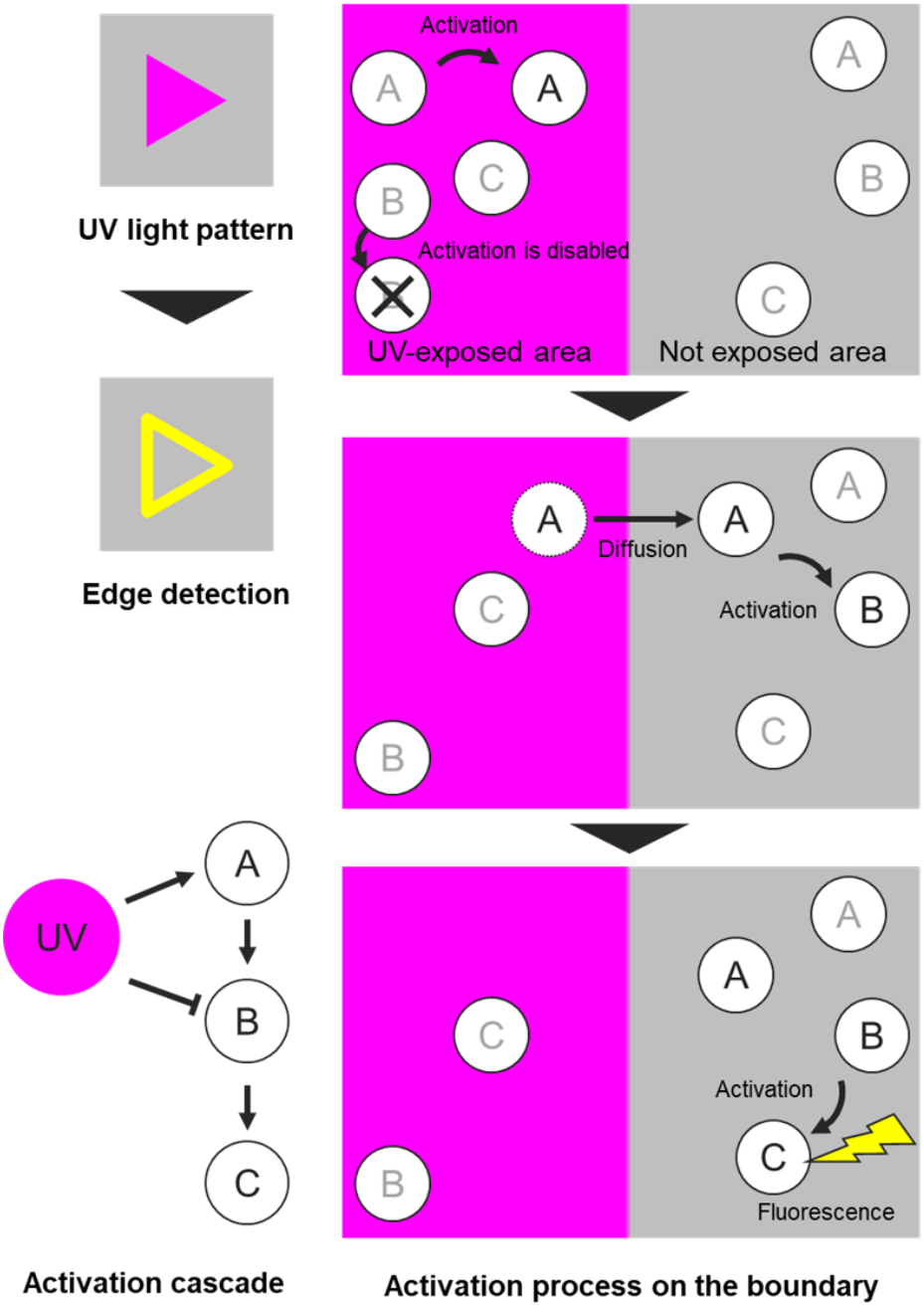

Figure 1.8 Edge detection in hydrogel using DNA circuit. The input UV light activates A and inhibit B. The reaction cascade proceeds only in the boundary region where diffused activated A and uninhibited B coexist, resulting in edge detection. Adapted from [70]

a reaction–diffusion system for pattern formation requires a design that balances between reaction and diffusion.

One approach to solve this is to employ a DNA reservoir. Zenk, *et. al.* set reservoirs in which they continuously replace the inner solution to maintain the DNA concentration in the reservoirs (Figure 1.7) [68]. They designed four DNA complexes (source, initiator, recapturer, and

reporter) for DNA release, recapture, and reporting and realized stable pattern formations. During the release reaction, the source and initiator react and release output. The output reacts with both recapturer and reporter, with different rates and reversibility. The recapture reaction is slow but irreversible and consumes the output. However, the reporting reaction is fast and reversible. Therefore, the released output is initially used for the reporting reaction, and then gradually consumed by the recapture reaction. They built a reaction–diffusion system where the recapturer and reporter are prepared in the whole area, and the source and initiator are stored in facing reservoirs. The reporting reaction was visualized using a fluorescent signal. In addition, the authors have also reported later that microfluidic devices can continuously supply DNA. The pattern formed there recovered from the disturbance [69].

Another well-known example is an edge detection system constructed in a polyacrylamide gel (Figure 1.8) [70]. This system detects the UV-irradiated area on the hydrogel using A, B, and C DNAs, which have active and inactive states and are initially inactive. The activated A and B activate inactive B and C, respectively, and fluorescent emission visualizes the C DNA activation. The input UV irradiation activates A and inhibits the B activation. Then, the active A diffuses into the unirradiated area and starts the activation cascade. Since inactive B and active A are around the irradiated area boundary, the cascade occurs only at the edge of the irradiated area.

1.3.4 Programming DNA diffusion

There are two main ways to maintain the patterns in methods described. In the first method, the pattern is dynamically maintained by balancing supply and dissipation. In the second method, it is statically maintained by immobilizing the molecules. The mechanism to change the diffusion of molecules also differs. Since the chemical gradient is lost by diffusion, the pattern formation in a reaction–diffusion system requires a mechanism to maintain the result. The methods for dynamic pattern require perpetual molecule supply or synthesis, while the systems for static pattern adopt mechanisms that decrease the diffusion of molecules.

The chemical approach described in section 1.2, uses the BZ reaction, which is a cyclic reaction, while the other two approaches involve molecule retention by precipitation. Most

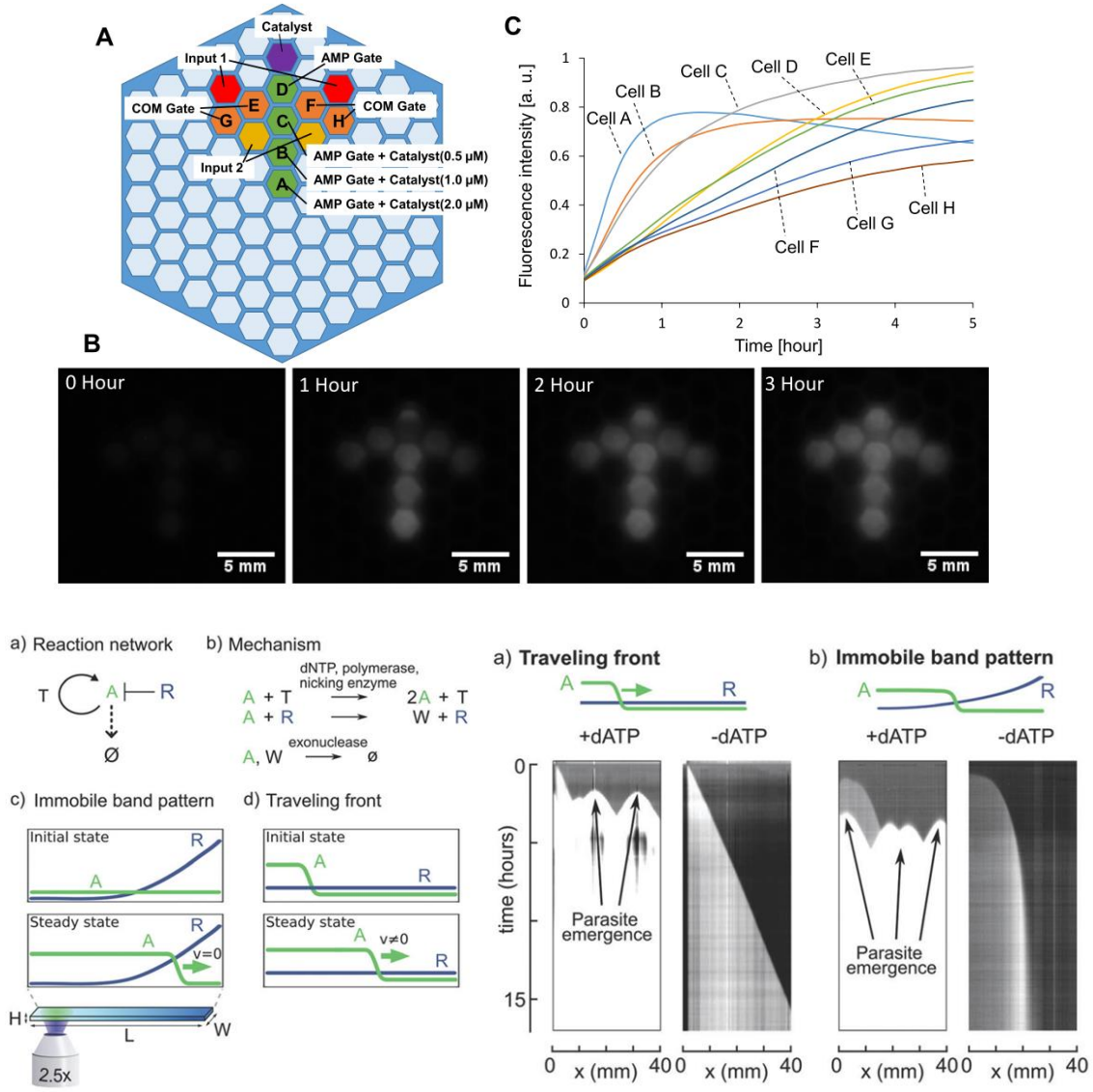

Figure 1.9 Pattern formation with programmed diffusion. Top, the anchor DNA remains in the cell and controls cell–cell signal propagation [71]. Bottom, the anchor DNA prevents the dissipation of the pattern created by the enzyme reaction [75].

DNA-based approaches mainly focus on the mechanism of dynamic pattern maintenance. This is because the advantage of DNA sequence design is usually applied to program reaction terms.

In contrast, previous studies have focused on the mechanisms that manipulate DNA diffusion (Figure 1.9), particularly the size dependence of molecular diffusion based on the Stokes–Einstein equation [71]. The size of single-stranded DNA depends on the number of bases, but long single-stranded DNA is not suitable for practical use because of the increase in undesired interactions. On the contrary, grafting even small DNA with a polymer suppress diffusion. The copolymerization of acrylamide with acryldite binds acrydite-modified DNA to the

polyacrylamide network. In particular, a specific DNA can be anchored to a certain space in the hydrogel.

This technique was developed to materialize gellular automata, a cellular automaton realized by separating compartments containing molecule solutions using hydrogel walls [72-74]. While the DNA signals diffuse in the hydrogel wall and propagate to the neighboring compartments, the acrylamide-modified DNA cannot diffuse into the neighbor compartment because it cannot penetrate the gel walls. The diffusion state of the signals can be switched by binding the anchor DNA. Combining the anchor DNA with DNA logic circuits realizes spatial state transitions of the cellular automata.

This anchoring technique can be combined with enzymatic reactions. Based on previously described reaction–diffusion system for French-flag pattern [61], combining the combination of the PEN DNA toolbox with the anchor DNA maintains the pattern formed for a long time [75].

This anchoring method has also been applied to the control diffusion speed of DNA molecule [76]. A toehold exchange reaction, in which two DNA strands compete for a toehold of the anchor DNA, is the reversible interaction that adjusts the degree of equilibrium to vary the diffusion coefficient. This changes the diffusion coefficient by a factor of six and causes sequence-specific adjustment between orthogonal DNA sequences. I have employed it in this study and described the detailed mechanism in section 3.1.

1.4 Purpose of this thesis

This study aim to develop a method to program pattern formation by DNA reaction–diffusion systems. I investigated a method for building a DNA-based reaction–diffusion system that mimics pattern formation process in biological development.

During biological development, biomolecules move and interact with each other to create ordered patterns, which are maintained for a certain time period to provide the positional information necessary to form the body. Mutually orthogonal positional information, such as front–back or top–bottom coordinates are simultaneously generated in a closed space called an

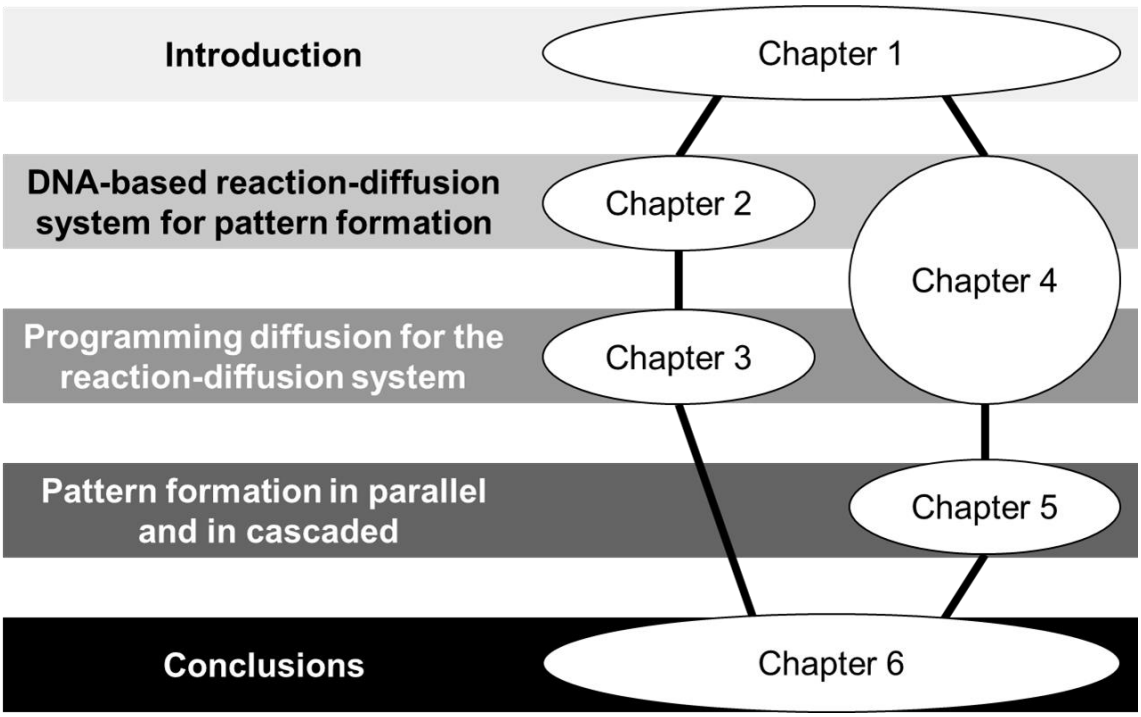

Figure 1.7 Construction of this thesis

embryo. The pattern formation occurs in multiple steps in an appropriate order, resulting in complex maturation as an individual. The following three issues must be addressed to realize such a phenomenon in artificial DNA reaction–diffusion systems.

1) To construct a reaction–diffusion system that switches the DNA diffusion state in the hydrogel to form static patterns.

2) To program the spatiotemporal DNA diffusion process by introducing a mechanism to inhibit diffusion and change the patterns formed.

3) To combine and link multiple pattern formation processes in a cascade.

I addressed these issues using two approaches. In Chapter 2, I have described the construction of a reaction–diffusion system that forms a static pattern by applying a DNA anchoring technique. Anchor DNA employment in a hydrogel medium and the program for logical operations realize a static pattern formation. In Chapter 3, I have introduced an additional technique to modulate diffusion, which is an extension of the reaction–diffusion system described in Chapter 2. In Chapter 4, I have described the polymerization approach developed after evaluating the effectiveness and problems of the approach described in Chapter 2 and 3.

In Chapter 5, I have described the realization of parallel and cascaded pattern sresults obtained and describe the future perspectives based on them.

2. Bisector pattern formation in hydrogel

In this chapter, I describe the construction of a reaction–diffusion system that forms the basic bisector pattern using synthetic DNA. The bisecting pattern can be formed by programming two molecules to diffuse form the left and right diffusion sources and stopping their diffusion when they react at the center.

2.1 Design and experimental system

2.1.1 DNA anchoring method

Bisector pattern formation requires stopping the diffusion of substances propagating from the sources. Here, I explain how to construct a reaction–diffusion system that stops the diffusion of two DNAs by combining the anchoring method and the DNA AND gate.

A method of attaching DNA to polymers has been reported as a DNA anchoring technique. By modifying DNA with acrydite and copolymerizing it with acrylamide, anchor DNA that attaches to long polyacrylamide chains and does not pass through the wall separated by the hydrogel can be produced [71]. The anchor DNA stops the diffusion of other DNA in the hydrogel medium by dispersing in the hydrogel.

The anchor DNA behaves in the same sequence-dependent manner as other DNA because molecular modifications to DNA ends do not affect the DNA properties. If the anchor DNA has a sequence complementary to the diffusing DNA sequence, they hybridize and stop the diffusion. Such diffusion-inhibiting properties can be introduced into a reaction system by sequence design.

2.1.2 DNA AND gate

To realize a reaction that stops the diffusion of two DNA strands on the bisector, I used a DNA AND gate that binds when two single-stranded DNA inputs A and B coexist. In the pattern

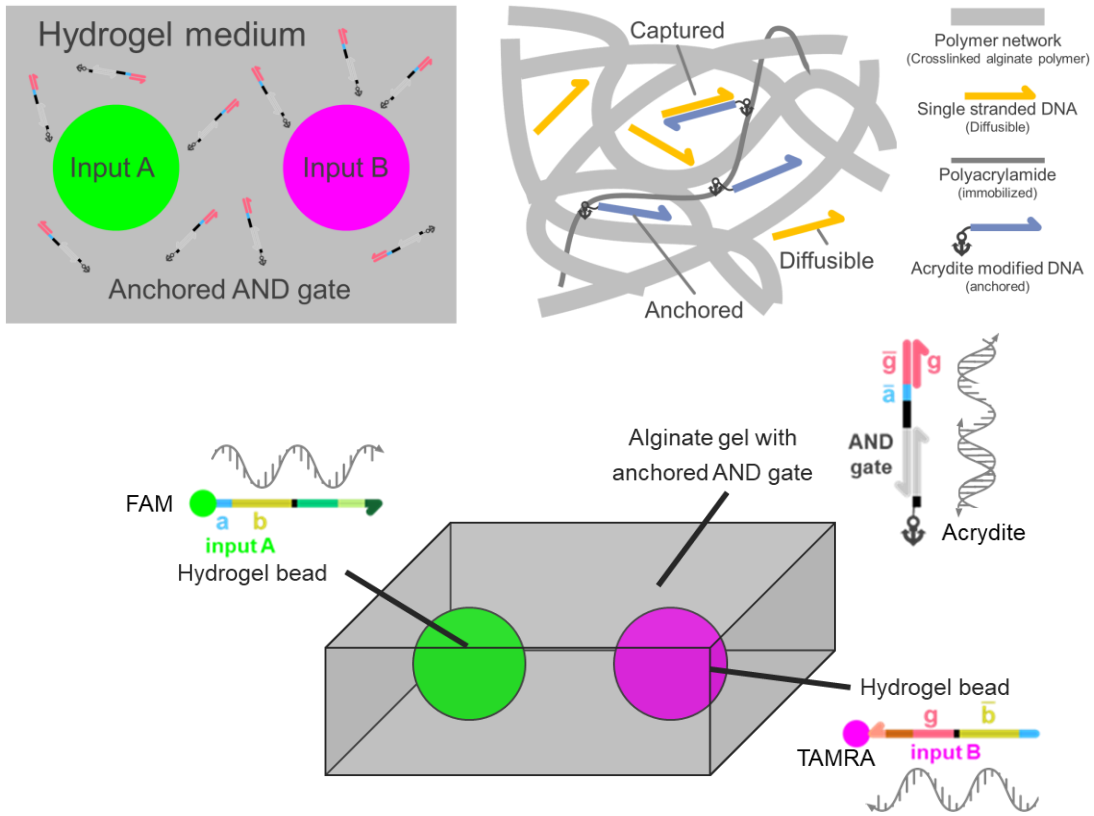

Figure 2.1 Schematics of the experimental system. In the initial state, the source of inputs A and B are placed in a hydrogel medium containing an anchored AND gate (upper left). DNA bound to polyacrylamide by acrydite modification not only prevents its diffusion but also to stops the diffusion of complementary DNA (upper right). This system was realized by filling the area around hydrogel beads with alginate gel with an anchored AND gate (lower).

formation system, hydrogel beads containing two types of single-stranded DNA inputs A and B face each other and are surrounded by hydrogel anchored with AND gate to construct a reaction–diffusion system.

This AND gate was designed based on the logic gate using the associative toehold activation reaction [34] (Figure 2.2). The AND gate is a DNA complex that operates to bind inputs A and B to the anchor DNA only in the presence of both. The details of the reaction are as follows: inputs A and B are first combined by hybridization in the reaction domain “b” to form an input A–B complex. Since the reaction domain “g” of input B and the reaction domain “a” of input A are adjacent by this reaction, AND gate joins input A-B complex via strand displacement reaction.

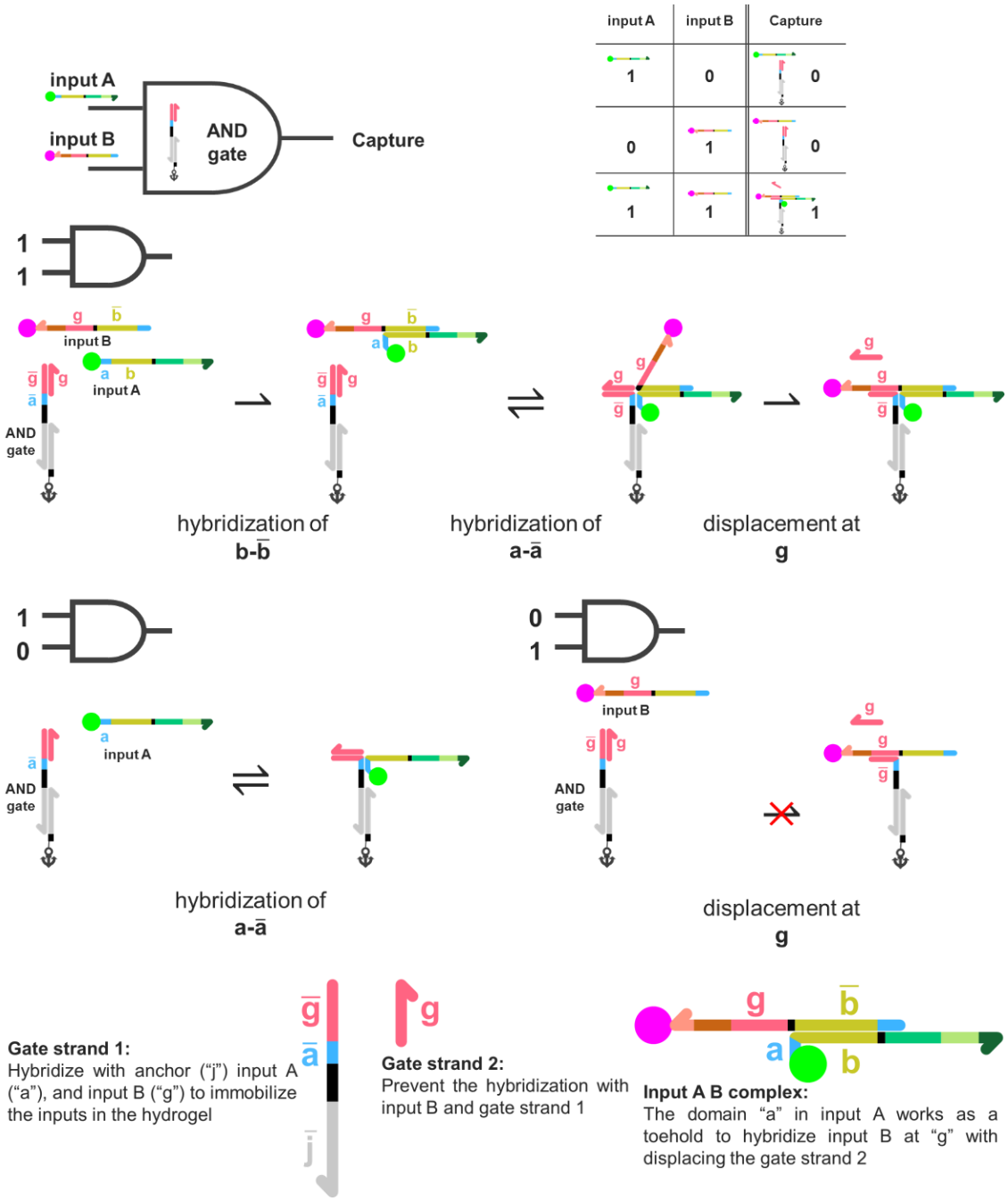

Figure 2.2 Design of our DNA logic gate. AND gate stably binds only to input A-B complex (upper panels). The AND gate consists of two strands (lower left). The inputs bind to each other in the reaction domain "b" (lower right).

In contrast, when only input A is present, input A hybridize with the AND gate at the 6 nt reaction domain a, it denatures immediately at room temperature. However, when input A is absent, the reaction domain "g" is covered by gate strand 2; thus, input B cannot hybridize with the AND gate.

2.1.3 Experimental setup

The reaction–diffusion system used in the experiment consists of the following four steps (Figure 2.3).

Step 1.Mix 1.5% acrylamide (BIORAD), 0.5% N, N'-methylenebisacrylamide (Bio-Rad Laboratories, Inc., CA, USA), and 40 μM acrydite-modified DNA in a 10 mM Tris-HCl buffer supplemented with 12.5 mM $MgCl_2$ (Fuji Film Wako Pure Chemical Corporation, Osaka, Japan) (Other solutions in Chapter 2 and 3 are also with the same condition) and add a polymerization initiator (10% TEMED; Bio-Rad Laboratories, Inc., CA, USA) and 10% APS (Fuji Film Wako Pure Chemical Corporation, Osaka, Japan). Leave it left overnight to attach the DNA to the polyacrylamide chain.

Step 2. Prepare pre-gel solutions for AND gate, input A, and B.

1) Mix the anchor DNA with other DNA.
2) Add the connector DNA which mediates the bind between the anchor and the inputs.
3) Mix each solution with 1.5% sodium alginate solution.

Step 3. Prepare hydrogel beads containing inputs A and B.

1) Drop 3 μL pre-gel solutions containing inputs A and B into 0.4 M $CaCl_2$ (Fuji Film Wako Pure Chemical Corporation, Osaka, Japan) solution. At this time, the alginate polymers in the solution cross-link and immediately congeals the solution (Figure 2.4 top). The inputs A and B bind to the anchor via the connectors and immobilized in the hydrogel.
2) Remove the $CaCl_2$ solution around the gel, add 150 μL Ca^{2+}-free buffer and exchange the buffer again to rinse the beads twice.

Step 4. Set up the initial state and start pattern formation.

1) Place the hydrogel beads to face each other in a silicon chamber and fill it with sodium alginate solution containing the anchored AND gate.

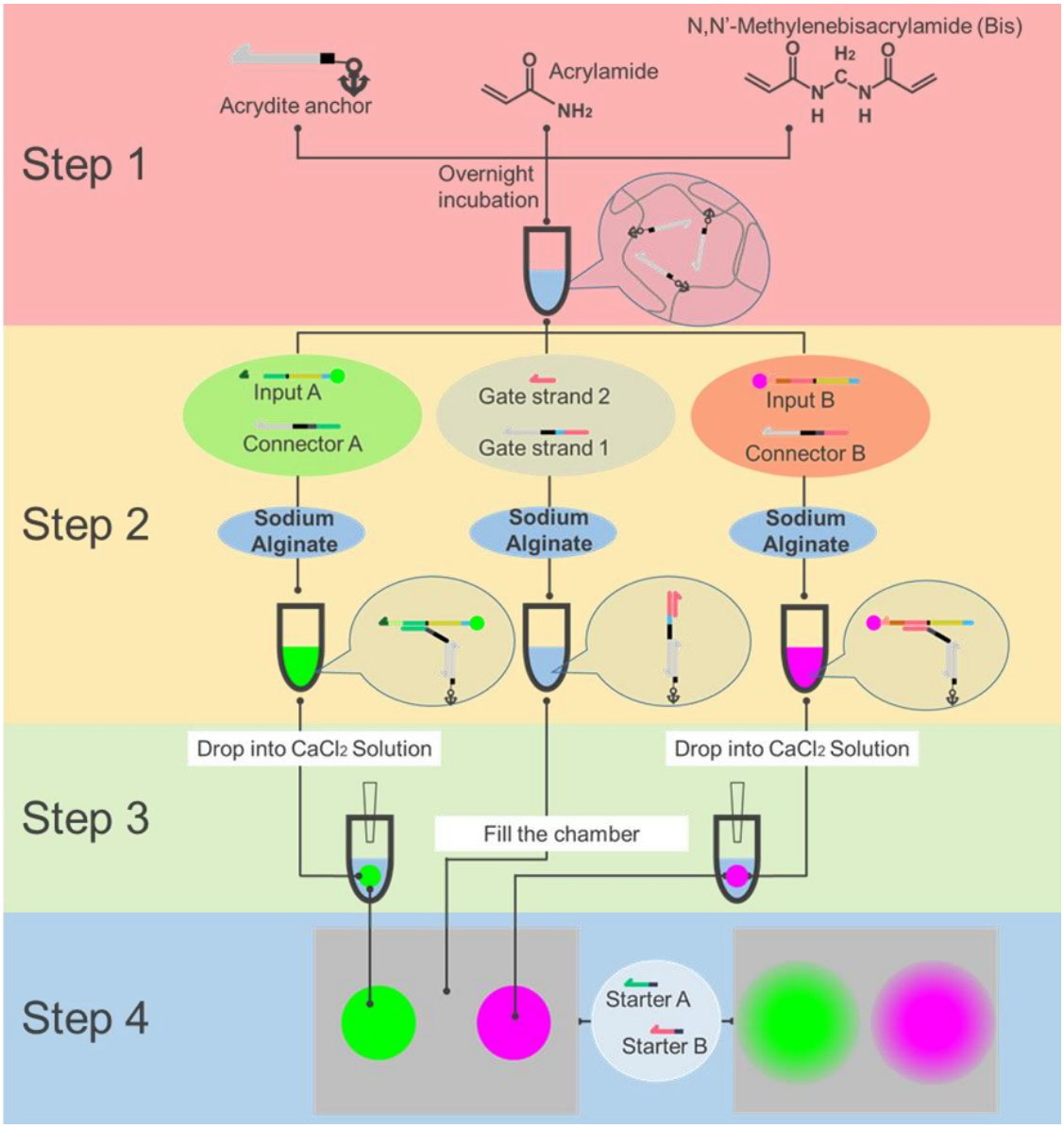

Figure 2.3 Steps for fabricating the reaction–diffusion system. The system was constructed in four steps: preparing anchored DNA, mixing pre-gel solution, preparing hydrogel beads containing inputs, and setting up initial conditions.

2) Pour $CaCl_2$ solution into the chamber and incubate it for 10 minutes (Figure 2.4 bottom).
3) Add 4 μL 8 μM starter DNAs, which release inputs A and B from their connectors through strand displacement reaction to initiate pattern formation after observation setup.

Input A and B were modified with fluorescent molecules FAM and TAMRA, respectively, to visualize pattern formation process.

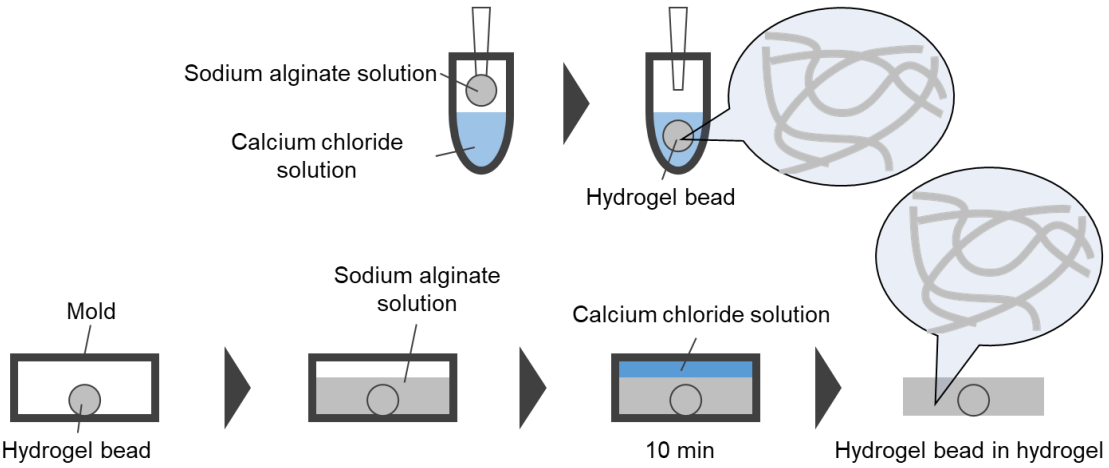

Figure. 2.4 Hydrogel preparation for medium

2.2 Results and discussion

2.2.1 DNA anchoring

The performance of DNA anchoring was evaluated by polyacrylamide electrophoresis (Figure 2.5). Lane 1 contains anchor DNA without step 1 treatment and Lane 2 contains DNA with a complementary sequence as a reference. Lane 3 shows a band in the upper position compared to than in Lane 2, representing hybridized DNA.

On the contrary, the lower fluorescent band indicating unanchored DNA disappears in Lane 4, and the area near the well has strong fluorescence. This indicates that the acrydite-modified DNA is bound to the polyacrylamide chain in step 1, increasing its molecular weight. When the complementary strands are added (Lane 5), the band observed in Lane 3 becomes faint. This is because the added complementary strand binds to the anchor DNA and stays near the well. Therefore, the result shows that anchoring is possible by binding acrydite-modified DNA to a polyacrylamide chain and does not damage that the sequence-dependent property.

2.2.2 Associative toehold activation reaction–based DNA logic gate

The behavior of the DNA logic gate was also evaluated by polyacrylamide gel electrophoresis (Figure 2.6).

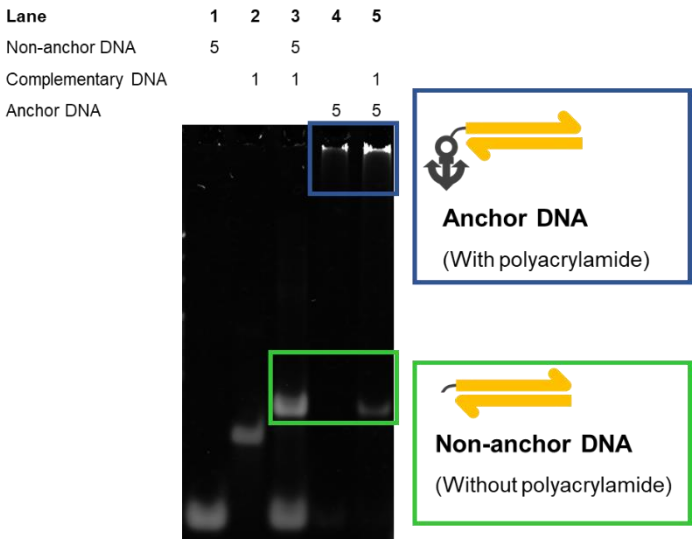

Figure. 2.5 Electrophoresis of anchor DNA. DNA was mixed to 1 μM, run on a 10% polyacrylamide gel for 60 min at 100 V and stained with SYBR Gold for 20 min.

Comparing to the bands in Lanes 1–4, which represent inputs A, B, A–B complex, and gate strand 1, no interaction between gate strand 1 and input A is observed in Lane 5, while input B and gate strand 1 bind to each other in Lane 6. Since the band in Lane 7 appears upper than that in Lane 6, three DNAs including gate strand 1 form a complex when both inputs A and B are added. Lanes 9–11 show that gate strand 2 does not interact with inputs A and B. Therefore, even if the AND gate reacts as designed, the released gate strand 2 will not affect the operation of other inputs.

When gate strands 1 and 2 are mixed to form an AND gate, the inputs do not react with the complex (Lanes 12–14). In contrast, when both inputs A and B are added (Lane 7), a complex band of input A, B, and gate strand 1 appears, confirming that the AND gate acts as a logic circuit as designed.

2.2.3 Pattern formation in hydrogel medium

The DNA was introduced into the hydrogel and the pattern formation process was observed. The inputs A and B were modified with FAM and TAMRA, and the changes in the concentration distribution were visualized as green and magenta fluorescence, respectively. Figure 2.7 shows the results of a system where input A is prepared on the left bead and input B on the right bead, and the AND gate is anchored to the surrounding hydrogel medium observed for 10 hours.

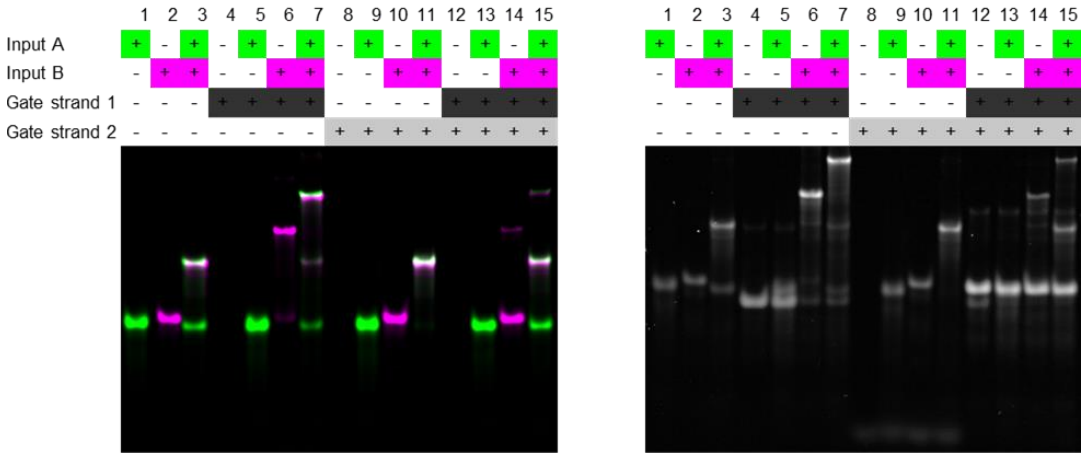

Figure. 2.6 Electrophoresis of DNA logic gate. DNA was mixed to 1 μM, for 30 min, and run on a 10% polyacrylamide gel for 60 min at 100 V. Left: a superimposed image of FAM (green) and TAMRA (magenta) fluorescence images, respectively. The bands of the DNA complexes that include both inputs A and B, such as Lane 3, are visualized in white. Right: stained with SYBR Gold for 20 min.

Inputs A and B diffuse into the hydrogel containing AND gate after 2 hours, and a white bisector appears weakly between the two beads after 4 hours (Figure 2.7). The white area indicates where both FAM and TAMRA fluorescence was observed, indicating that the co-localization of inputs A and B in this reaction–diffusion system resulted in the appearance of the bisector line. This bisector remained throughout the observation period (10 hours), even as the DNA in the left and right beads diffused. This suggests that the bisector is not a temporary pattern due to the overlap of the diffusion fronts, but a static pattern formed by the programed DNA reaction.

Furthermore, when the same inputs are provided for both the left and the right sides, or when the AND gate is not anchored to the surrounding hydrogel, such bisector lines did not appear (Figure 2.8). Thus, the bisector pattern did not form when the inputs A and B do not react to the AND gate. Therefore, the bisector pattern formed and remained by the operation of the anchored AND gate.

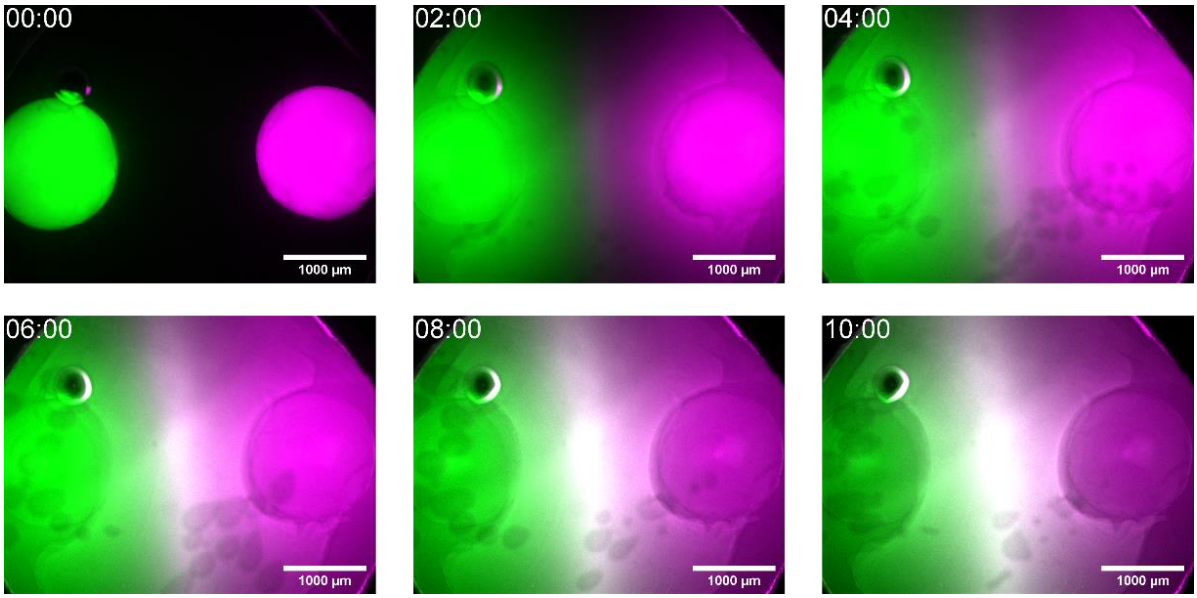

Figure. 2.7 Bisector pattern formation in hydrogel medium. The results are superimposed FAM and TAMRA fluorescence images (green and magenta, respectively). The area where inputs A and B coexist is visualized in white.

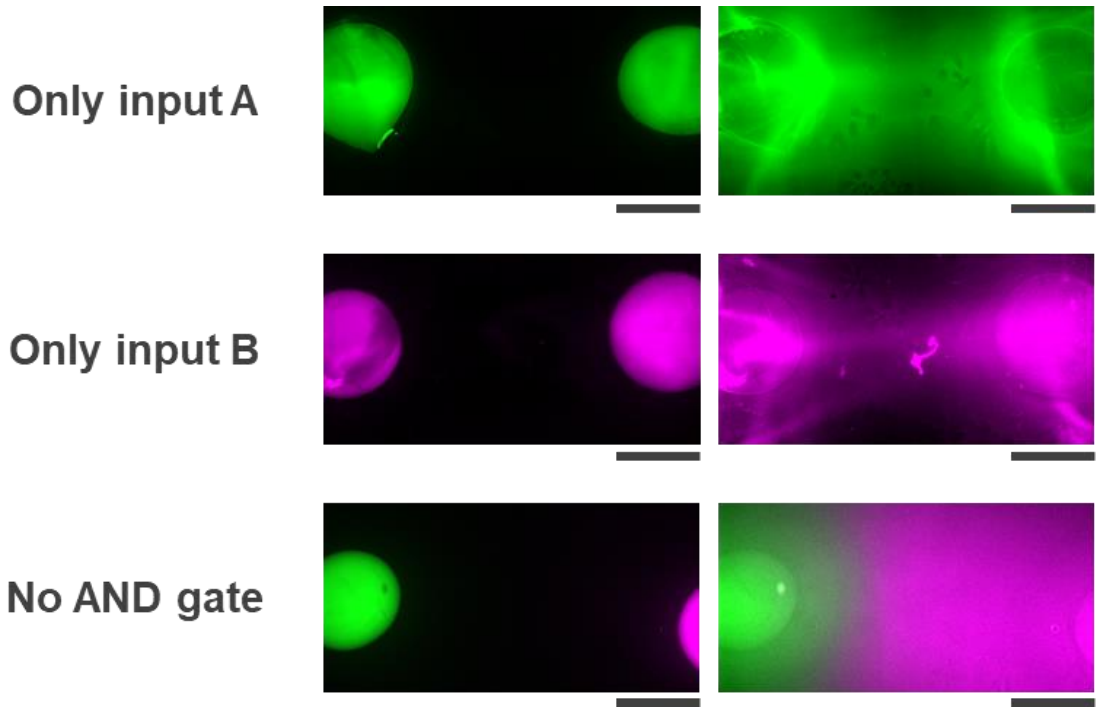

Figure. 2.8 Reaction–diffusion system in hydrogel medium insufficient for bisector pattern formation. The results are superimposed FAM and TAMRA fluorescence images (green and magenta, respectively. (Scale bar: 1 mm).

2.2.4 Reaction–diffusion simulation

The reactions were verified by simulations based on a reaction–diffusion system model. First, the molecules involved in the reaction were classified as follows.

I_A : Input A

I_B : Input B

I_{AB} : Input A–B complex

A_1 : AND gate

A'_1 : AND gate–input A complex (which denatures easily)

A_2 :AND gate–input A–B complex

The reaction and diffusion for each molecules were described by the following partial differential equations and simulated using the reaction–diffusion simulator "Ready" [77] (https://github.com/GollyGang/ready) for solving the partial differential equations numerically.

$$\frac{\partial}{\partial t}[\mathrm{I_A}] = D\Delta[\mathrm{I_A}] - k_\mathrm{h}[\mathrm{I_A}][\mathrm{I_A}] - k_\mathrm{h}[\mathrm{I_A}][\mathrm{A_1}] + k_\mathrm{d}[\mathrm{A'_1}],$$

$$\frac{\partial}{\partial \mathrm{t}}[\mathrm{I_B}] = D\Delta[\mathrm{I_B}] - k_\mathrm{h}[\mathrm{I_A}][\mathrm{I_B}] - \mathrm{k_s}[\mathrm{I_B}][\mathrm{A'_1}],$$

$$\frac{\partial}{\partial t}[\mathrm{I_{AB}}] = D\Delta[\mathrm{I_{AB}}] + k_\mathrm{h}[\mathrm{I_A}][\mathrm{I_B}] + k_\mathrm{s}[\mathrm{I_{AB}}][\mathrm{A_1}],$$

$$\frac{\partial}{\partial t}[\mathrm{A_1}] = D'\Delta[\mathrm{A_1}] - k_\mathrm{h}[\mathrm{I_A}][\mathrm{A_1}] - k_\mathrm{s}[\mathrm{I_{AB}}][\mathrm{A_1}] - k_\mathrm{d}[\mathrm{A_1}],$$

$$\frac{\partial}{\partial t}[\mathrm{A'_1}] = D'\Delta[\mathrm{A'_1}] + k_\mathrm{h}[\mathrm{I_A}][\mathrm{A'_1}] - k_\mathrm{d}[\mathrm{A'_1}] - k_\mathrm{s}[\mathrm{I_B}][\mathrm{A'_1}],$$

$$\frac{\partial}{\partial \mathrm{t}}[\mathrm{A_2}] = D'\Delta[\mathrm{A_2}] + k_\mathrm{s}[\mathrm{I_{AB}}][\mathrm{A_1}] + k_\mathrm{s}[\mathrm{I_B}][\mathrm{A'_1}],$$

[X] is the concentration of the chemical X at the time, D is the diffusion coefficient of DNA in the hydrogel medium, and D' is the diffusion coefficient of anchored DNA. The rate constant k_h, k_sd, and k_d are correspond to hybridization, strand displacement, and denaturation, respectively. The values consistent with the experimental results were obtained by changing the diffusion coefficient and rate constants based on those reported earlier. The reaction–diffusion field was set up in two dimensions (32×64 pixels), and calculations were performed by changing the time t corresponding to seconds (sec) in increments of 0.01. The results were

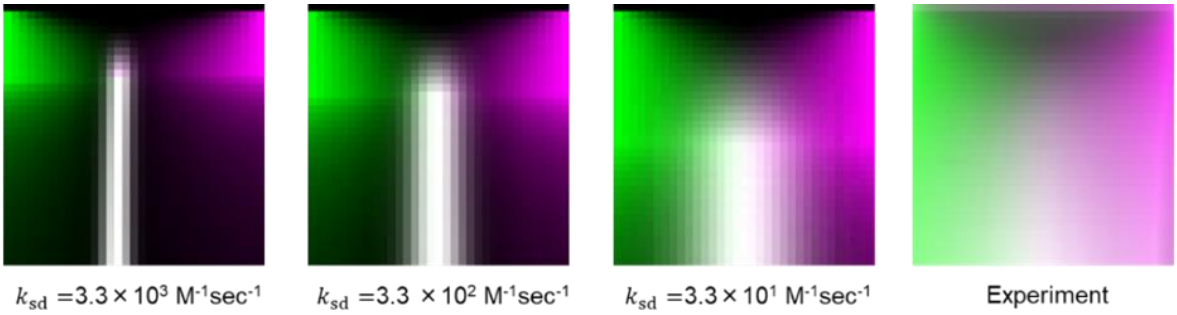

Figure. 2.9 Kymographs of bisector pattern formation in simulation with several rate constants and in experiment. The larger the rate constant of the strand displacement reaction, the thinner the bisector becomes. If the value is too large, the reaction proceeds immediately before A'$_1$ denatures, and the position of the bisector shifts slightly toward the diffusion source of input A.

output every 10 minutes (6000 timesteps), which is the same interval as experimental observation.

First, the D of DNA in hydrogel was set to 70 μm^2/sec based on the DNA diffusion in high-viscosity solvents [76], and D' for anchored DNA was set to 0 μm^2/sec, which is close to the experimental results. However, the rate constant of 3.3 × 10^6 /M/sec, which is close to the value of 3.0 × 10^6 /M/sec shown in [31] that investigated the rate of the strand displacement in buffer, was too large to reproduce the pattern formation process obtained in the experiment. Then, the simulation was conducted at lower rate constant and the results are compared.

To evaluate the effect of the rate constant, a kymograph was used to visualize the spatiotemporal changes in the chemical distribution (Figure 2.9). The leftmost image is the ideal case where most inputs reaching the bisector are immediately coupled to the AND gate. However, the bisector formed in the experiment has a wide and blurred co-localization area possibly due to the low sensitivity of the AND gate. The k_{sd} was decreased, and a result close to the experimental result was obtained at k_{sd}= 3.3 × 10^1 [/M/sec]. This value is five orders of magnitude lower than that reported previously, and it is expected that there are other reasons for the small reaction rate besides the AND gate efficiency.

One possible cause is the difference in reaction field conditions. In particular, the mesh structure of the alginate polymer inhibits molecular diffusion, which reduces the probability of DNA collisions, thus decreasing the reaction rate. There is also a difference in the buffer condition between our system and the reference.

As the result, the pattern formation in the hydrogel can be reproduced by a simulation with D = 70 μm^2/s, D'= 0 μm^2/s, and k_{sd}= 3.3 × 10^1 /M/s. However, if the rate constant is increased, a finer pattern can be obtained. Although the use of a hydrogel reaction–diffusion field is difficult to be improved due to DNA anchoring, the rate constant may be improved by changing the logic circuit.

2.3 Summary

In this chapter, I report a method to construct an artificial reaction–diffusion system in hydrogel by combining a DNA logic gate and anchoring technique. First, I devised a method to create a reaction–diffusion field using alginate gel, and verified the effect of anchoring in the hydrogel to introduce the DNA anchoring technique into it. Furthermore, I employed an AND gate, where the reaction proceeds only when two specific DNA strands (inputs A and B) are presented to form a DNA complex and developed a reaction–diffusion system that forms a bisector pattern. The obtained bisector pattern remained for 10 hours, whereas no pattern formed when the AND gate condition was not satisfied or not anchored. Simulations were also performed using partial differential equations based on the reaction–diffusion model to reproduce the bisector pattern formation. Through these results, a reaction–diffusion system that forms static patterns using DNA, although some issues such as pattern resolution remained.

3. Diffusion modulation for pattern formation

In the reaction–diffusion system described in Chapter 2, if the left and right molecules diffuse at different rates, the position of bisector line appears will change. In other words, the position of the bisector can be set by programming DNA diffusion speed. In this chapter, I report the construction of a system that combines diffusion modulation to program DNA diffusion and evaluate its effect on pattern.

3.1 Diffusion modulation mechanism

I employed diffusion modulation [76], combines DNA anchoring with a reversible reaction that utilizes toehold exchange to tune diffusion coefficient without changing the target DNA sequence or concentration, to program diffusion.

Diffusion modulation involves introducing two types of DNA, trap and competitor, to control net diffusion coefficient of target DNA. The competitor DNA has the same number of bases as the target DNA and binds to the trap, but not stably. The target and competitor bind to the trap, replacing each other in a competing manner. In the hydrogel medium, the target stops diffusing when it binds to the anchored trap and can diffuse again when it is replaced by the competitor. Since the target can also release the competitor from the trap, this process is reversible. The diffusion of the target is not stopped completely but decrease than free diffusion by this mechanism.

The balance of the reversible reaction defines the degree of inhibition for the diffusion. Here, the equilibrium constant is assumed to be 1, the relationship between each chemical concentration can be described as follows:

$$[D][CT]=[C][TD]$$

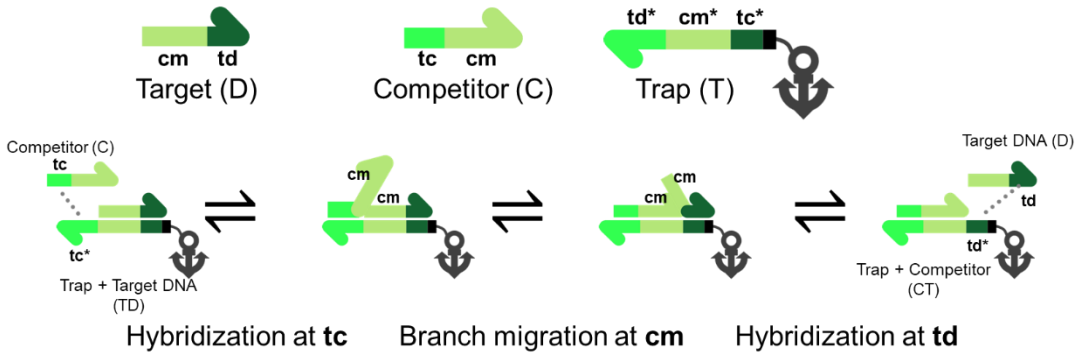

Figure. 3.1 Mechanism of diffusion modulation

where [D], [CT], [C], and [TD] are the concentration of target, competitor–trap complex, competitor, and trap–target complex, respectively. When [D] is constant and the field is homogeneous, this equation can be transformed as follows:

$$[D]_{total}=[D]+[TD]=\left(1+\frac{[C]}{[CT]}\right)[TD]=\frac{[C]+[CT]}{[CT]}[TD]$$

$$[C]_{total}=[C]+[CT]$$

$$[D]_{total}=\frac{[C]_{total}}{[CT]}[TD]$$

$$\frac{[D]_{total}}{[C]_{total}}=\frac{[TD]}{[CT]}$$

Here, the trapped target to trapped competitor ratio is equal to the ratio of the total amount of target to that of competitor. Small TD indicates that the target DNA diffusion is similar to free diffusion.

Sequence design using three reaction domains “cm,” “td,” and “tc” (and their complementary domains “cm*,” “td*,” and “tc*”) realizes this reaction. For the trap, complementary reaction domains are designed from the 5’ end in the order of “td*”, “cm*”, and “tc*” (Figure 3.1). Without the competitor, the target and trap are bound by hybridization at “cm” and “td” domains, while the trap “tc*” domain remains single-stranded (TD). In the presence of the competitor, the binding of “cm” is recombined by branch migration with the reaction domain “tc” as the toehold. Then, only the target “td” domain cannot maintain a stable bond with the trap and

dissociates. This process is reversible, and conversely, the target can bind to the trap while the competitor is dissociated by branch migration with “td” as the toehold.

By applying this mechanism to the system described in Chapter 2, a program of diffusion necessary for designing a sequence orthogonal to the base sequence used for the AND gate can be developed. The sequence design requires that this mechanism and the AND gate work independently and not intermingle with each other.

3.2 Results and discussion

3.2.1 Diffusion modulation with DNA logic gate

First, trap A and competitor A were prepared for input A, and their coexistence with the AND gate reaction was examined by polyacrylamide electrophoresis (Figure 3.2).

When competitor A was added to each solution under the conditions for the AND gate explained in 2.2.1, the fluorescence image was unchanged from those obtained when the DNAs for the AND gate alone was added (Figure 2.8). SYBR Gold staining showed a band at the same position in the lower part of all lanes. The position of the band is almost the same as that of the 15 nt gate strand 2 and indicates the presence of 16 nt competitor A. Thus, competitor A does not affect the AND gate operation.

Interestingly, when the trap is added, the position of the input A band shifts slightly upward. However, other bands are at the same position as in Figure 2.8, indicating that the AND gate functions properly. A new band appears at the bottom of lanes that do not include input A (Lanes 0, 2, 4, 6, 8, 10, 12, and 14). Since this band appears slightly above the gate strand 2, it indicates the presence of 25 nt trap A. This result shows that trap A binds to input A but does not inhibit the AND gate reaction.

These results show that diffusion modulation and AND gate react in an appropriate combination without interfering with each other. Thus, they can be used in the same reaction–diffusion system to program the diffusion in bisector pattern formation.

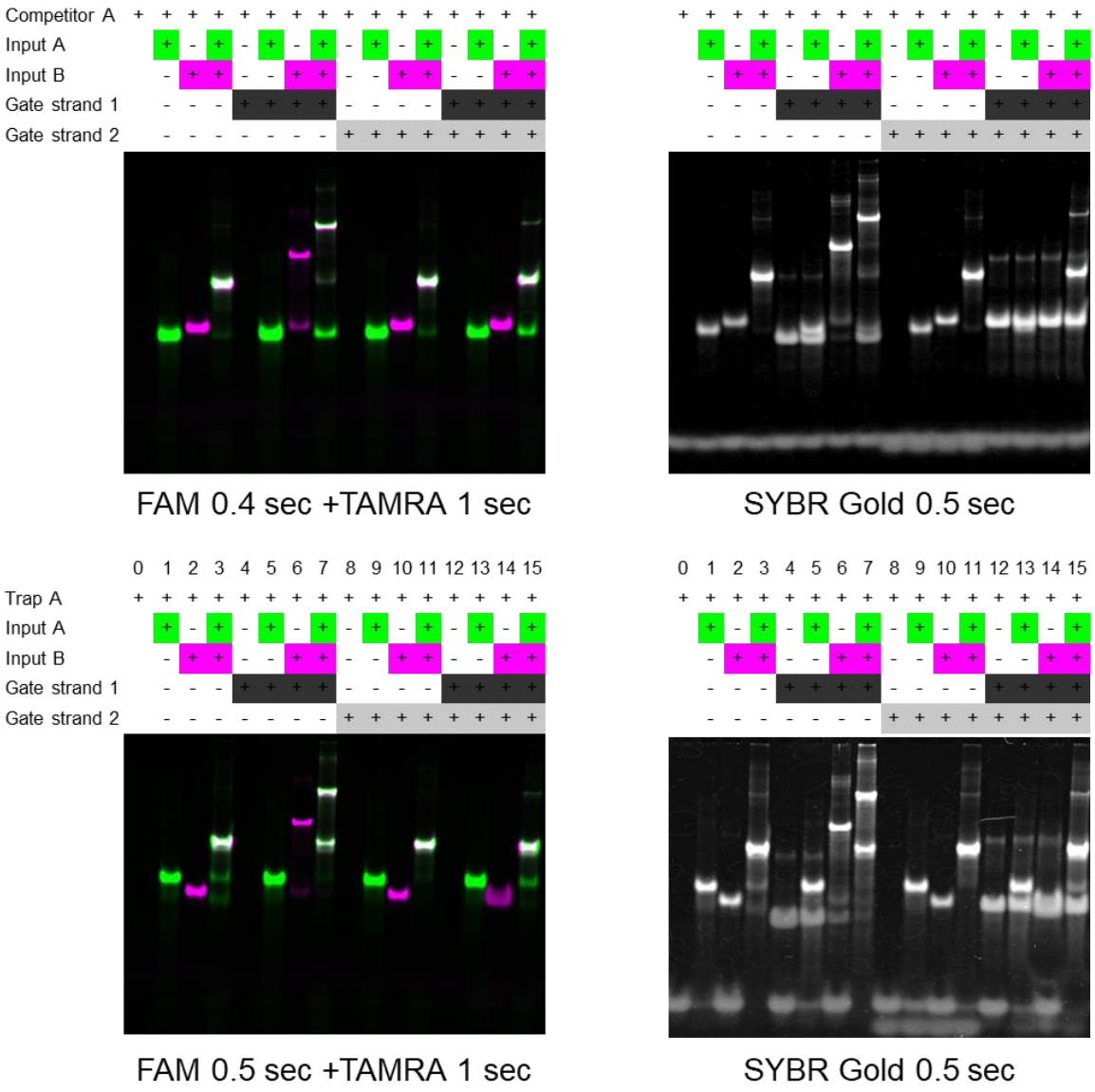

Figure. 3.2 Electrophoresis of competitor (above) and trap (below) for input A with DNA logic gate. DNA was mixed to 1 μM, for 30 min and run on a 10% polyacrylamide gel for 60 min at 100 V. Left: superimposed image of FAM and TAMRA fluorescence (green and magenta, respectively). The bands of the DNA complexes that include both inputs A and B, such as Lane 3, are visualized in white. Right: stained with SYBR Gold for 20 min.

3.2.2 Pattern formation in hydrogel

The trap and competitor are then introduced into the hydrogel containing AND gate to program diffusion in the bisector pattern formation. The process was observed using the same procedure as in Chapter 2.

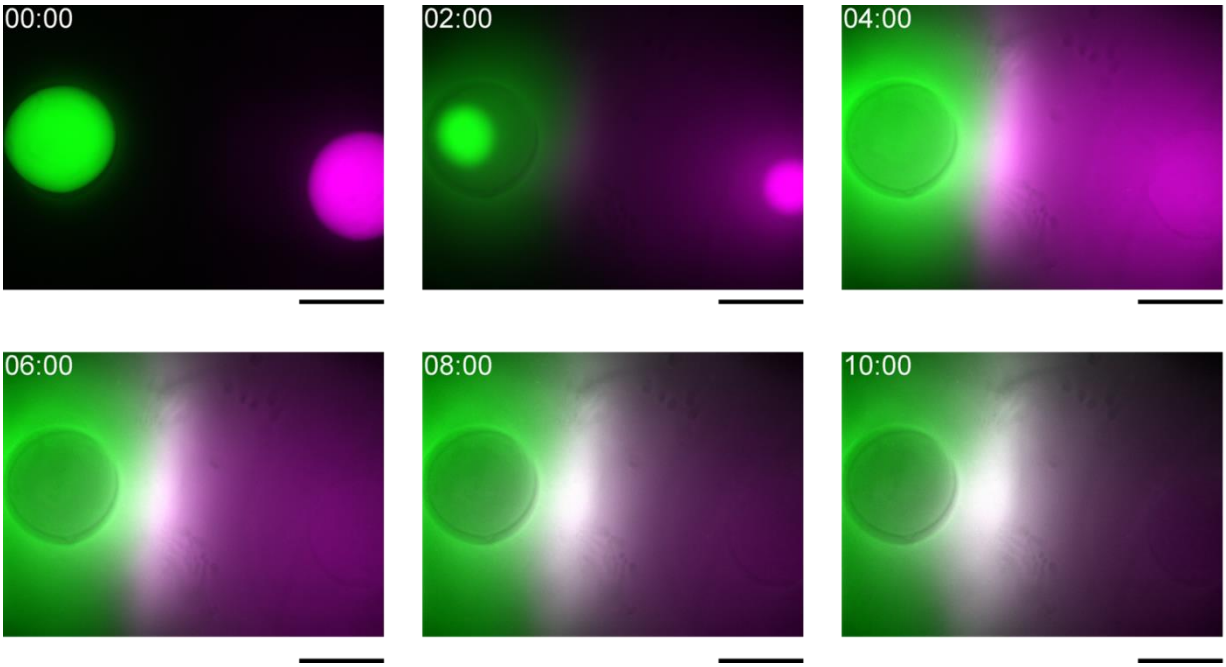

Figure. 3.3 Bisector pattern formation with diffusion modulation. The results are superimposed FAM and TAMRA fluorescence images (green and magenta, respectively) as same as Figure 2.8.

Figure 3.3 shows bisector pattern formation using 2 μM competitor and trap were for 4 hours. The position of the bisector is closer to the source of input A than the position equidistant from the two diffusion sources.

The effect of the competitor concentration was examined by changing the competitor to trap ratio to 1:0, 1:1, and 1:2, while the trap concentration is fixed at 2 μM. The fluorescence images after 6 hours showed that the white bisector did not appear when no competitor was added, while the bisector appeared farther from the diffusion source when the competitor concentration was doubled. This result indicates that the bisector position shifts depending on competitor concentration.

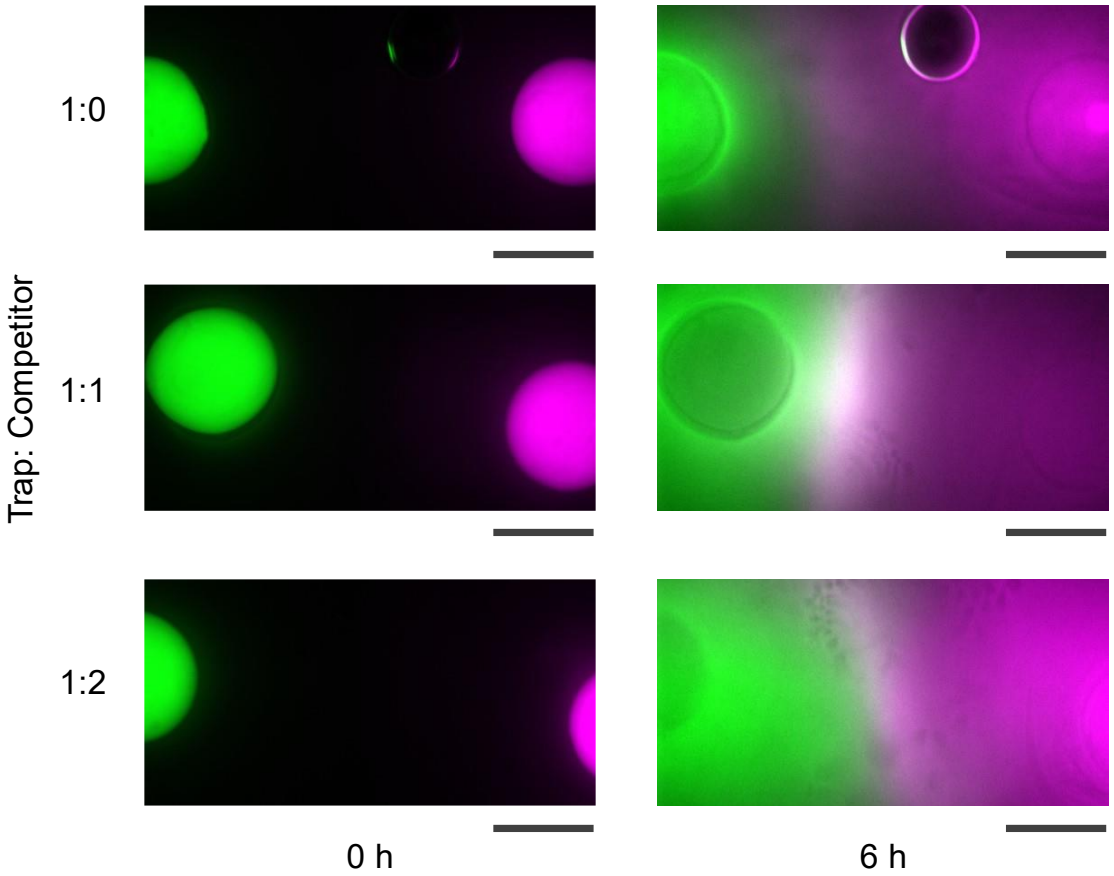

Figure. 3.4 Modulated bisector pattern formations. The amount of competitor to trap was varied from none, to equal, to double. The results are superimposed of FAM and TAMRA fluorescence images assigned to the green and magenta channels, respectively as same as Figure 2.8. (The scale bar is 1 mm).

3.2.3 Reaction–diffusion simulation

To verify the correspondence of the obtained results with the theory of reaction–diffusion systems, the behavior of bisector pattern formation was described by partial differential equations formulated by adding trap A and competitor A terms to the equations described in 2.2.4 and its numerical simulation was compared with the experimental results. The chemical species are labeled as follows:

I_A : Input A

I_B : Input B

I_{AB} : Input A–B complex

A_1 : AND gate

A'_1 : AND gate–input A complex (which denatures easily)

A_2 : AND gate–input A–B complex

C : Competitor A

T : Trap A

T_I : Trap A–input A complex

T_C : Trap A–competitor A complex

$$\frac{\partial}{\partial t}[I_A] = D\Delta[I_A] - k_h[I_A][I_A] - k_h[I_A][A_1] + k_d[A'_1] - k_h[I_A][T] - k_s[I_A][T_C] + k_s[C][T_I],$$

$$\frac{\partial}{\partial t}[I_B] = D\Delta[I_B] - k_h[I_A][I_B] - k_s[I_B][A'_1],$$

$$\frac{\partial}{\partial t}[I_{AB}] = D\Delta[I_{AB}] + k_h[I_A][I_B] + k_s[I_{AB}][A_1],$$

$$\frac{\partial}{\partial t}[A_1] = D'\Delta[A_1] - k_h[I_A][A_1] - k_s[I_{AB}][A_1] - k_d[A_1],$$

$$\frac{\partial}{\partial t}[A'_1] = D'\Delta[A'_1] + k_h[I_A][A'_1] - k_d[A'_1] - k_s[I_B][A'_1],$$

$$\frac{\partial}{\partial t}[A_2] = D'\Delta[A_2] + k_s[I_{AB}][A_1] + k_s[I_B][A'_1],$$

$$\frac{\partial}{\partial t}[C] = D\Delta[C] - k_h[C][T] + k_s[C][T_I],$$

$$\frac{\partial}{\partial t}[T] = D'\Delta[T] - k_h[I_A][T] - k_h[C][T],$$

$$\frac{\partial}{\partial t}[T_I] = D'\Delta[T_I] + k_h[I_A][T] + k_s[I_A][T_C] - k_s[C][T_I],$$

$$\frac{\partial}{\partial t}[T_C] = D'\Delta[T_C] + k_s[I_A][T_C] + k_s[C][T_I] - k_s[I_A][T_C].$$

where the notation and parameters are the same as those described in 2.2.4. These partial differential equations were solved numerically.

The pattern obtained in the simulation (Figure 3.5) shows that the position of the bisector shifts with the competitor concentration corresponding with the experimental result (Figure 3.4). The intensity of the bisector formed when the competitor concentration is equal to the trap concentration is weaker than that formed when the concentration is double. This is because the

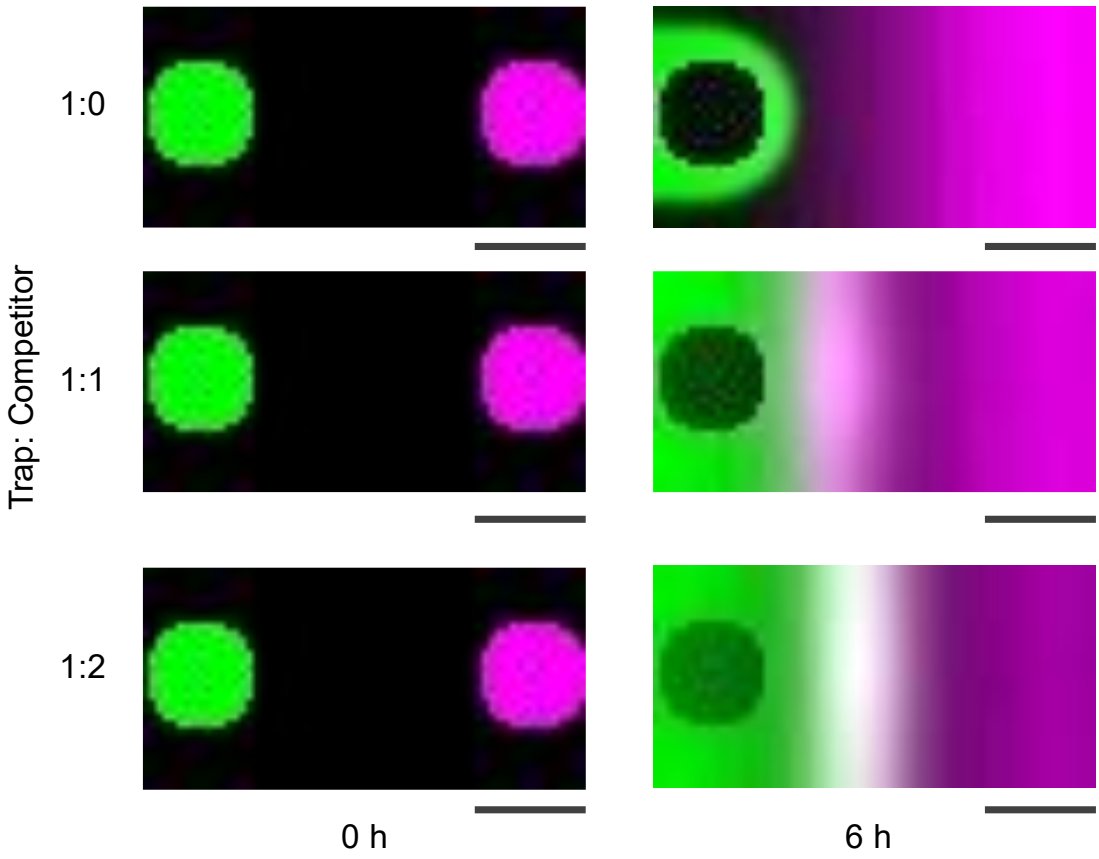

Figure. 3.5 Bisector pattern formation in simulation with several modulation condition. The intensities of green and magenta correspond directly to the concentrations of inputs A and B, respectively. As in Figure 3.4, the simulation was performed with a fixed trap concentration and no, equal, or double competitor concentration. (Scale bar: 1 mm).

diffusion of input B is the same in both cases, and it takes longer for input B to reach the left side, which is farther from the source. The left side has low input B concentration and the reaction is less likely to proceed. Then, slow diffusion increases the time necessary for pattern formation. The time necessary for pattern formation is also affected by the distance between the diffusion sources.

The kymograph shows that increasing the competitor concentration increases the speed at which the green region spreads, and reaches close to the magenta region. This indicates that the pattern also depends on input A diffusion speed. The simulation results agree with the experimental results, suggesting that this pattern formation is caused by the designed interaction.

The graph on the right of Figure 3.6 quantitatively shows that the bisector position varies depending on the conditions. The horizontal axis represents the position of the line drawn from

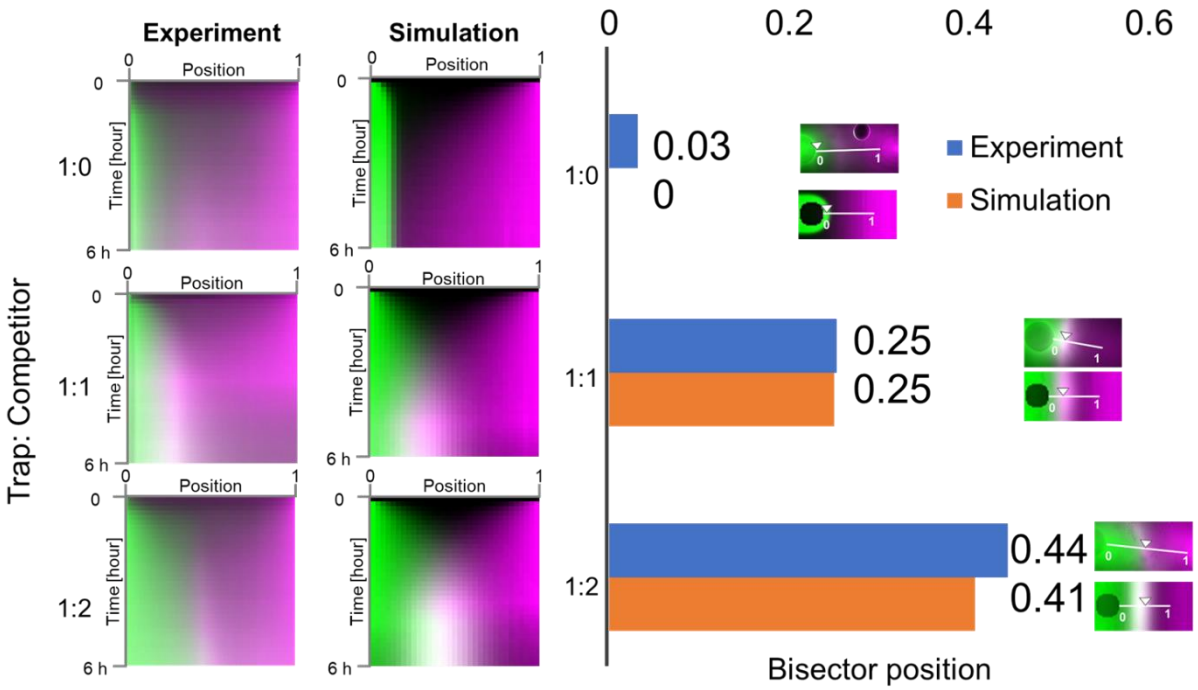

Figure. 3.6 Bisector pattern formation in simulation with several modulation condition. The left kymograph represents the fluorescent distribution between the sources. The right graph shows the position of the peak of bisectors in experiment and simulation.

the source of input A to that of input B. The distances between the sources are normalized to [0, 1]. Without the competitor, the calculated positions are close to zero because input A diffusion stops around the source, which is verified in the simulation. When the competitor concentration is equal to the trap concentration, the bisector forms at 0.25, which is halfway from the midpoint of the sources. In contrast, when the competitor concentration is twice the trap concentration, the bisector appeared at 0.44, indicating that by increasing the competitor, the input behaves more like free diffusion, which also occurs without diffusion modulation.

Interestingly, bisector position also depends on the spacing of the diffusion sources as mentioned previously. The bisector width and the time it appears are affected by the distance between the diffusion sources.

3.2.4 Diffusion modulation for Weighted Volonoi pattern formation

As a demonstration, four sources (two sets of input A and B sources) were used to form two-dimensional Voronoi patterns. When no competitor or trap was used, the system formed a cross pattern at the center of the four diffusion sources. When diffusion modulation was applied to

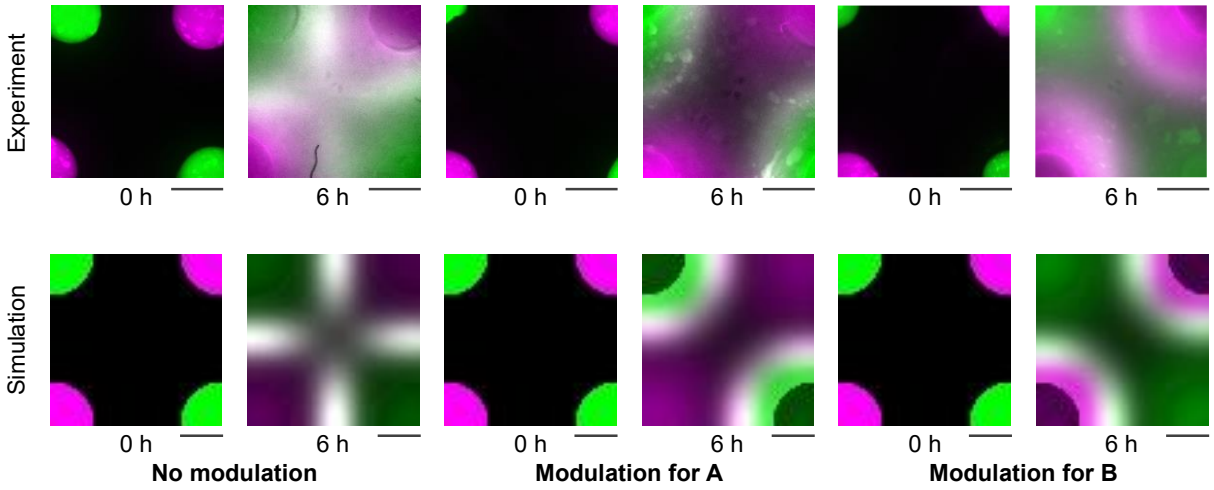

Figure. 3.7 Weighted Voronoi pattern formation in experiment and simulation. The sources of input A are at the upper left and lower right (green) and that of input B are at the upper right and lower left (magenta). (The scale bar is 1 mm).

input A, the cross was broken and two curved lines appeared around the input A sources. Next, an additional trap and competitor are introduced to modulate input B diffusion. Then, two curves appeared around the input B sources. Comparing these patterns, the connectivity of the regions varied for different parameters, indicating that diffusion modulation formed the weighted Voronoi pattern.

3.3 Summary

The reaction–diffusion system reported in Chapter 2 is extended to include diffusion modulation to change DNA diffusion. Tuning input A diffusion also shifted the bisector the positions. Moreover, the degree of the shift can be adjusted by changing the competitor concentration. The various weighted Voronoi pattern formations in two-dimensional space were demonstrated.

The white region indicating the co-localization of inputs A and B was blurred when diffusion modulation was used, particularly in the weighted Voronoi patterns. The problem in the reaction kinetics mentioned in Chapter 2 seems to become more apparent here since the added DNA complicates the reaction and less DNA reaches the reaction site by the suppression of diffusion.

In the next chapter, I will discuss the construction of a reaction–diffusion system that forms sharp patterns.

4. Polymerization approach for high resolution pattern

In Chapters 2 and 3, I have discussed the development of a reaction–diffusion system for various pattern formations by programming both reaction and diffusion. However, issues of bisector pattern resolution (steepness and width) remain to be addressed for forming advanced patterns. In this chapter, I describe a method to develop a reaction–diffusion system that forms high resolution patterns. Two points will be discussed: an experimental method and DNA reaction system design. For the experimental method, I have considered methods that defines the source locations to evaluate the pattern, while reducing factors that can affect the reactions. The reaction system have been redesigned to achieve the behavior in which two molecules interact and stop diffusing with high rate constant, while still shifting the bisector by adjusting diffusion like the method in Chapter 3.

4.1 Experimental method

The type of hydrogel used and setting the initial conditions are particularly important for DNA reaction–diffusion system. The hydrogel used in the experiment reported in the previous chapter was an alginate gel prepared by adding sodium alginate solution to $CaCl_2$ solution. In this method, the alginate polymer congeals immediately, but since the alginate solution is in contact with the solution, the diffusion of molecules is not suppressed. Moreover, the DNA was prepared in the alginate polymer solution, and there was concern that it would diffuse into the $CaCl_2$ solution. In addition, the high calcium ion concentration ions may affect the DNA–DNA interaction.

Agarose and polyacrylamide gels are used in electrophoresis because of their high compatibility with DNA. In this chapter, we have reported the use of polyacrylamide gel, which can be prepared without temperature manipulation and can directly bind to acridite-modified DNA.

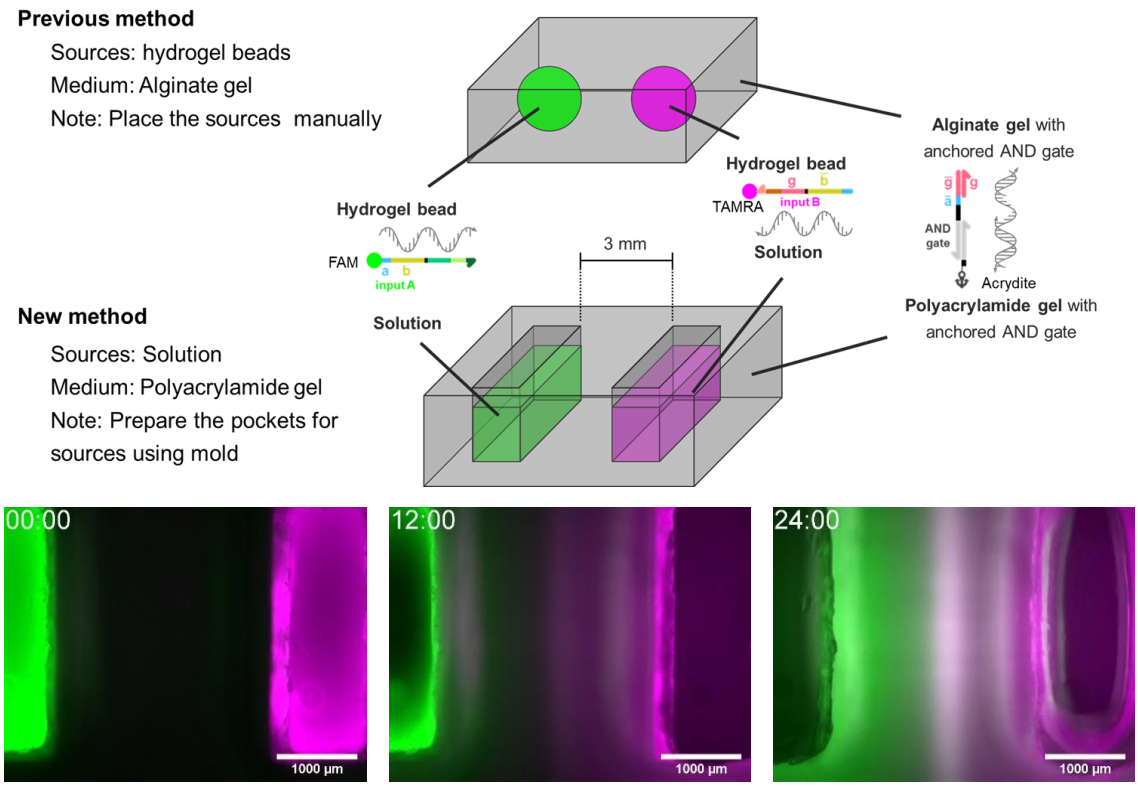

Figure. 4.1 A polyacrylamide-based reaction–diffusion system. The results indicate superimposed FAM and TAMRA fluorescence images (green and magenta, respectively), similar to that reported in Figure 2.8.

When we employ the polyacrylamide gel as the medium, we can determine the source location as follows. A rectangular polyacrylamide gel with two 3mm apart rectangle holes was prepared using a mold (Figure 4.1). The polyacrylamide gel was mixed with the anchor and the AND gate DNA during polymerization to anchor the AND gate. The inputs A and B were in solutions, and pattern formation starts with dropping them into the left and right square holes, respectively.

Using this method, a bisector pattern was observed as in the experiment using alginate gel. Since the distance between the sources was 3 mm, which is farther than in the previous experiments, pattern formation is slow. This result confirms that this experimental method is effective in constructing a DNA reaction–diffusion system.

4.2 Design of DNA reaction for sharp bisector formation

4.2.1 Polymerization approach for bisector pattern formation

To form a bisector pattern, we need a reaction field where the molecules diffuse from the left and right sources and stop diffusing when they react with each other. As reported in the previous chapter, DNA AND gates releases the output DNA when both input DNAs are present. The AND gates need to be homogeneously distributed in the medium for spatiotemporal development, so the amount of DNA required per experiment is large.

The logic gate used, an associative toehold activation, does not form stable bonds with the gate when only one input DNA is present. While this property is required to form bisector patterns, the reaction process become complicated. In addition, pattern resolution implies that the reaction term is not as large as the diffusion term. Thus, this property is an obstacle to obtain sharp pattern.

In this chapter, I propose a method named "polymerization approach." Based on the Einstein–Stokes equation, the molecular size is inversely proportional to the diffusion coefficient. I designed 46nt DNAs (L1 and R1) comprising two 23nt complementary segments, that hybridize alternately, and form a polymer (Figure 4.2). The polymerization process is based on hybridization, faster than complex strand displacement reaction and increases the molecular size of the DNA strands rapidly, thus rapidly decreasing the diffusion coefficient. I placed the L1 and R1 solutions facing each other on the hydrogel medium. The DNAs diffuse into the hydrogel medium, react on the bisector, and immobilize to form a bisector pattern. The DNA logic gate needs five DNAs including an anchoring DNA, whereas this approach requires only two DNA strands. Since the number of DNAs constituting the system is small, it is less likely to cause undesired reactions and develop into parallel and cascaded reactions.

4.2.2 Adjuster DNA for shifting position of bisector

As mentioned in Chapter 3, different DNA diffusion coefficients shift the bisector. The diffusion modulation can adjust the diffusion coefficient of the target according to competitor concentration, but it requires anchoring DNA throughout the medium.

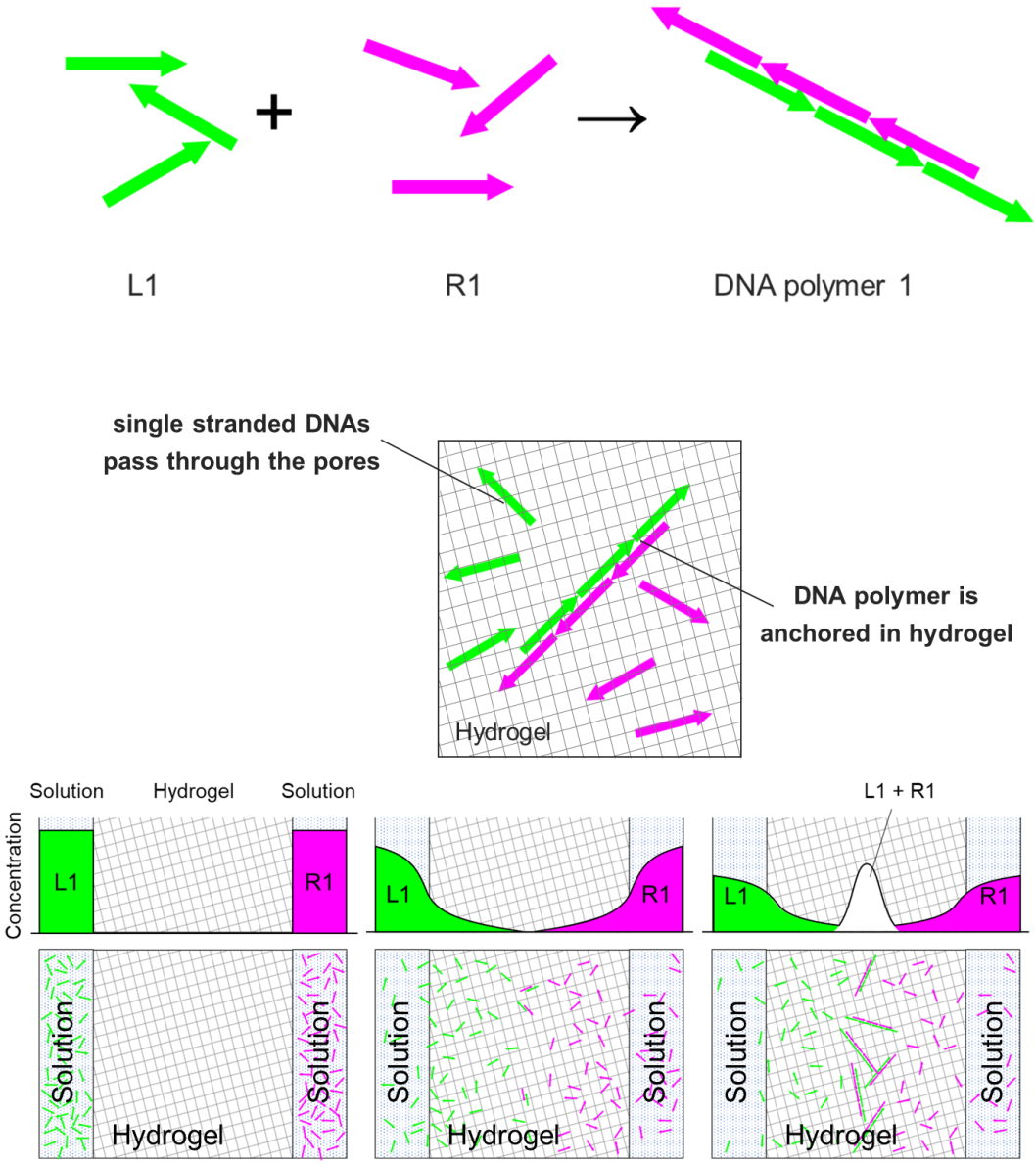

Figure. 4.2 Polymerization approach for bisector pattern formation. L1 and R1 form a polymer (upper). Single-stranded L1 and R1 diffuse in the hydrogel, but the polymer is trapped in the network (middle). When they diffuse from the left and right sides, they react at the midpoint to form the polymer, stop diffusion, immobilize, and form a bisector pattern (lower).

To overcome these difficulties, I introduced adjuster DNA for tuning the diffusion more directly with less DNA. The adjuster binds to target DNA by hybridization and its single-stranded length can tune the molecule size.

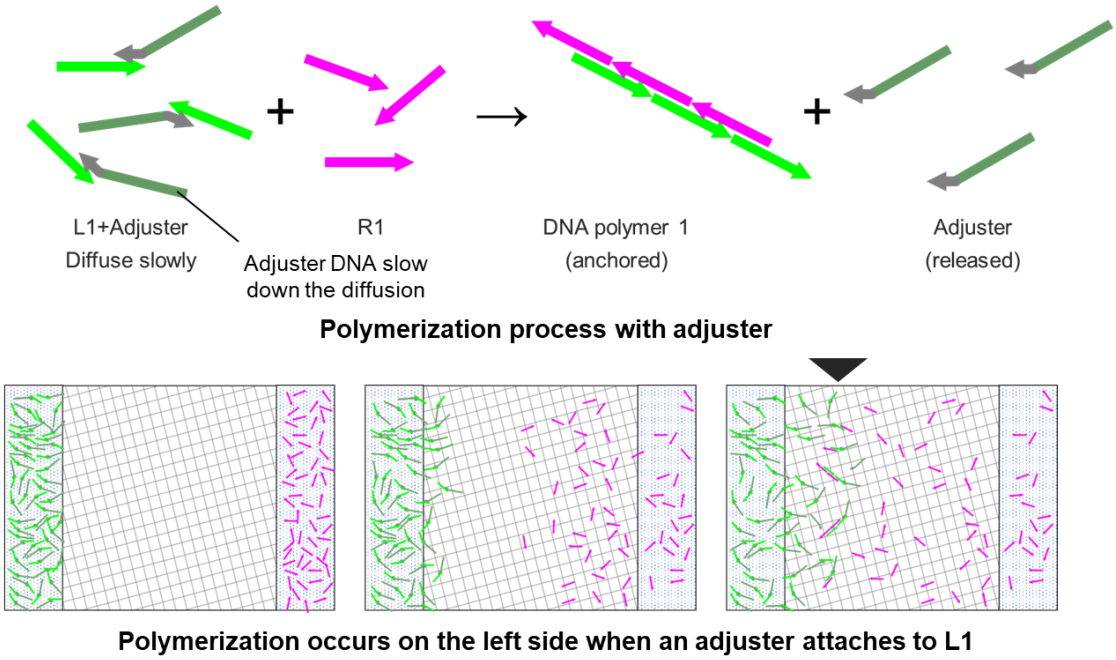

Figure. 4.3 Adjuster for shifting position of bisector. The adjuster increases the molecular size but is released during the polymerization process, thus adjusting the diffusion but not inhibiting the reaction for pattern formation.

I design an adjuster hybridizing with L1 on the 3' end (Figure 4.3). The adjuster slows down L1 diffusion and is released in the polymerization process. Since the adjuster hybridize to a 15 nt segment of the 23 nt domain necessary for polymerization, the reaction with R1 in that domain is a strand displacement reaction mediated by an 8 nt toehold from hybridization. However, the rate of strand displacement reaction mediated by over 6 nt toehold is only about 15% slower than that of hybridization. The other domain for the polymerization on the 5' end is still single-stranded, so the adjuster weakly affects polymerization.

4.3 Results and discussion

4.3.1 DNA polymer diffusion in hydrogel

The behavior of the DNA polymer formed by polymerization, was verified using polyacrylamide gel electrophoresis and fluorescence recovery after photobleaching (FRAP).

The result of the polyacrylamide gel electrophoresis is shown in upper left of Figure 4.4. A band at a higher position in Lane 3 (mixed L1 and R1) indicates the formation of a high

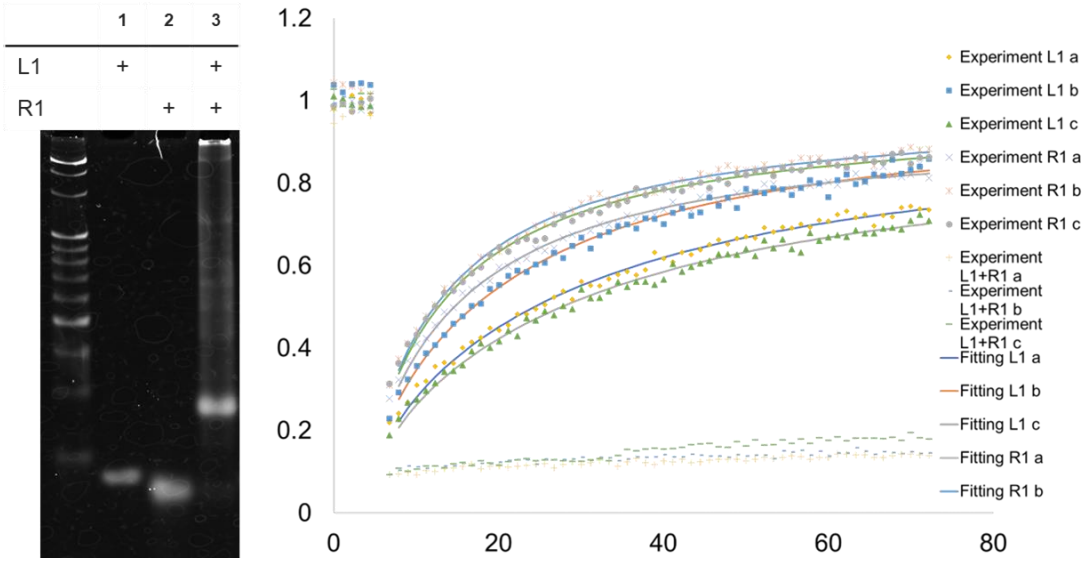

Figure. 4.4 Electrophoresis and fluorescence recovery after photobleaching (FRAP) of the L1 and R1. DNA was mixed to 200 nM and then run on a 10% polyacrylamide gel for 120 min at 50 V and stained with SYBR Gold for 20 min (left). In the FRPA, the intensity of the fluorescent recovery was normalized by reference to that of background and unstimulated areas, and its change over time was plotted (right). Details of the analysis are in A.9.

molecular weight structure by the interaction between L1 and R1. The highest band in the lane appeared slightly above the 500 bp ladder.

The change in diffusion in the hydrogel due to polymerization was quantified by FRAP. Briefly10% polyacrylamide gels were prepared in 10 μL tubes, placed in a silicon chamber, covered with liquid paraffin to prevent evaporation and photo-stimulated using a confocal unit for microscopy.

Fluorescent recovery was measured at three points in the hydrogel in the presence of absence L1 and/or R1. No recovery was observed when L1 and R1 are mixed, indicating that diffusion is suppressed by polymerization. The L1 and R1 diffusion were calculated by fitting (42.3 and 84.0 $\mu m^2/s$ for L1 and R1, respectively). The values suggest that R1 is smaller and has a higher diffusion coefficient than L1; however, the value is about twice as large as that of L1 though they have the same number of bases. Since DNAs with the same length and different sequences have different molecular weights and possible structures, they may have different diffusion coefficients; however, such a large difference may be due to not only the differences in DNA itself, but also environmental factors, such as the medium heterogeneity. Therefore, its reliability should be considered.

4.3.2 Pattern formation in hydrogel medium

I built the rectangular polyacrylamide gel with two rectangular holes 3 mm apart like section 4.1 and added the 4 μM DNA solutions into the holes (Figure 4.5). The L1 and R1 are labeled with FAM and Cy5, respectively, and visualized as green and magenta, respectively. Then, L1 and R1 co-localization was visualized as white superimposed image.

The L1 and R1 were in left and right sources in the initial state and diffused into hydrogel medium. Six hours later, a very weak white bisector appeared and the intensity increased over time. The bisector remained for 24 hours, implying that the DNAs are immobilized on the bisector.

I compared the DNA type and amount used to form a single bisector, the width of the bisector formed, and the average normalized fluorescence intensity. Compared with the DNA logic circuit, which requires five anchor DNA in addition to two inputs and two AND gates, the polymerization approach requires only two DNA for polymerization. The amount of DNA used in one experiment is 80 pmol for the two types of DNA, 4 μL each of 10 μM DNA added as input. The polymerization approach requires much less DNA than the DNA logic gate. In this experiment, 2 μM DNA for the AND gate and 4 μM anchor DNA were added to 160 μL polyacrylamide gel. Thus 1280 pmol DNA should be present in the hydrogel. The polymerization approach reduces the amount of DNA required for a bisector formation by 94%.

Next, I examined the fluorescence intensity distribution among the sources at 24 hours and normalized them to [0:1]. The degree of co-localization was then quantified by calculating the synergistic mean normalized fluorescence intensity for each combination of inputs A and B, L1, and R1.

Bisector width is defined as the width around the bisector at 0.5 intensity, which was approximately one-fourth of the value obtained by the DNA logic circuit.

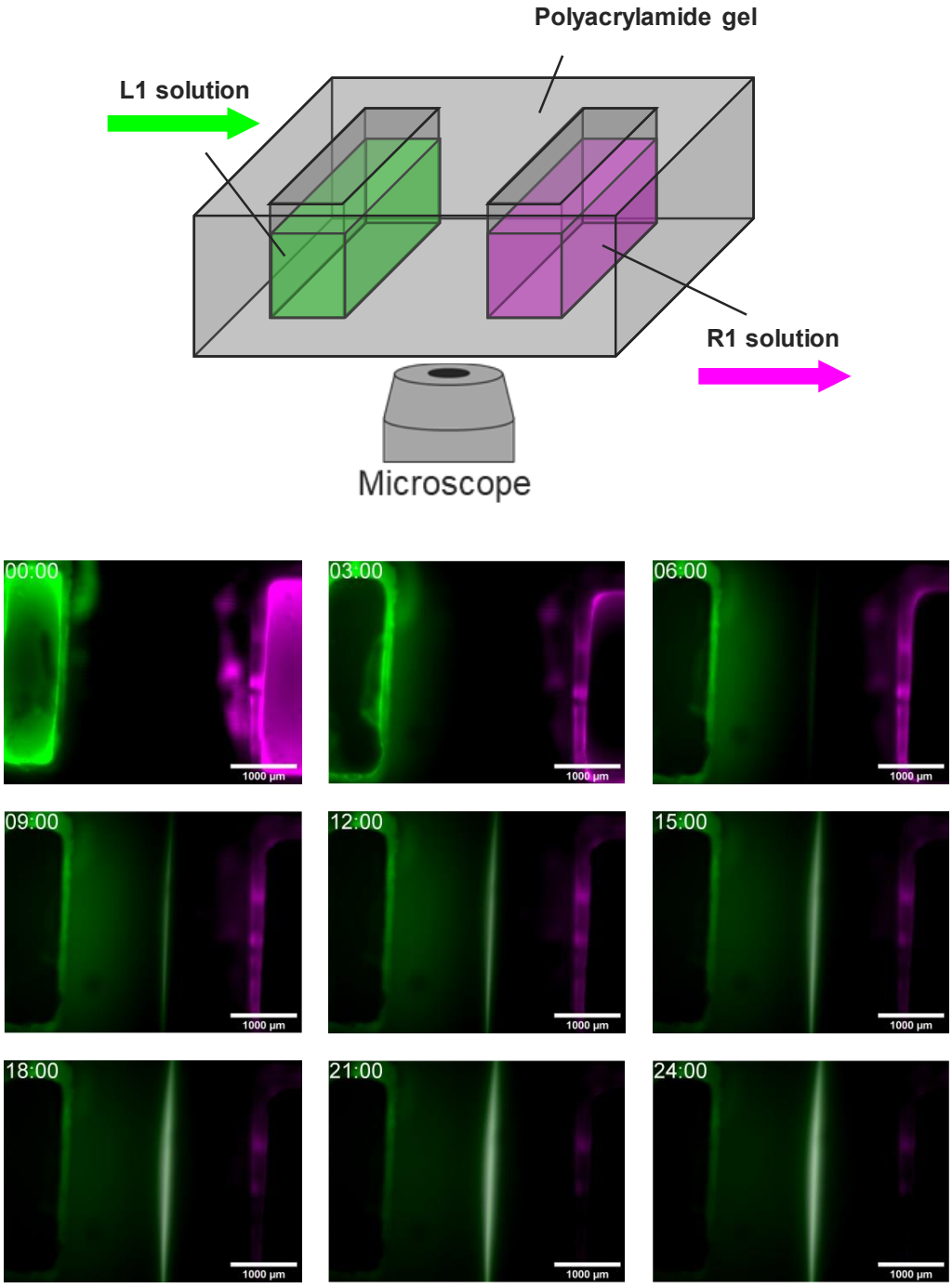

Figure. 4.5 Bisector pattern formation using polymerization approach. The reaction–diffusion system was set up as shown above. The results indicate superimposed FAM and Cy5 fluorescence images (green and magenta, respectively). The area of L1 and R1 colocalization is visualized in white.

The average normalized intensity obtained by the logic circuit approach is approximately one-fourth the value obtained by the polymerization approach. This value corresponds to the size of the area where both types of fluorescence are at the same level. In particular, the small value indicates that the diffusion of DNA is immediately suppressed on the bisector and

Table. 4.1 Quantitative comparison of the two methods.

	Logic gate	Polymerization approach
DNA species	5	2
Amount of DNA	1360 pmol	80 pmol
Width of the bisector	738 μm	181 μm
Intensity average	0.48	0.11

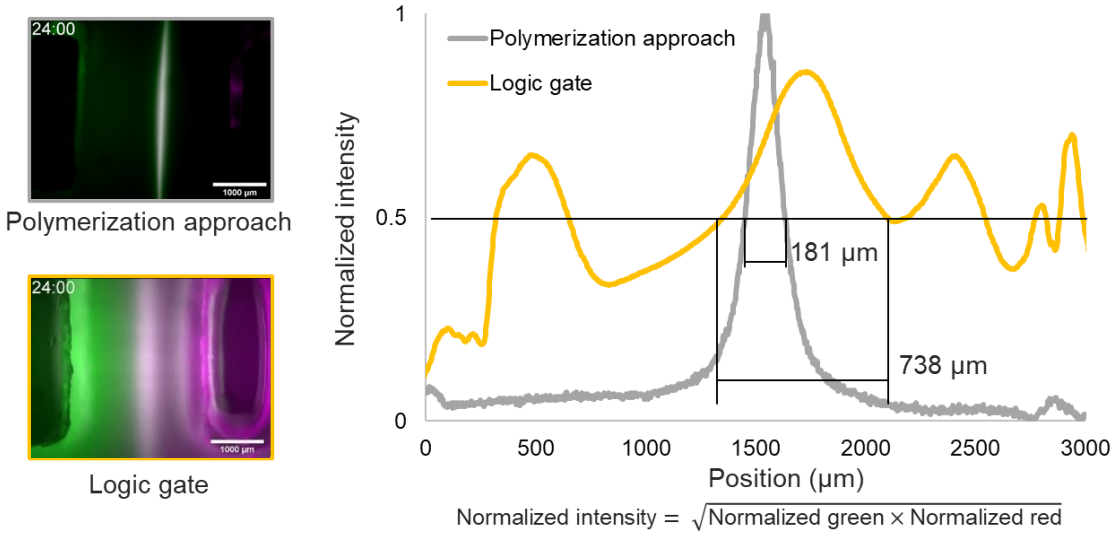

Figure. 4.6 Comparison of bisector patterns between the logic gate and the polymerization approach. The plotted intensity is a geometrical mean of the intensity of inputs A and B or L1 and R1.

localized on the bisector. Overall, the results suggest that the polymerization approach can rapidly form a sharp bisector pattern with less DNA by suppressing strong DNA diffusion.

4.3.3 Bisector pattern with adjusters

Before conducting pattern formation experiments, the adjuster performance was evaluated by polyacrylamide gel electrophoresis. Lanes 1, 2, and 3 show the L1, R1, and the polymer, respectively, while Lanes 4, 5, and 6 show the adjuster A0, A46, and A92, respectively. The bands in Lanes 7, 8, and 9, which has L1 and each adjuster, respectively, appear above the band

	1	2	3	4	5	6	7	8	9	10	11	12
L1	+		+				+	+	+	+	+	+
R1		+	+							+	+	+
A0				+			+			+		
A46					+			+			+	
A92						+			+			+

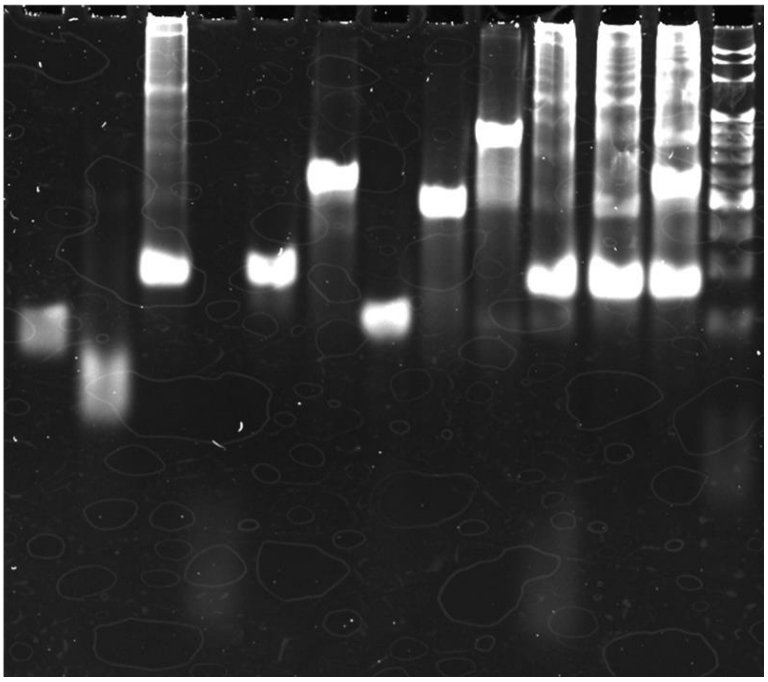

Figure. 4.7 Electrophoresis of anchor DNA. DNA was mixed to 200 nM and then run on a 10% polyacrylamide gel for 120 min at 50 V and stained with SYBR Gold for 20 min.

indicating L1. In the Lanes, band shift increases with the adjuster length, suggesting that binding L1 to the adjuster increased the molecular size and reduced its mobility. However, the bands did not shift after adding R1 to the adjusters (Lanes 10, 11, and 12). The result shows that binding to the adjusters does not inhibit L1 and R1 polymerization.

Then, I used the adjusters to shift the bisector. I prepared four reaction–diffusion systems for bisector pattern formation: without adjuster DNA, with A0, with A46, and with A92. Each bisector formed at the shifted position between the sources 24 hours later. The plot of the geometric means of the fluorescent intensity representing the bisector shape shows that the distance between the left L1 source and the peaks without adjusters, A0, A46, and A92 were $(1.65\pm0.03)\times10^3$, $(1.27\pm0.07)\times10^3$, $(1.05\pm0.05)\times10^3$, and $(0.98\pm0.02)\times10^3$ μm, respectively. The results mean that the long adjuster shifts the peak to the left.

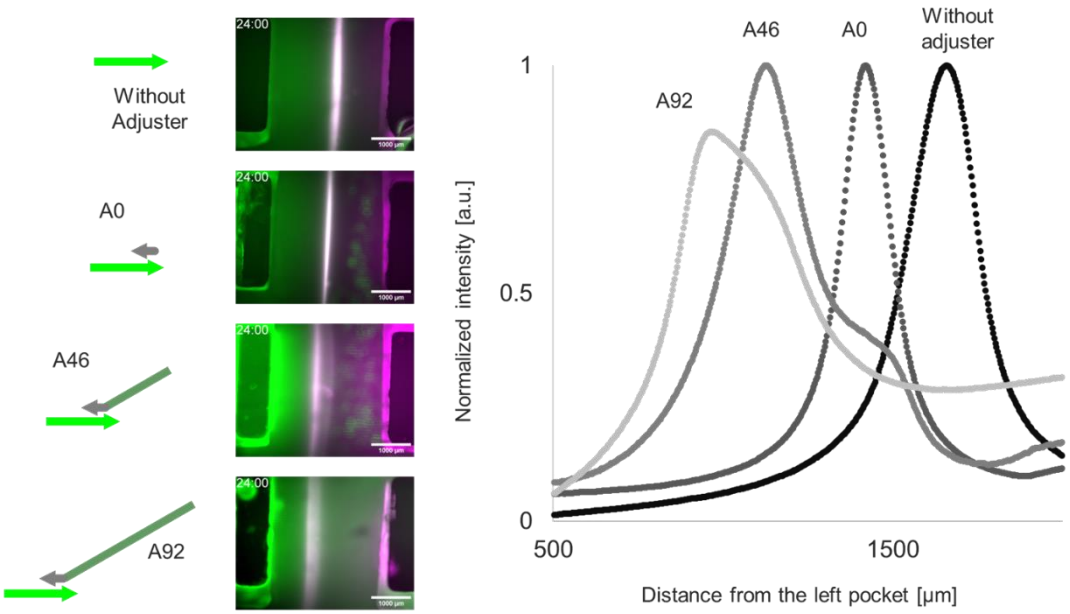

Figure. 4.8 Bisector patterns with A0, A46 or A92. The images are superimposed FAM and Cy5 fluorescence images (green and magenta, respectively), same as that in Figure 4.5. Based on the images, the geometric mean of the fluorescent intensity representing L1 and R1 was calculated to compare the peak position.

4.4 Reaction–diffusion simulation

4.4.1 Polymerization reaction model

A numerical simulation based on a reaction–diffusion system is a powerful tool for the design. Describing the partial differential equation representing the whole process is difficult because polymerization occurs unlimitedly, so that the intermediate products are also unlimited. I modeled the reaction by categorizing the reactivity and the number of polymer strands and limiting the maximum polymer size. In Figure 4.9, the polymers are classified into three types: a linear polymer with an L1 at the left end (α), an R1 at the left end (β), and a complex with no single-stranded part (γ). The subscripts represent the number of strands (i.e., α_m means a polymer that consists of m strands and is classified into α). Based on the type and the number of the strands (subscript number of α, β, or γ), the reactivity of the polymer can be categorized into five: α_{2n-1} reacts with β_{2n-1}, α_{2n}, and β_{2n}, to produce $\alpha_{2(n-1)}$ or $\beta_{2(n-1)}$, $\alpha_{2(2n)-1}$, and $\beta_{2(2n)-1}$, respectively. β_{2n-1} reacts with α_{2n-1}, α_{2n}, and β_{2n}, to produce $\alpha_{2(n-1)}$ or $\beta_{2(n-1)}$,

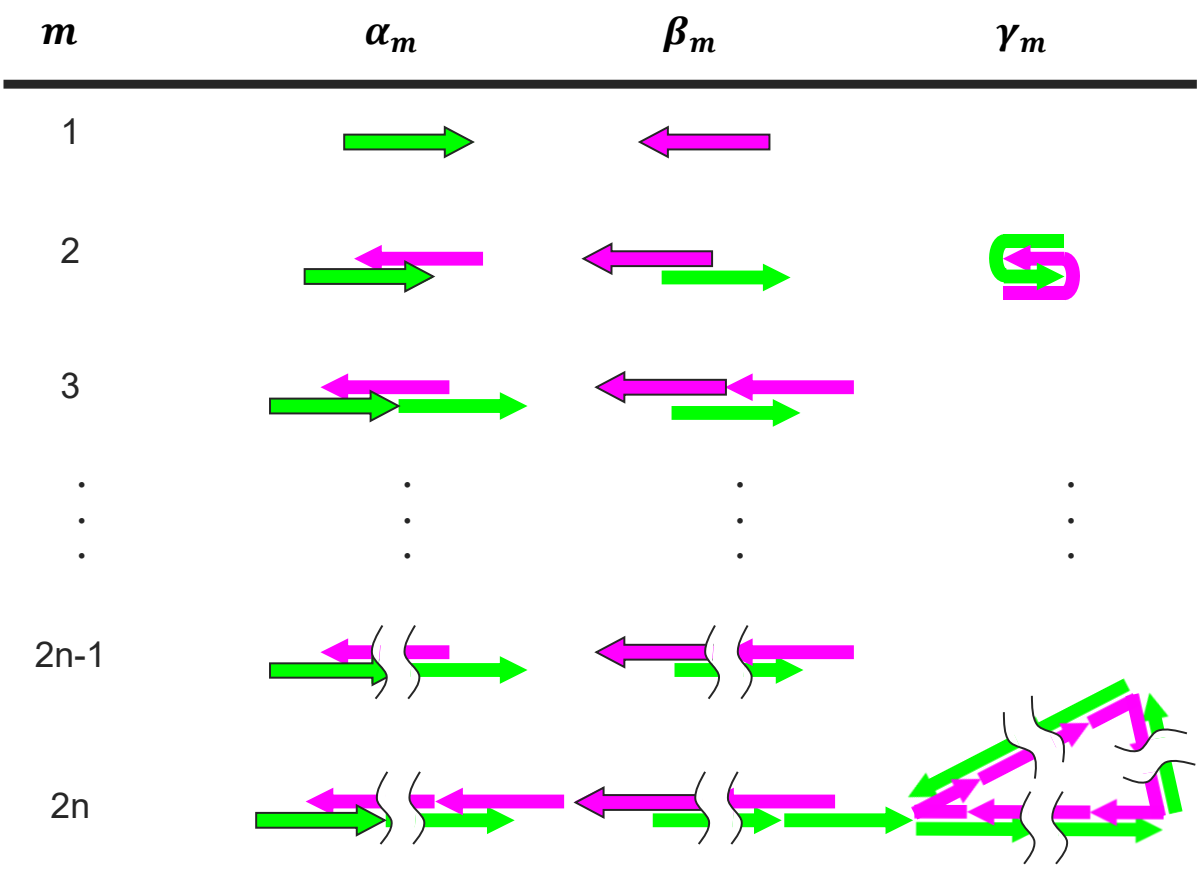

Figure. 4.9 Classification of the polymers. The reactions of the polymerization process are covered by summarizing the reaction relationships for five types of molecules when classified by the arrangement of the strands and the number of DNA.

$\beta_{2(2n)-1}$, and $\alpha_{2(2n)-1}$, respectively. α_{2n} reacts with α_{2n-1}, β_{2n-1}, and α_{2n}, to produce $\alpha_{2(2n)-1}$, $\beta_{2(2n)-1}$, and $\alpha_{2(2n)}$, respectively. β_{2n} reacts with α_{2n-1}, β_{2n-1}, and β_{2n}, to produce $\alpha_{2(2n)-1}$, $\beta_{2(2n)-1}$, and $\beta_{2(2n)}$, respectively. γ_{2n} is a circular structure produced by the intramolecular reaction of α_{2n} or β_{2n} and does not react with anything (Figure 4.10).

When I set the maximum number of DNA in a polymer to *N*, the reaction–diffusion system can be described as partial differential equations as follows:

$$\frac{\partial}{\partial t}[\alpha_{2n-1}] = D_{2n-1}\Delta[\alpha_{2n-1}] + \sum_{i\le n}\sum_{j\le n-i}(k_h[\alpha_{2i-1}][\alpha_{2j}] + k_h[\alpha_{2i-1}][\beta_{2j}]) - \sum_{2i\le N-2n}(k_h[\alpha_{2n-1}][\alpha_{2i}] + k_h[\alpha_{2n-1}][\beta_{2i}] + k_h[\alpha_{2n-1}][\beta_{2i-1}] + k_h[\beta_{2i-1}][\alpha_{2n-1}])$$

$$\frac{\partial}{\partial t}[\beta_{2n-1}] = D_{2n-1}\Delta[\beta_{2n-1}] + \sum_{i\le n}\sum_{j\le n-i}(k_h[\beta_{2i-1}][\alpha_{2j}] + k_h[\beta_{2i-1}][\beta_{2j}]) - \sum_{2i\le N-2n}(k_h[\beta_{2n-1}][\alpha_{2i}] + k_h[\beta_{2n-1}][\beta_{2i}] + k_h[\alpha_{2i-1}][\beta_{2n-1}] + k_h[\beta_{2n-1}][\alpha_{2i-1}])$$

$$\frac{\partial}{\partial t}[\alpha_{2n}] = D_{2n}\Delta[\alpha_{2n}] + \sum_{i\le n}\sum_{j\le n-i}(k_h[\alpha_{2i}][\alpha_{2j}] + k_h[\alpha_{2j}][\alpha_{2i}] + k_h[\alpha_{2n-1}][\beta_{2i-1}]) - \sum_{2i\le N-2n}(k_h[\alpha_{2n}][\alpha_{2i}] + k_h[\alpha_{2i}][\alpha_{2n}] + k_h[\alpha_{2i-1}][\alpha_{2n}] + k_h[\alpha_{2n}][\beta_{2i-1}]) - k_c[\alpha_{2n}]$$

$$\frac{\partial}{\partial t}[\beta_{2n}] = D_{2n}\Delta[\beta_{2n}] + \sum_{i\le n}\sum_{j\le n-i}(k_h[\beta_{2i}][\beta_{2j}] + k_h[\beta_{2j}][\beta_{2i}] + k_h[\alpha_{2n-1}][\beta_{2i-1}]) - \sum_{2i\le N-2n}(k_h[\beta_{2n}][\beta_{2i}] + k_h[\beta_{2i}][\beta_{2n}] + k_h[\beta_{2n}][\alpha_{2i-1}] + k_h[\beta_{2n}][\beta_{2i-1}]) - k_c[\beta_{2n}]$$

$$\frac{\partial}{\partial t}[\gamma_{2n}] = D_{2n}\Delta[\beta_{2n}] + k_c[\alpha_{2n}] + k_c[\beta_{2n}]$$

where k_h and k_c represent the rate constants of intermolecular and intramolecular hybridization. D_m is the diffusion coefficient of polymers consisting of m strands and calculated as follows.

$$D_m = \frac{D_1}{n}(1 \le m < N)$$

$$D_N = 0$$

Here, m is in the range of [1, *N*]. Since the polymerization proceeds unlimitedly, *N* was used as the maximum number of strands to limit the number of chemical species in the simulation. Considering the electrophoresis results (Figure 4.4), *N*=16 was used in the following simulation.

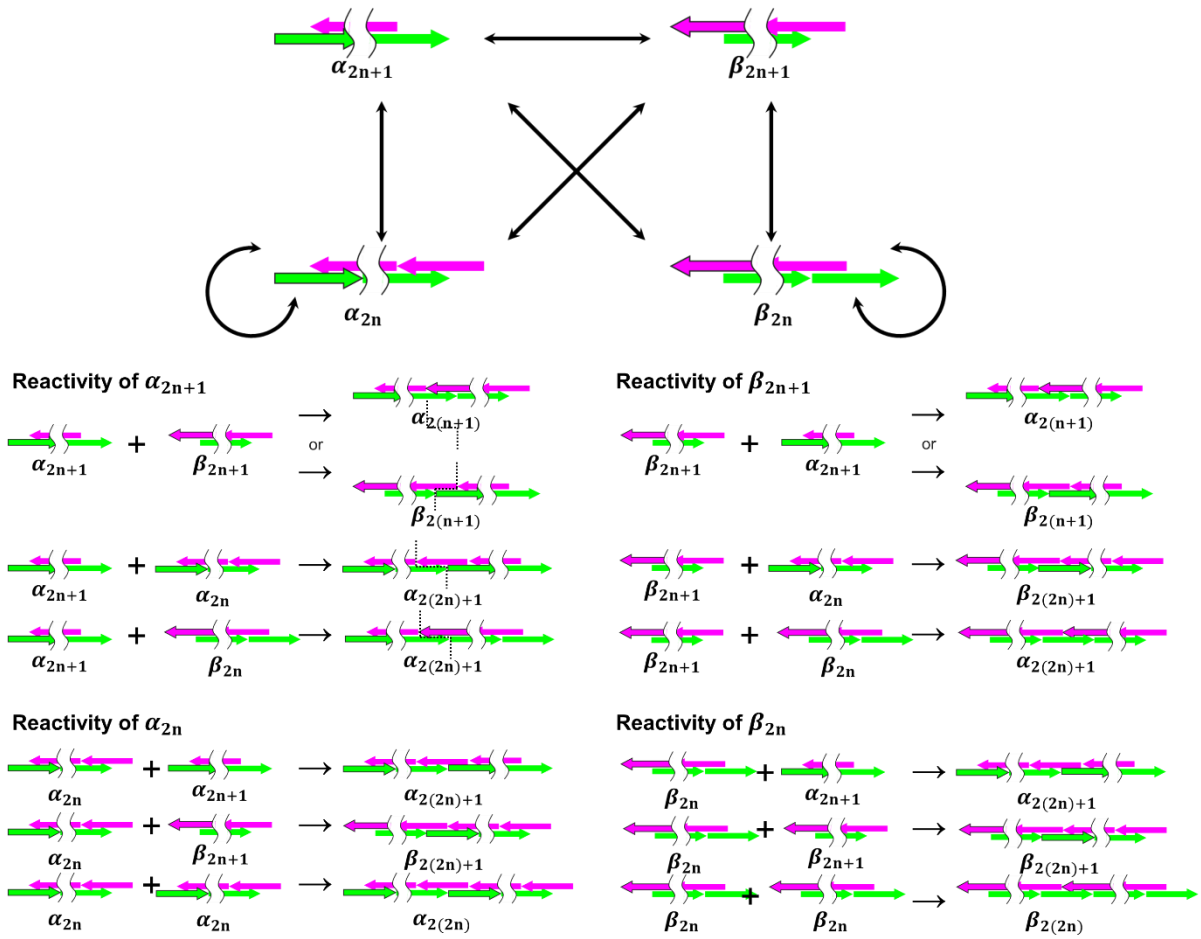

Figure 4.10 Reaction relationships of four types of polymers. In the schematics, γ, which has no reaction domain, is omitted.

D_1(the diffusion coefficient of single-stranded DNA), k_h, and k_c values were decided based on experimental results. Moreover, the D_1 value obtained by FRAP in 4.3.1 was large to reproduce the pattern formation. Therefore, I set lower D_1 values according to the obtained L1 diffusion coefficient. The values are summarized in Table 4.2. The simulation was compared with experimental results in two points: bisector formation process and shape after 24 hours. I evaluated the results for each condition by calculating error E as follows

$$E = \sum \left(I_{\text{experiment}}(t) - I_{\text{simulation}}(t) \right)^2,$$

where $I_{\text{experiment}}(t)$ and $I_{\text{simulation}}(t)$ represent the bisector intensities obtained as the geometric means of L1 and R1 intensities.

Table 4.2 Parameter conditions for simulation

Condition #	D_1 [μm²/sec]	k_h [/M/s]	k_c [/s]	Error value
1	10	3.5×10^{3}	1.0×10^{-3}	19.9
2	10	3.5×10^{3}	2.0×10^{-3}	21.5
3	10	3.5×10^{3}	3.0×10^{-3}	22.1
4	10	3.5×10^{4}	1.0×10^{-3}	4.24
5	10	3.5×10^{4}	2.0×10^{-3}	7.62
6	10	3.5×10^{4}	3.0×10^{-3}	11.0
7	10	3.5×10^{5}	1.0×10^{-3}	74.9
8	10	3.5×10^{5}	2.0×10^{-3}	52.1
9	10	3.5×10^{5}	3.0×10^{-3}	36.1
10	20	3.5×10^{3}	1.0×10^{-3}	10.4
11	20	3.5×10^{3}	2.0×10^{-3}	14.5
12	20	3.5×10^{3}	3.0×10^{-3}	16.0
13	20	3.5×10^{4}	1.0×10^{-3}	20.4
14	20	3.5×10^{4}	2.0×10^{-3}	3.69
15	20	3.5×10^{4}	3.0×10^{-3}	0.28
16	20	3.5×10^{5}	1.0×10^{-3}	576
17	20	3.5×10^{5}	2.0×10^{-3}	457
18	20	3.5×10^{5}	3.0×10^{-3}	367
19	40	3.5×10^{3}	1.0×10^{-3}	5.89
20	40	3.5×10^{3}	2.0×10^{-3}	11.5
21	40	3.5×10^{3}	3.0×10^{-3}	13.8
22	40	3.5×10^{4}	1.0×10^{-3}	76.9
23	40	3.5×10^{4}	2.0×10^{-3}	28.0
24	40	3.5×10^{4}	3.0×10^{-3}	9.20
25	40	3.5×10^{5}	1.0×10^{-3}	1302
26	40	3.5×10^{5}	2.0×10^{-3}	1079
27	40	3.5×10^{5}	3.0×10^{-3}	897

For condition #15, which agreed best with the experimental result, the obtained kymograph and the graphs showing pattern growth and shape over 24 hours are shown in Figure 4.11. The difference in the time when the bisector intensity reached 0.5 was less than 1 hour. The half-widths of the bisectors were 1.8 $\times10^{2}$ and 1.4 $\times10^{2}$ μm in the experiment and simulation, respectively. Due to the resolution of the simulation, the difference was less than 2 pixels.

The graphs of other conditions (Figure 4.12 and 4.13) suggest that each of three parameters has a characteristic effect on the pattern formation process. When D_1 (monomer diffusion

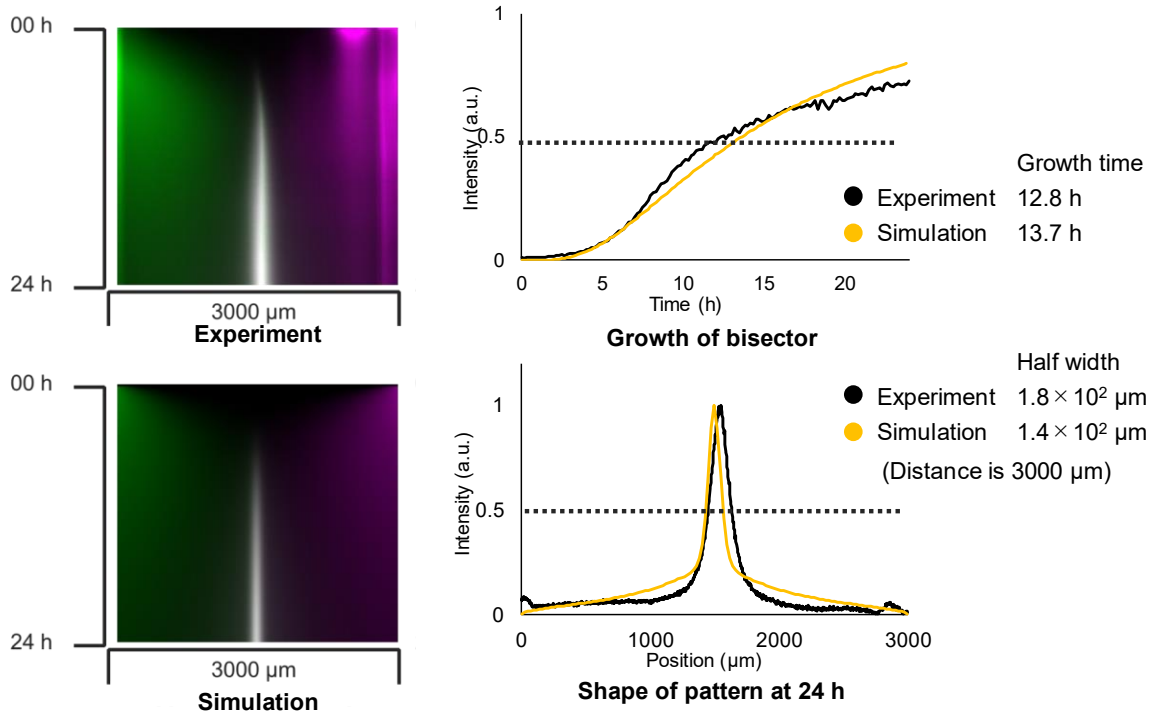

Figure 4.11 Simulated pattern formation with condition #15. Left: kymographs of experimental and simulated pattern formation. Right: the growth and shape of the bisector pattern.

coefficient) is large, the bisector intensity and half-width increases rapidly. This indicates that when the diffusion coefficient is large, L1 and R1 meet quickly to form the bisector, but the line formed is blurred due to dissipation before sufficient polymerization. When k_h (the rate constant of hybridization) is high, the rise of bisector intensity is rapid and the half-width is small because the time between the start of polymerization and growth is short, and the DNA stays in place before being dissipated by diffusion. When k_c (the rate constant of cyclization) is large, the bisector intensity rises slowly and the half-width is large. This is the rate of intramolecular reaction at which α_{2n} and β_{2n} become γ_{2n}. Since γ_{2n} does not polymerize further, a large rate constant means that the polymerization is less likely to proceed. As $\gamma_m (m < N)$, where $D_m > 0$, increase, the bisector pattern becomes blurred.

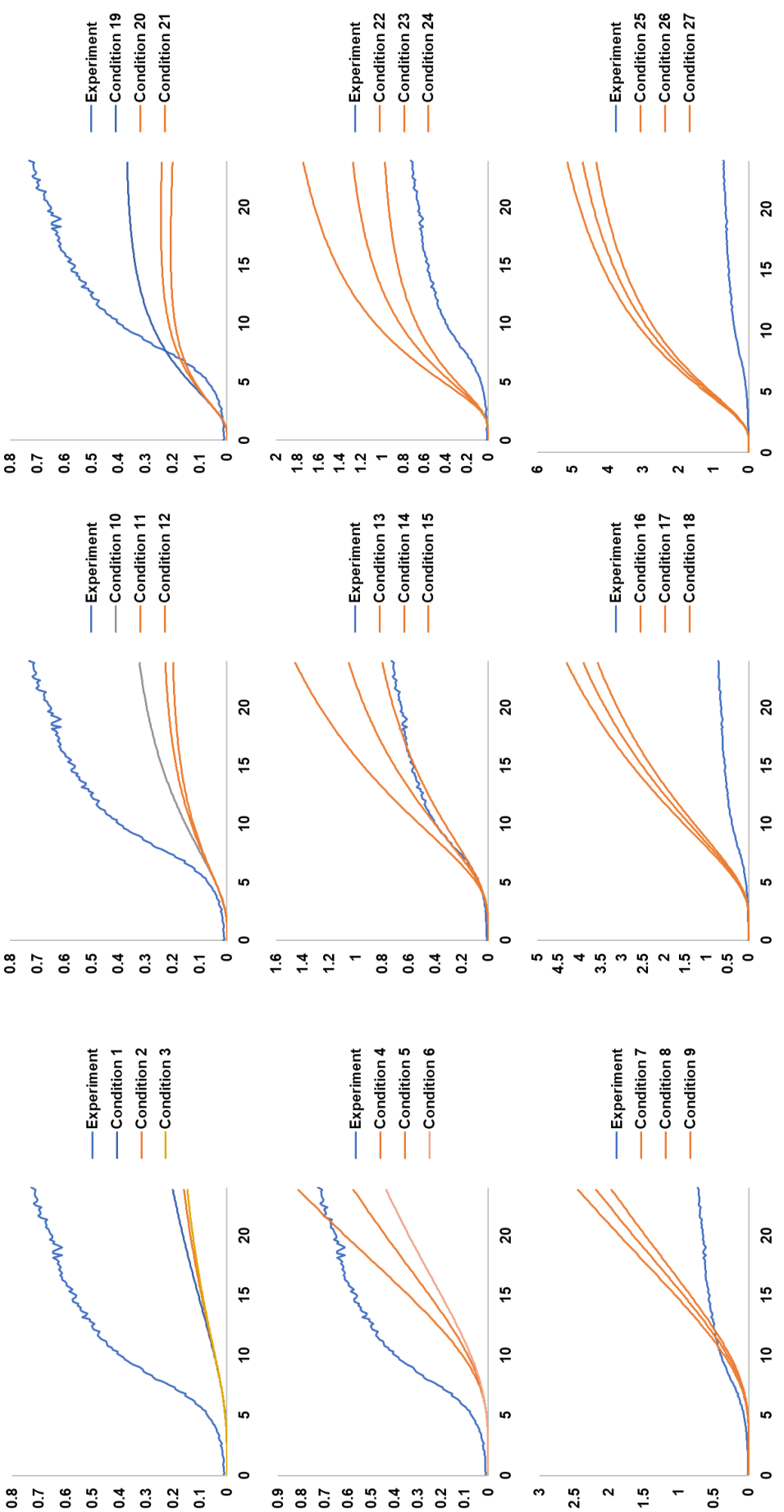

Figure 4.12 Growth of the bisector pattern in simulation with 27 conditions. A single graph is plotted series with the same D_1 and k_h but different k_c. The same rows show the differences in the k_h, whereas the same columns show the differences in the D_1.

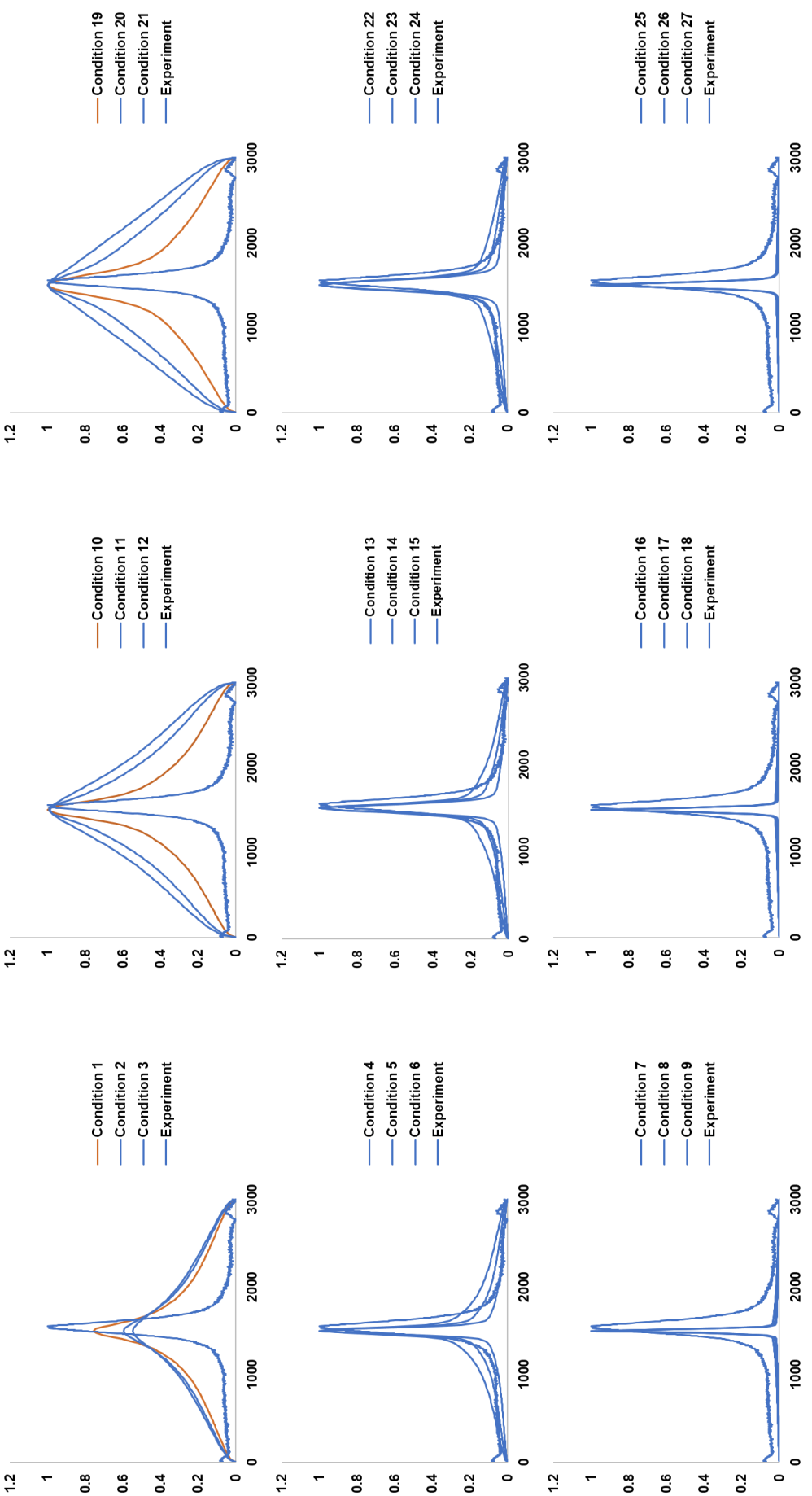

Figure 4.13 Shape of the bisector pattern in simulation with 27 conditions. As Figure 4.12, a single graph is plotted series with the same D_1 and k_h but different k_c. The same rows show the differences in the k_h, whereas the same columns show the differences in the D_1.

4.4.2 Spatiotemporal effect of adjuster DNAs for the bisector

I compared the bisector pattern positions after 24 hours by decreasing L1 diffusion coefficient while that of R1 was fixed. Based on the fitted value, the diffusion coefficient of L1, which is assumed to bind the adjuster, was 4–15 μm^2/sec.

Here, since the reaction in the adjuster-bound domain changes from a 23 nt hybridization to a 8 nt toehold-mediated strand displacement reaction, a new rate constant k_s for the reaction is introduced. The equations were revised as follows:

$$\frac{\partial}{\partial t}[\alpha_{2n-1}] = D_{2n}\Delta[\alpha_{2n-1}] + \sum_{i\le n}\sum_{j\le n-i}(k_h[\alpha_{2i-1}][\alpha_{2j}] + k_s[\alpha_{2i-1}][\beta_{2j}]) - \sum_{2i\le N-2n}(k_h[\alpha_{2n-1}][\alpha_{2i}] + k_s[\alpha_{2n-1}][\beta_{2i}] + k_s[\alpha_{2n-1}][\beta_{2i-1}] + k_h[\beta_{2i-1}][\alpha_{2n-1}])$$

$$\frac{\partial}{\partial t}[\beta_{2n-1}] = D_{2n}\Delta[\beta_{2n-1}] + \sum_{i\le n}\sum_{j\le n-i}(k_h[\beta_{2i-1}][\alpha_{2j}] + k_s[\beta_{2i-1}][\beta_{2j}]) - \sum_{2i\le N-2n}(k_h[\beta_{2n-1}][\alpha_{2i}] + k_s[\beta_{2n-1}][\beta_{2i}] + k_s[\alpha_{2i-1}][\beta_{2n-1}] + k_h[\beta_{2n-1}][\alpha_{2i-1}])$$

$$\frac{\partial}{\partial t}[\alpha_{2n}] = D_{2n}\Delta[\alpha_{2n}] + \sum_{i\le n}\sum_{j\le n-i}(k_h[\alpha_{2i}][\alpha_{2j}] + k_h[\alpha_{2j}][\alpha_{2i}] + k_s[\alpha_{2n-1}][\beta_{2i-1}]) - \sum_{2i\le N-2n}(k_h[\alpha_{2n}][\alpha_{2i}] + k_h[\alpha_{2i}][\alpha_{2n}] + k_h[\alpha_{2i-1}][\alpha_{2n}] + k_h[\alpha_{2n}][\beta_{2i-1}]) - k_c[\alpha_{2n}]$$

$$\frac{\partial}{\partial t}[\beta_{2n}] = D_{2n}\Delta[\beta_{2n}] + \sum_{i\le n}\sum_{j\le n-i}(k_s[\beta_{2i}][\beta_{2j}] + k_s[\beta_{2j}][\beta_{2i}] + k_h[\alpha_{2n-1}][\beta_{2i-1}]) - \sum_{2i\le N-2n}(k_s[\beta_{2n}][\beta_{2i}] + k_s[\beta_{2i}][\beta_{2n}] + k_s[\beta_{2n}][\alpha_{2i-1}] + k_s[\beta_{2n}][\beta_{2i-1}]) - k_c[\beta_{2n}]$$

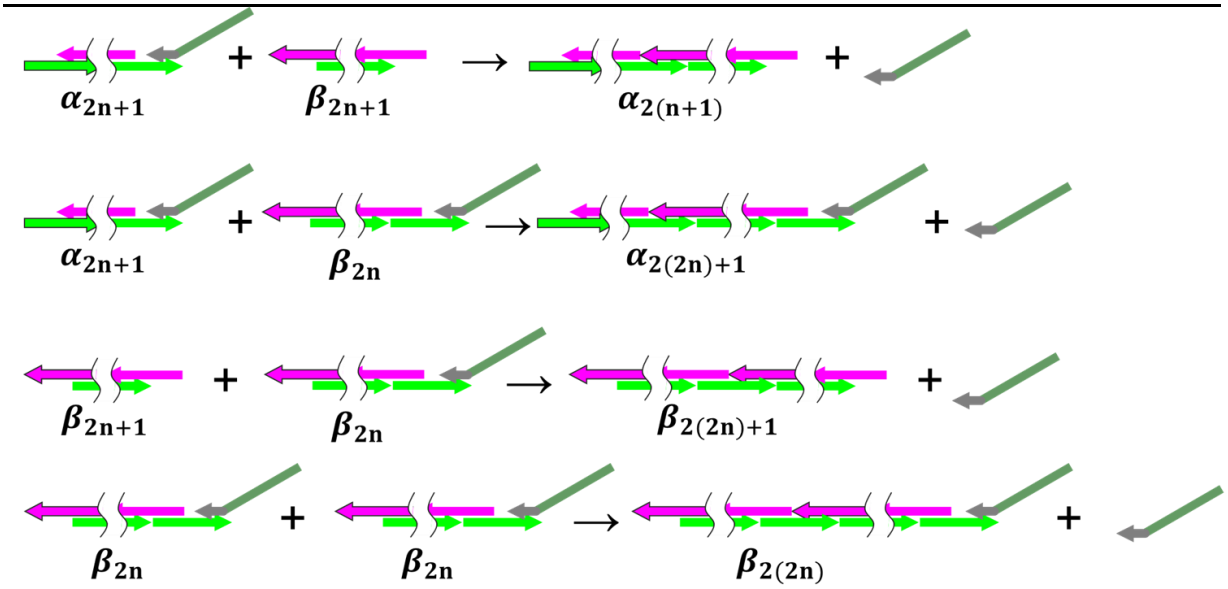

Figure 4.14 Reactions releasing adjusters. The reaction involving the domain at the 3' end of L1 is replaced by a strand displacement reaction when the adjuster is used.

$$\frac{\partial}{\partial t}[\gamma_{2n}] = D_{2n}\Delta[\beta_{2n}] + k_c[\alpha_{2n}] + k_c[\beta_{2n}]$$

Note that the four reactions whose rate constants were changed to k_s are shown in Figure 4.14.

Small L1 diffusion coefficient, shift the bisector to the left (Figure 1.14). The relationship between the peak position and the diffusion coefficient obtained from the graph was approximated by the least-squares method to the following exponential function.

$$D = 0.669\exp(0.0023b)$$

The equation represents the relationship between D (L1 diffusion coefficient) and b (bisector position) by finding the parameter using the least-squares approximation.

Based on the equation and the result shown in Figure 4.8, the diffusion coefficients for L1+A0, L1+A46, and L1+A92 are 8.9, 5.3, and 4.5 μm^2/s, respectively. These values suggest that the diffusion coefficient decreases as the adjuster length increases, and the degree of the decrement reduces.

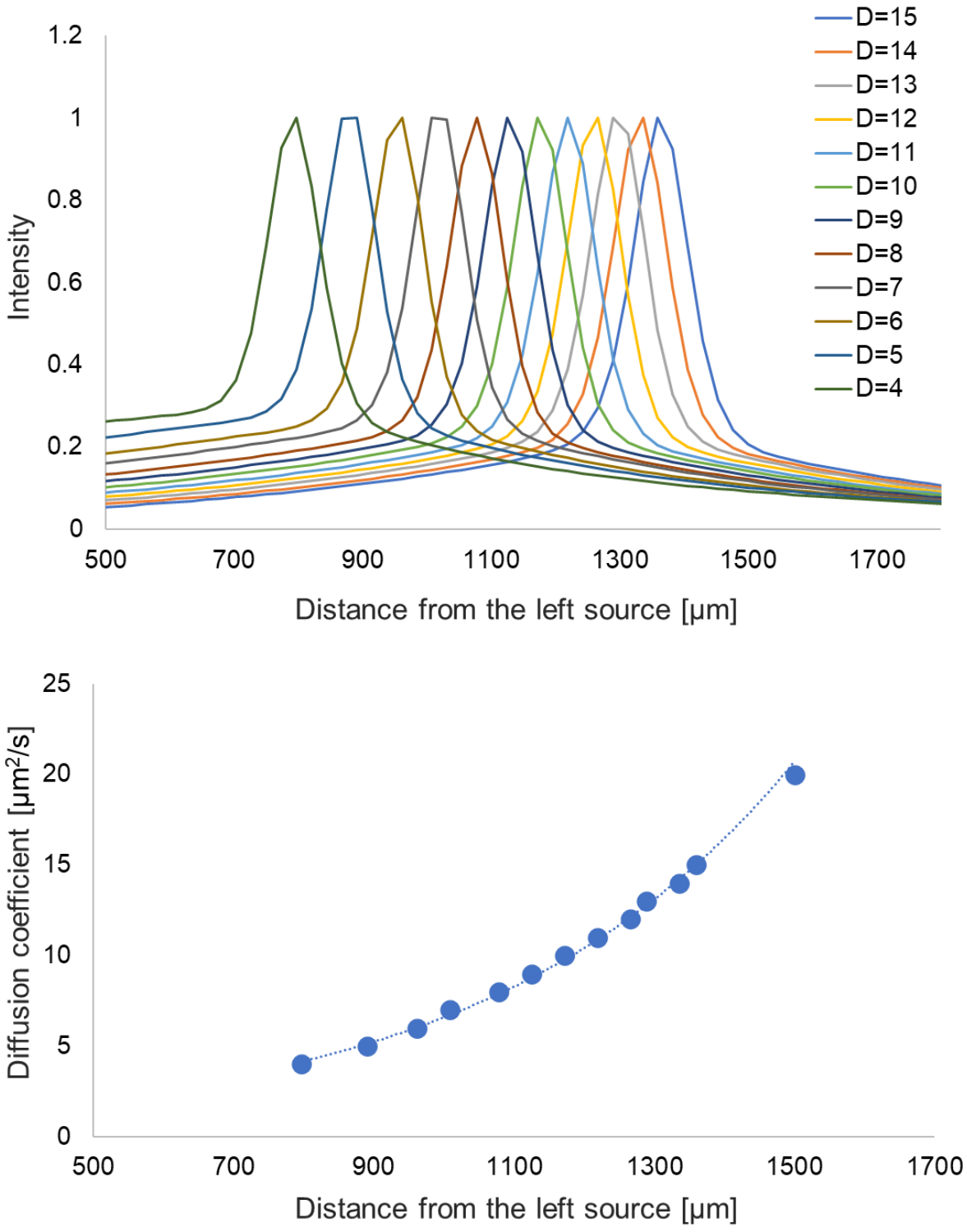

Figure 4.14 Relationship between bisector position and L1 diffusion coefficient. The bisector shifts following the change in the L1 diffusion coefficient (above). The relationship can be fit by an exponential function (below).

This result can be explained by focusing on the behavior of single-stranded DNA in solution. Single-stranded DNA has shorter persistent length than double-stranded DNA [78] and behaves

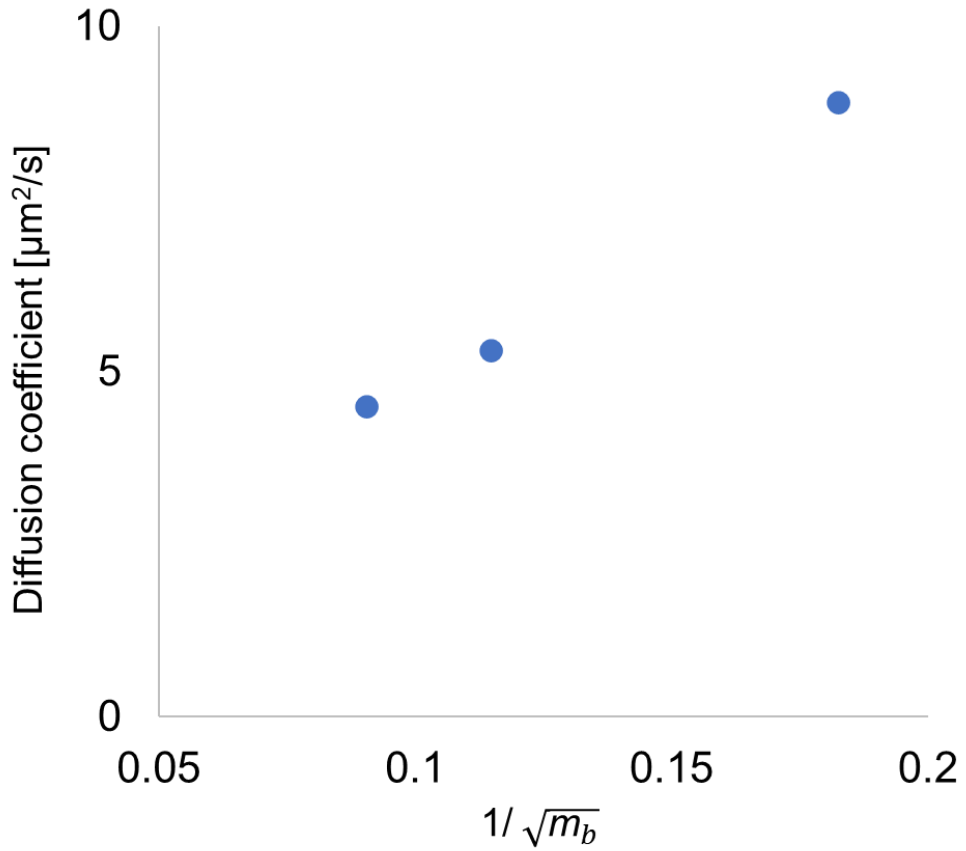

Figure 4.15 Relationship between diffusion coefficient and the length of single-stranded domain. m_b is the number of bases in single strand. The three plots represent L1+A0, L1+A46, and L1+A92.

as a string-like molecule in solution. R_g, the radius of gyration of a polymer consisting of x monomers of length l, can be obtained by the following equation:

$$R_g = l\sqrt{\frac{x}{6}}$$

Substituting R_g for r in the Einstein-Stokes equation yields the following equation.

$$D = \frac{k_B T}{6\pi\eta l}\sqrt{\frac{6}{x}} = \frac{A}{\sqrt{m}}, \left(A = \frac{k_B T}{\sqrt{6}\pi\eta l}\right)$$

Note that when the temperature and the viscosity are constant, A is also a constant.

For the patterns with adjusters, a linear relationship is suggested when the horizontal axis is plotted as $1/\sqrt{m_b}$, where m_b is the number of bases in a single strand, and the vertical axis indicates the calculated diffusion coefficients (Figure 4.16). The graph suggests that the effect

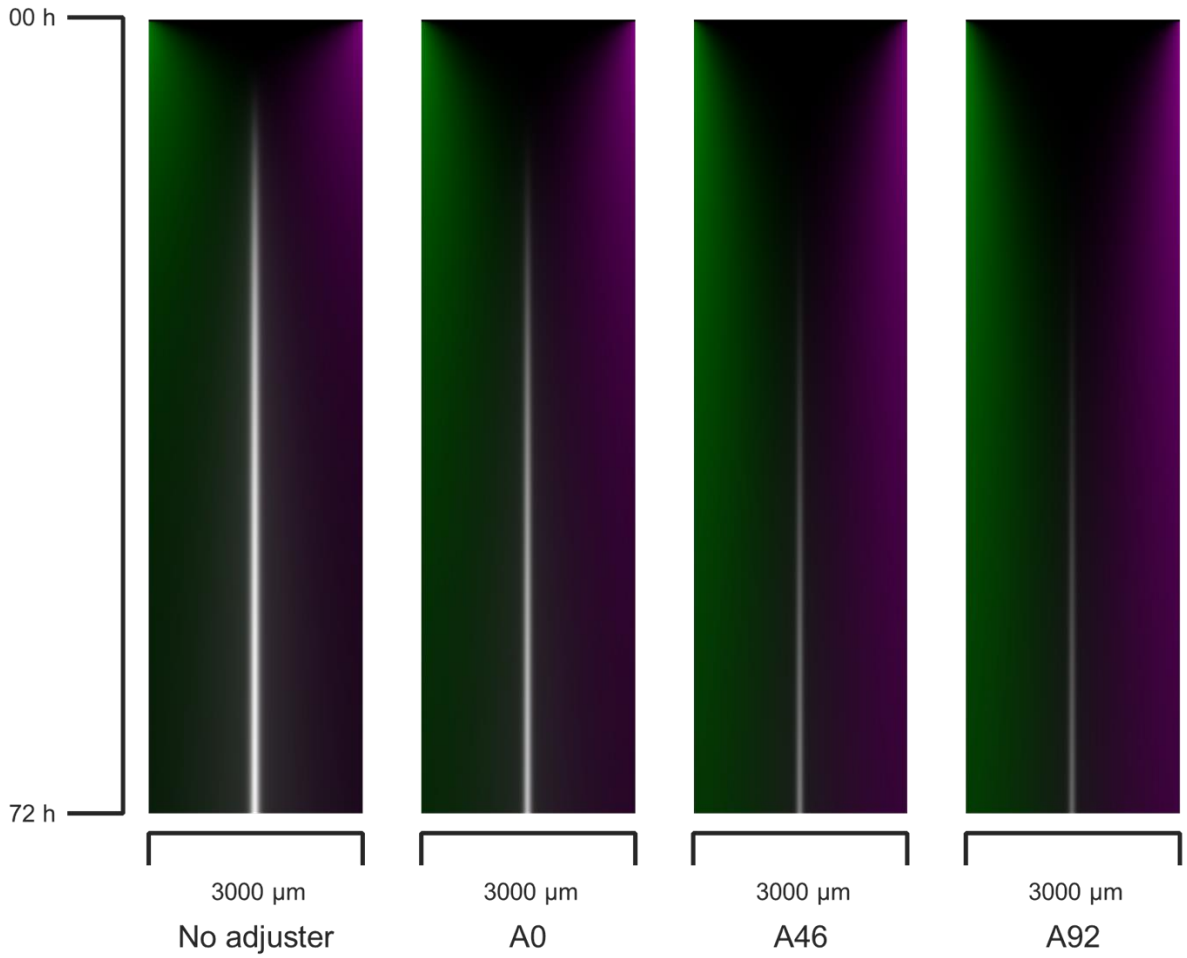

Figure 4.16 Temporal effect of adjuster for bisector pattern formation. Assuming that adjusters are used for L1 and R1, the diffusion coefficient was set to that of L1+A0, L1+A46, and L1+A92.

of the adjuster can be formulated by its length. We must note that the L1-adjuster complex is not a single-stranded DNA as shown in Figure 4.3 and the DNA structure potentially affects the diffusion coefficient. It seems possible to predict the effects of adjusters with other lengths since there was a certain correspondence with theory.

Next, I investigated the effect of the adjuster on the time necessary for bisector pattern formation (Figure 4.16). The simulation was performed assuming that adjusters were used for both L1 and R1. The diffusion coefficients were set to the calculated values. The kymographs show that the time at which the bisector appears has changed compared to that in the absence of adjusters.

4.5 Summary

In this chapter, I report a method for constructing a reaction–diffusion system using polyacrylamide gel and designed a polymerization-based reaction system by hybridization for bisector pattern formation (polymerization approach). The bisector pattern gradually appeared after 6 hours within 3 mm and was observed for 24 hours. Compared to the design in Chapter 2, this method required 94% DNA, while the resulting pattern was four times sharper.

By introducing adjuster DNA to suppress the diffusion, the bisector shifted successfully. The degree of shift can be modulated by different adjuster lengths. We modeled the polymerization approach to simulate the pattern formation process. The diffusion coefficients and rate constants that reproduce the experimental results were obtained. Additionally, the partial differential equations were modified to reproduce the experiments using the adjusters. The influence of the adjuster was quantitatively evaluated by comparing it with the experimental results, and the possibility of applying the adjuster to time control of pattern formation was also suggested.

Compared to the system in Chapter 2 and 3, a system with higher resolution was achieved. They are beneficial for parallel and cascaded pattern formation described in the next chapter.

5. Cascaded pattern formation in hydrogel medium

In this chapter, I describe a method for parallel and cascaded pattern formation by the polymerization approach described in Chapter 4. I focused on DNA orthogonality for parallelization of DNA, and utilized the DNA released in the polymerization process for the cascade. Furthermore, I applied the model in the experiment described in previous chapter and discuss the correspondence between these pattern formations and the model here.

5.1 Mechanism

5.1.1 DNA orthogonality for parallel reactions

In DNA nanotechnology, orthogonal sequence design enables parallelized DNA-based reactions. In this polymerization approach, introducing DNA pairs with similar reaction domains but different sequences allow to parallelize the DNA interactions for superimposing the pattern formation. Here, I designed L2 and R2, an additional DNA pair (pair 2) for bisector pattern formation. L2 and R2 are 46 nt long and polymerize by hybridization using the 23 nt segment also used by the L1 and R1 (pair 1), where the base sequence is orthogonal to avoid confusing the reactions.

In this design, pairs 1 and 2 form the bisector at the same area. Then, the adjuster for R2 is prepared to shift the bisector to the right. When L2 and R2 are added to the left and right sources, respectively, with the adjuster for R2, R2 diffuses slower than L2. Using pairs 1 and 2 in the same medium, L1 and R1 react at the left and L2 and R2 react at the right. The two bisectors consist of the superimposed patterns formed for pairs 1 and 2 in the hydrogel medium (Figure 5.1).

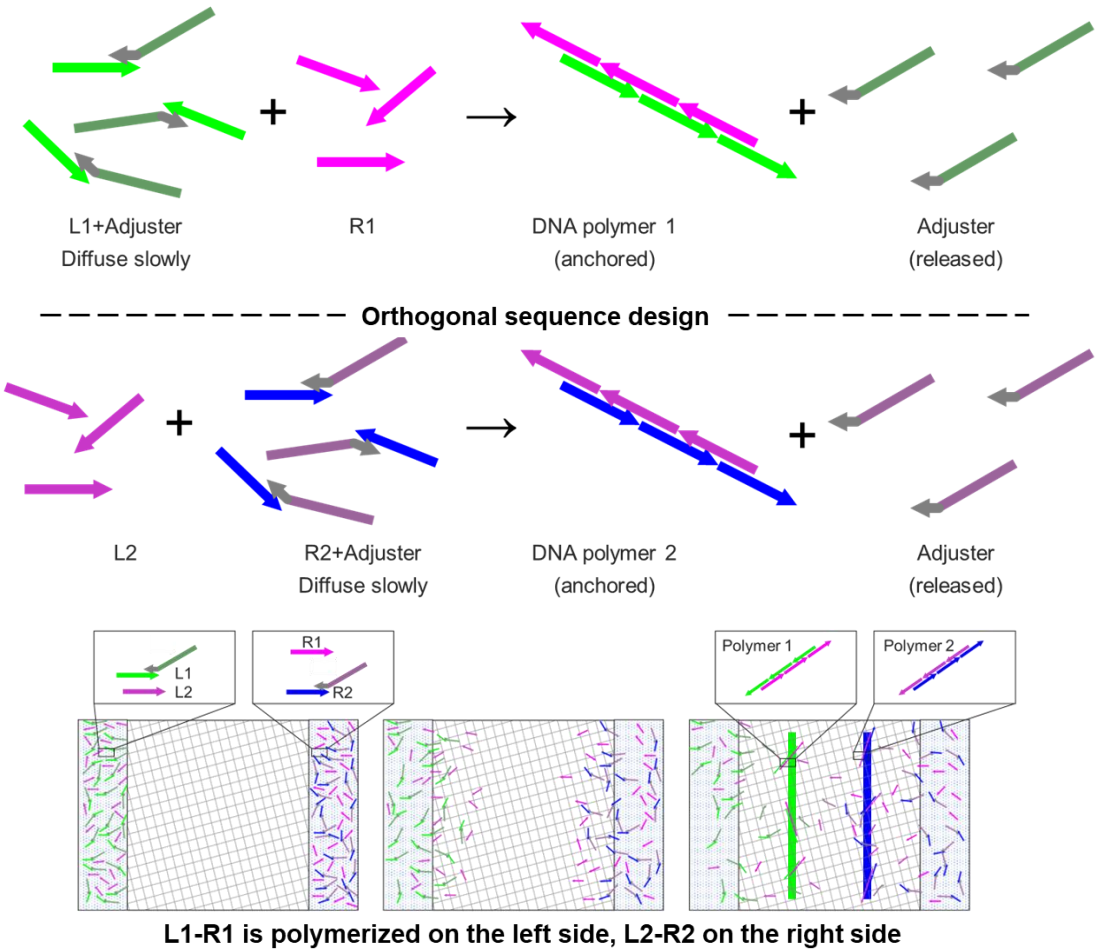

Figure 5.1 Superimposition of parallel pattern formation. Since pairs 1 and 2 are orthogonal, they do not interact with crossing pairs but form a polymer in each pair (above). In the reaction–diffusion system, pairs 1 and 2 act to form bisectors in the left and right, respectively (below).

5.1.2 Mechanism to make pattern formation cascaded

The cascaded pattern formation can be achieved by establishing a relationship within a single DNA reaction–diffusion system in which one pattern acts as a source of chemicals in subsequent pattern formation. Here, we built a DNA reaction system in which two superimposed bisector patterns are used to form a third bisector pattern. In addition to pairs 1 and 2, this system uses AL1-L3 and AR2-R3, which add 15 nt connector domains that bind to L1 and R2, respectively, to the third orthogonal DNA pair (L3 and R3). These initially act as adjusters for L1 and R2 and are released during the polymerization of pairs 1 and 2. Then, they diffuse from the two bisectors as a single strand and polymerize with each other to form the third bisector. The bisectors of pairs 1, 2, and 3 are labeled in green, red, and blue, respectively. First, green and

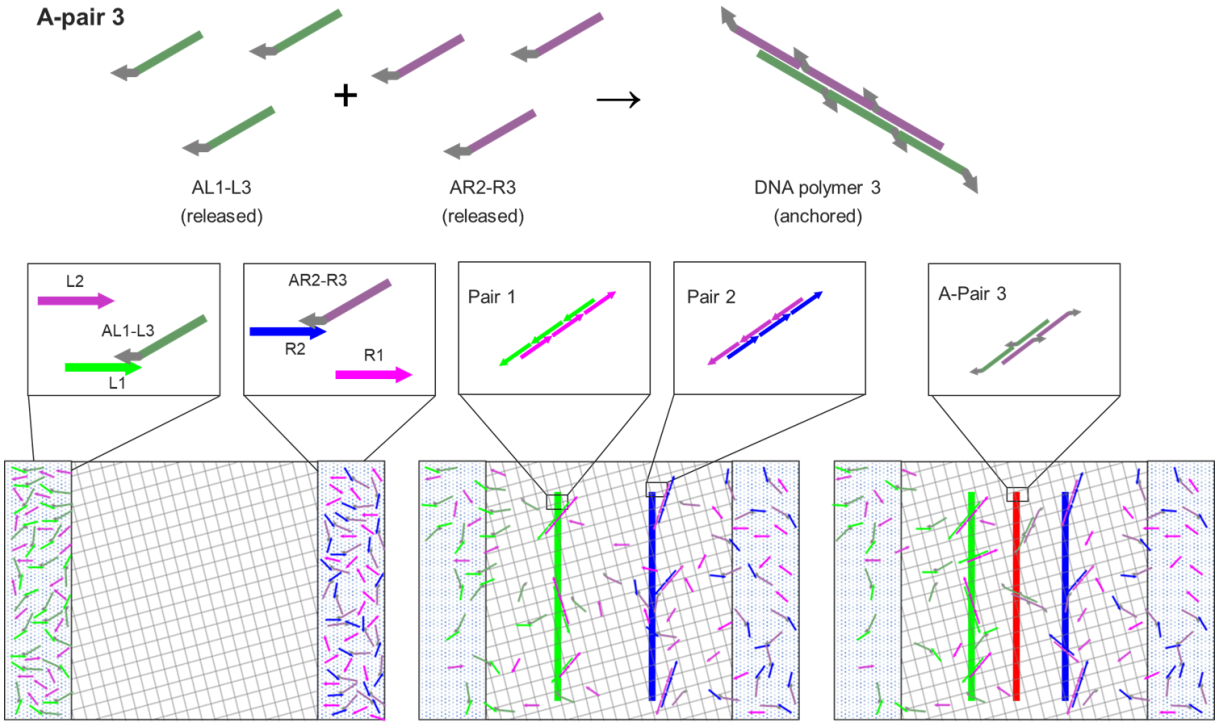

Figure 5.2 Design for cascaded pattern formation. AL1-L3 and AR2-R3 act as adjuster at first, are released in the polymerization of other pairs, and form a polymer.

blue bisectors appear on the left and right at first, and then a red bisector appears between them (Figure 5.2).

5.2 Results and discussion

5.2.1 DNA pair orthogonality

The orthogonality of the designed pairs 1 and 2 was evaluated by polyacrylamide gel electrophoresis (Figure 5.3). Lanes 1, 2, and 3 show the bands of L1, R1, and their mix, respectively. Lanes 4–7 show the bands of L1+R2, R1+R2, and their mix+R2, respectively, and Lanes 8–11 show the bands of L1+L2, R1+L2, and their mix+L2 instead, respectively. Both bands of polymers and a monomer were observed in Lanes 7 and 11, which contain both L1 and R1, while only the band of the monomer was observed in the others. This result indicates that L2 and R2 do not affect pair 1 polymerization.

For pair 2, bands of polymers similar to those in Lane 3 appeared in Lane 12, which contain both L2 and R2. When L1 and R1 were added (Lanes 13 and 14), bands showing the polymers and a monomer appeared as those in Lanes 7 and 11. In Lane 15, to which all DNAs of pairs 1

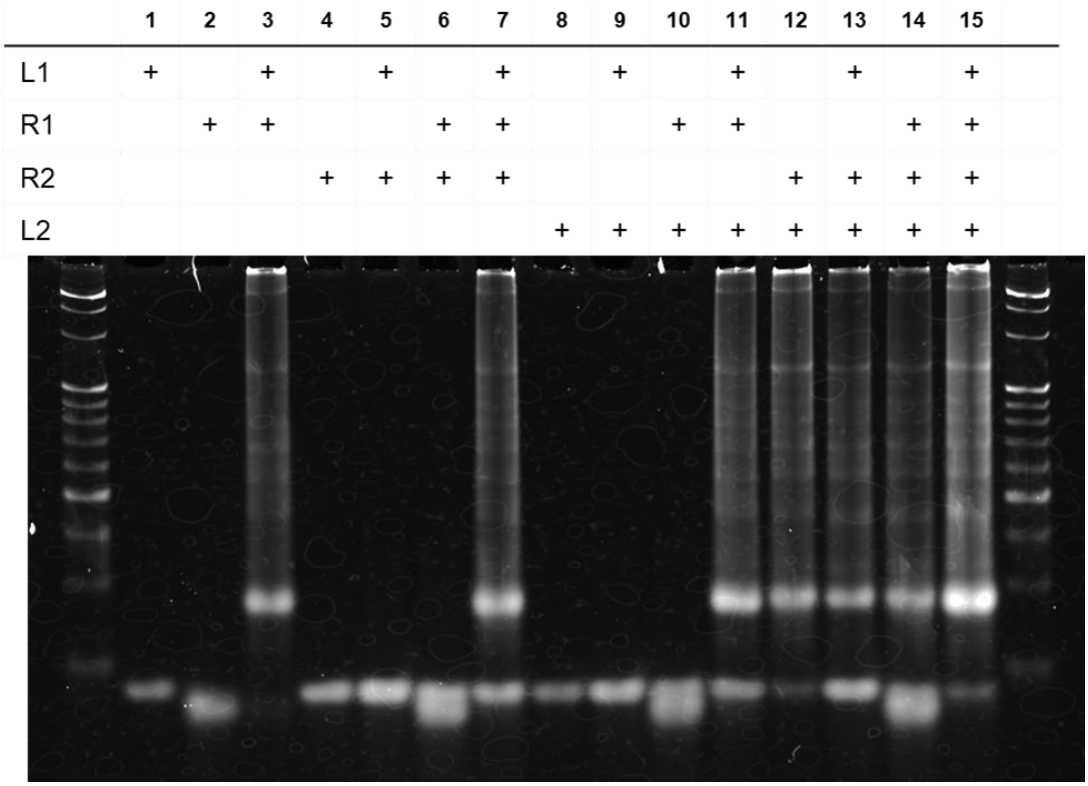

Figure 5.3 Orthogonality of pairs 1 and 2. DNA was mixed to 200 nM and then run on a 10% polyacrylamide gel for 120 min at 50 V and stained with SYBR Gold for 20 min.

and 2 were added, the bands showing the polymer were denser than those in Lanes 3, 7, and 11, and the band indicating the monomer was weaker, suggesting that both pairs polymerize at the same time. Therefore, this result shows that pairs 1 and 2 do not interact with each other and undergo similar polymerization.

5.2.2 Superimposed pattern formation

Superimposed pattern formation was demonstrated using the two pairs and adjusters for L1 and R2. L1, R1, L2 and R2 were modified with FAM, Cy5, Cy3 and AMCA, respectively, and the pattern formation processes of the pairs was visualized by four-channel fluorescence imaging. In Figure 5.4, images of FAM and AMCA fluorescence representing L1 and R2 distribution are indicated in green and blue, respectively. Within 24 hours two lines appeared. In the channels representing R1 and L2, which are omitted in Figure 5.4, the bisectors appeared and their positions were the same for the correct pair combinations (Figure 5.5). This implies that the pattern formed due to the orthogonal polymerization of the pairs.

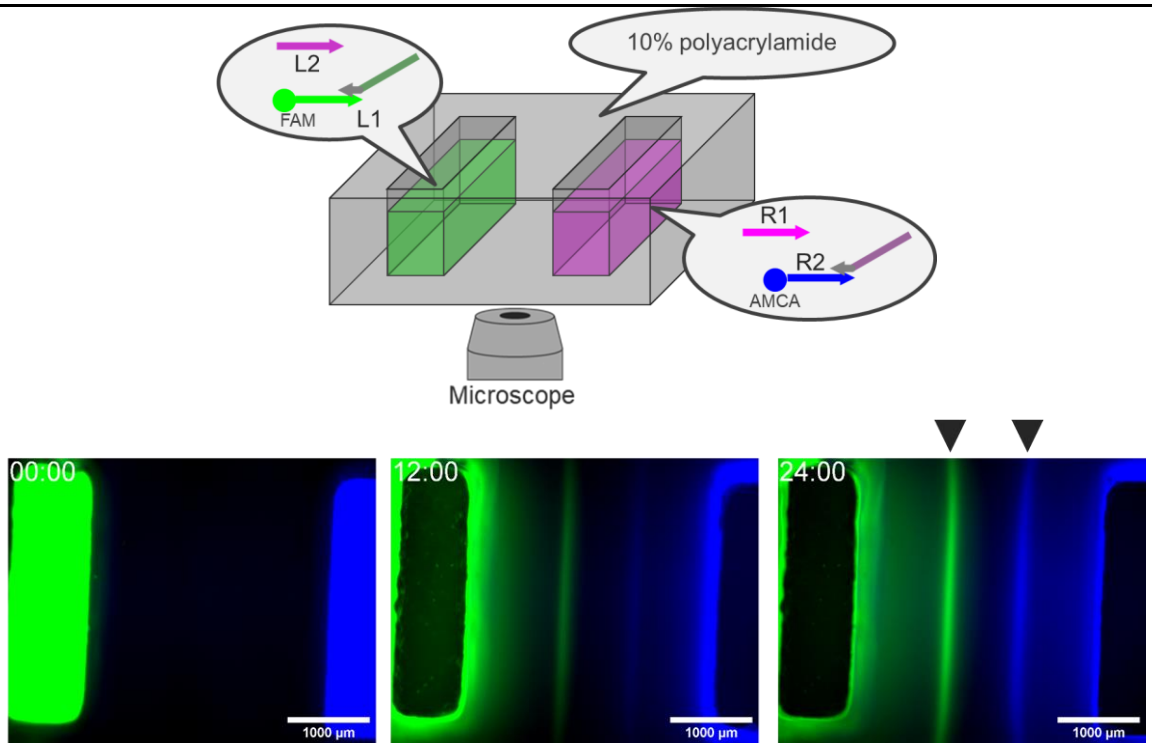

Figure 5.4 Superimposed pattern formation using two DNA pairs. The reaction–diffusion system was set up as shown above. The results are superimposed FAM and AMCA fluorescence images indicated in green and blue, respectively.

In the superimposed patterns with two pairs facing each other on a horizontal axis, the space is divided into three regions: to the left of the green bisector, between the green and blue bisectors, and the right of the blue bisector. Increasing the number of DNA pairs and the placing axes enables us to generate several partitions in the space. For example, if pairs 1 and 2 are placed horizontally and vertically facing each other, respectively, vertical and horizontal bisectors appear and divide the region into four regions.

Increasing the number of pairs requires designing DNA with orthogonal sequences. Four bases are available for DNA sequences. Thus, there are 4^{23} possible 23 nt sequences, which is the reaction domain length in this design. On the contrary, there is only one sequence that is fully complementary to a sequence. Since two reaction domains are required for the polymerization approach, four different sequences are used for each pair. That means that maximum 4^{22} pairs of fully complementary sequences are available.

Binding is possible despite a mismatch of a few bases (for example, the adjuster binds stably at room temperature using 16 nt segment, which is not fully complementary to the 23 nt), so

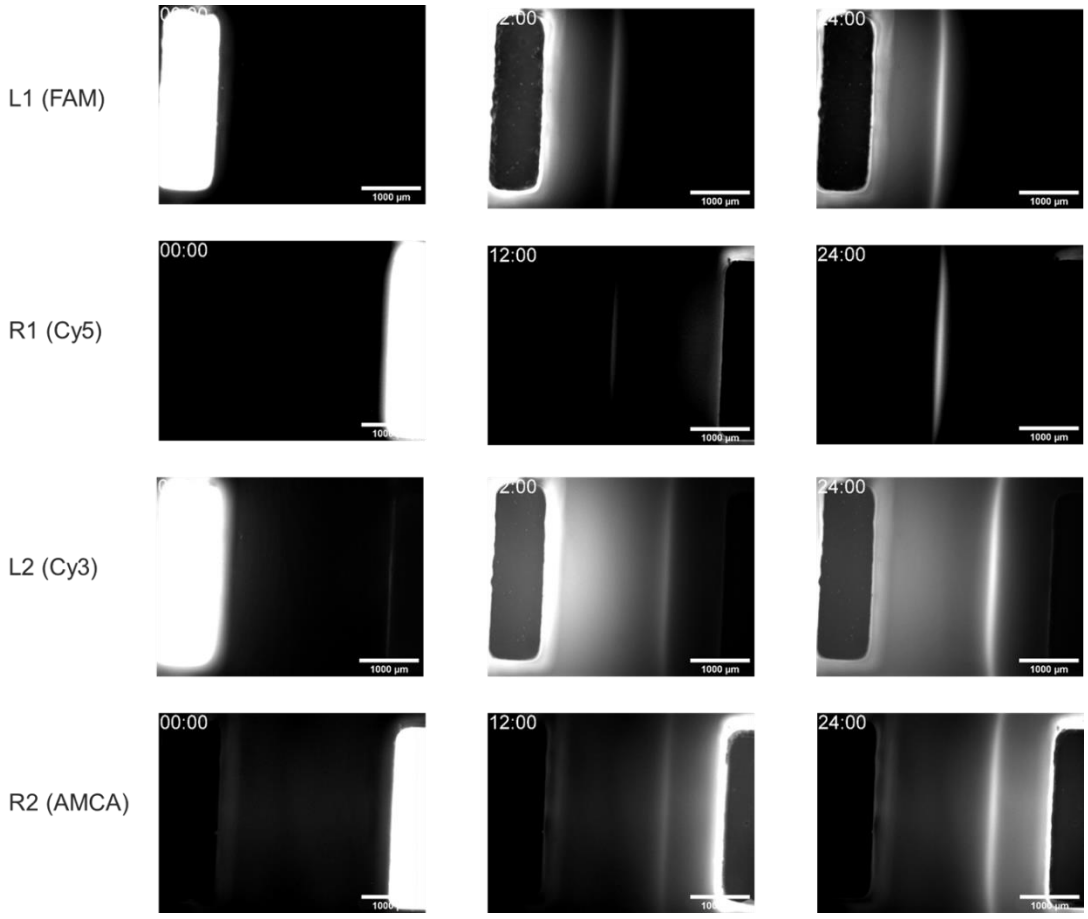

Figure 5.5 Fluorescence images before the composition. Although the images of Cy5 and Cy3 are omitted in the color image in Figure 5.4, the bisector appears at the same site with their correct pairs.

preparation of orthogonal DNA pairs requires proper sequence. It is reported that 300 orthogonal sequences with 23 nt are possible, and that sufficient orthogonality was experimentally examined using at least 37 of them [79]. Therefore, based on the sequences reported previously, at least nine orthogonal DNA pairs can be prepared.

When the pattern formation process is observed by fluorescent modification, the number of pairs that can be observed simultaneously is further limited. This is because combinations of fluorescent molecules with less leakage should be selected and to assign at least one fluorescent channel should be assigned to each pair.

Based on this, we next attempted to superimpose four bisectors by utilizing four channels of fluorescence that can be observed simultaneously. Two new DNA pairs (L3–R3 and L4–R4) were prepared, and the pattern formation process was observed by placing pairs 1 and 2 on the left and right, and pairs 3 and 4 facing each other on the top and bottom. L1 and R2 were

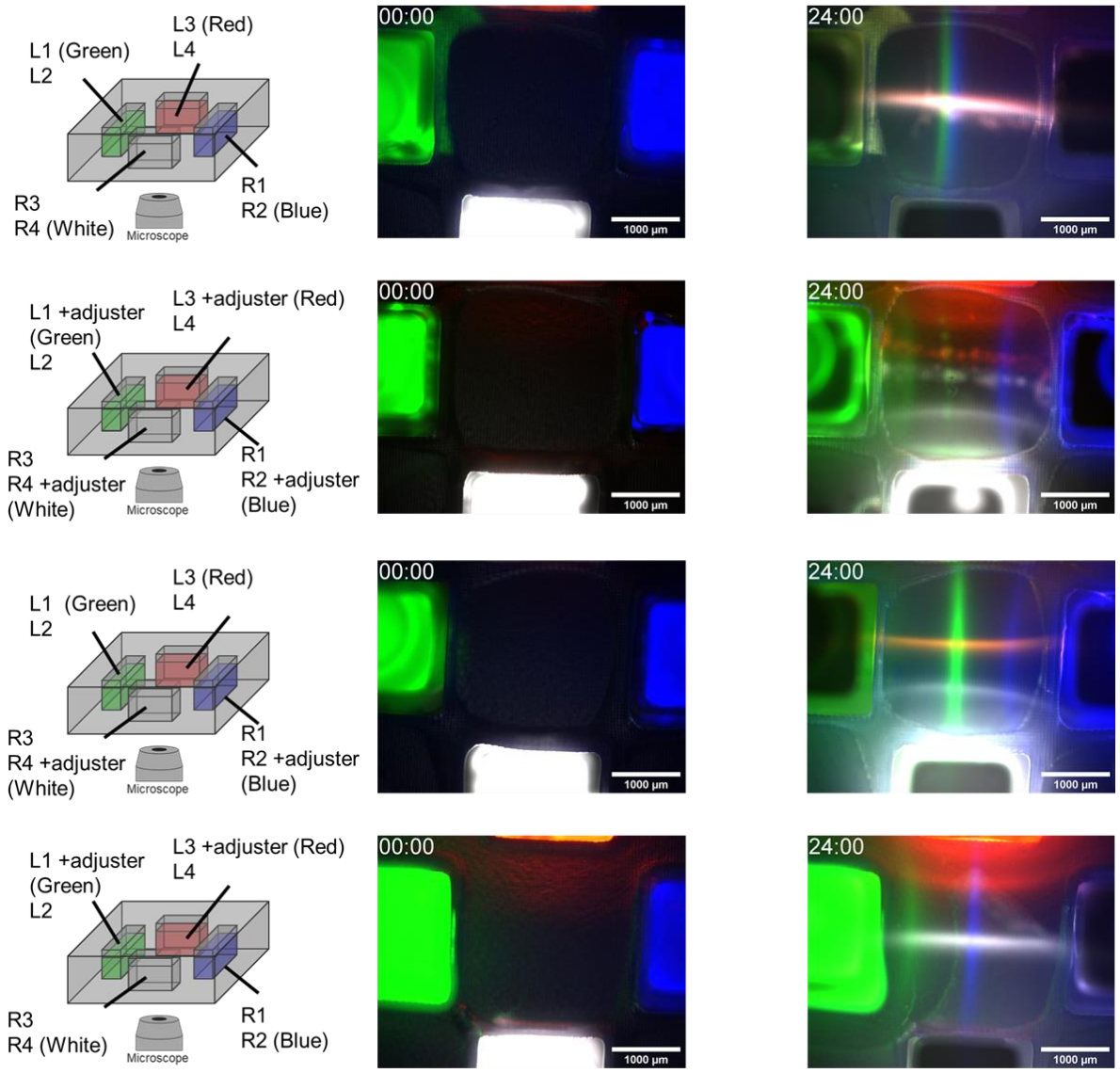

Figure 5.6 Super imposed pattern formation using four DNA pairs two-dimensionally. The reaction–diffusion system was set up as shown the left. The results are superimposed FAM, AMCA, Cy3 and Cy5 fluorescence images indicated in green, blue, red, and white, respectively.

modified with FAM and AMCA, respectively, as in the previous experiment. L3 of pair 3 and R4 of pair 4 were modified with Cy3 and Cy5 to observe fluorescence in four channels (blue, green, orange, and red). The position of the bisectors was changed by using an adjuster for the four labeled DNAs. The images of each fluorescent channel are indicated in blue, green, red, and white, respectively (Figure 5.6). Interestingly, the regions with blue, green, and red fluorescence to the same extent are visualized in white, so the composite image does not visualize the four channels independently at the same time. Thus, there are regions where the fluorescence intensity does not correctly correspond to the DNA concentration. However, since

the bisectors obtained in this design appeared sharply with high intensity, they were considered to show the positional relationship of the superimposed bisector pattern.

Without adjusters, the bisectors on the same axis appear in the same position. The green and blue vertical bisectors and the white and red horizontal bisectors appear in the same position 24 hours later, dividing the space into four regions. In contrast, when the adjusters are bound to the four DNAs, the green and blue vertical bisectors appear on the left and right, respectively, and the red and white horizontal bisectors appear on the upper and lower sides, respectively. These four lines form a lattice pattern with nine regions. The bisectors that appear here are slightly curved probably because the four sources are smaller than those in the previous system. The diffusion perpendicular to the axis affects the shape, forming a two-dimensional weighted Voronoi diagram that reported in Chapter 3.

Furthermore, when adjusters are applied to only R2 (blue) and R4 (white), the green and red bisectors intersect in the center, while the blue and white lines shift to the right and bottom, respectively, and intersect in the lower right corner. In this situation, the lattice shifts to the lower left, with the upper right corner is larger and the left corner smaller. On the contrary, when adjusters are applied to L1 (green) and L3 (red), the lattice shifts to the upper right corner. These results indicate that the reactions of the four DNA pairs are orthogonal to each other and the adjusters also work independently, showing the possibility of superimposition of at least four pattern formation in a reaction–diffusion system.

5.2.3 Cascaded pattern formation

A-pair 3 (AL1–L3 and AR2–R3), which has the sequence of pair 3 and connector domains to act as adjusters for L1 and R1 was prepared for the cascaded pattern formation. The reactivity of the A-pair 3 evaluated by polyacrylamide gel electrophoresis is shown in Figure 5.7.

Comparing to the bands in Lanes 1–3, which contain pair 1, and Lanes 4–7, which contain AL–L3, the band in Lane 5 shifts upward. The bands indicating R1 and pair 1 polymer appeared in Lanes 6 and 7, showing that AL1–L3 does not interact with R1 or inhibit the polymerization. In Lanes 8–11, only the bands seen in Lanes 1–3 and AR2–R3 were observed, indicating that pair 1 does not interact with AR2–R3. Both AL1–L3 and AR2–R3 are 61 nt long and the band in Lane 13 shifted upward, suggesting that it represents a one-to-one conformation. The bands

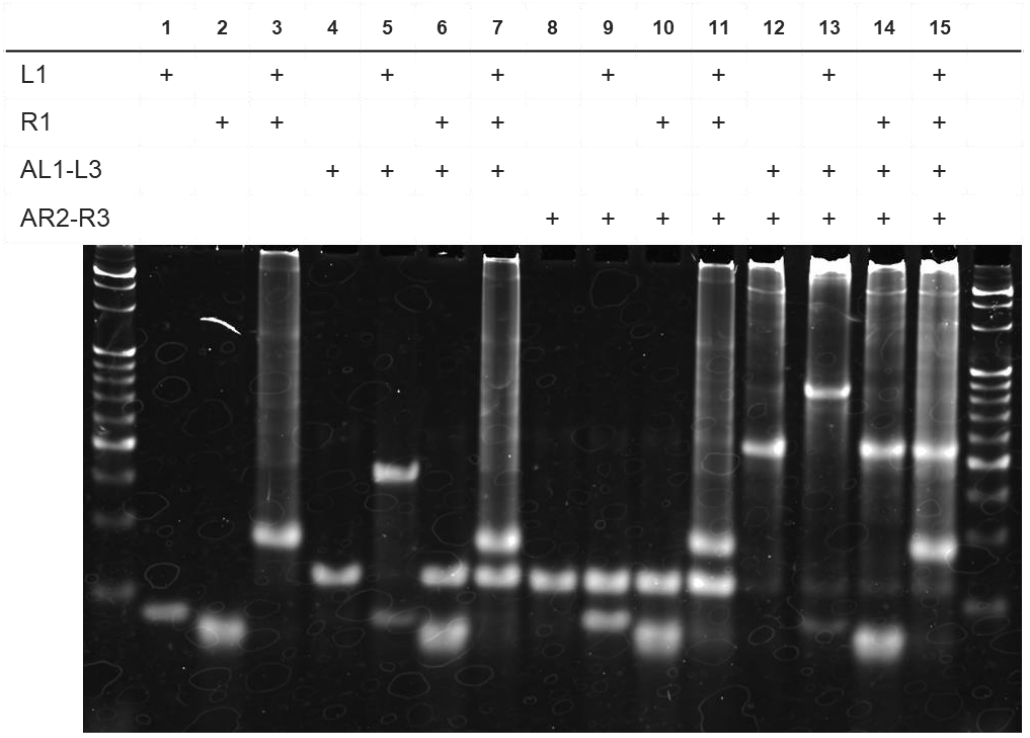

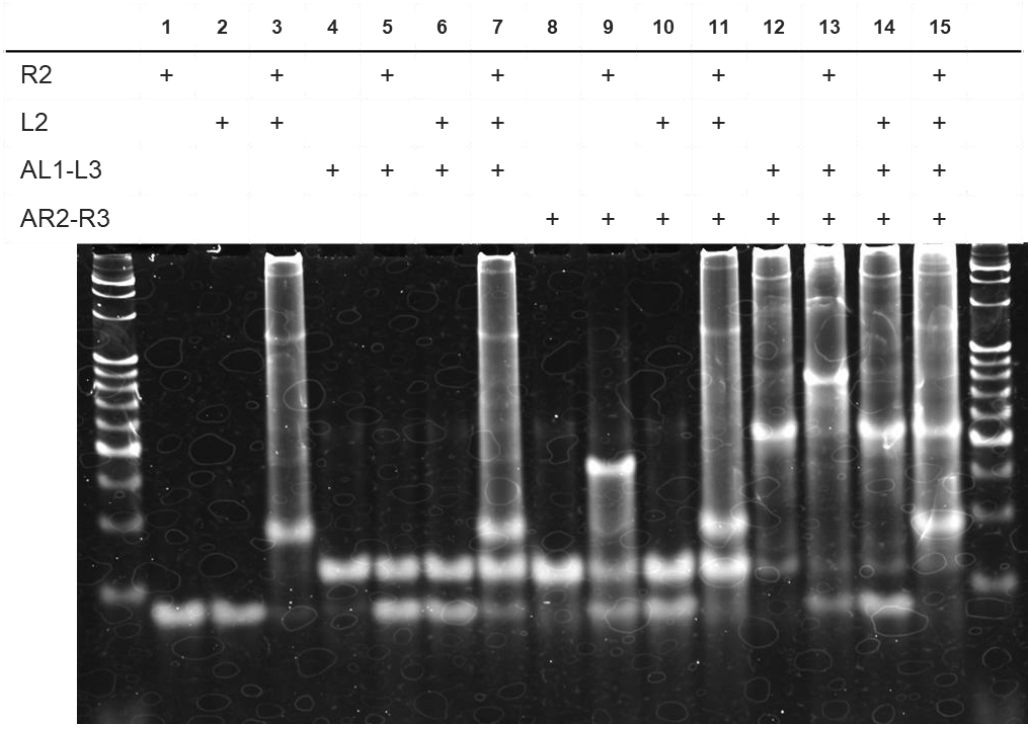

Figure 5.7 Interaction between A-pair 3 and other pairs. DNA was mixed to 200 nM, run on a 10% polyacrylamide gel for 120 min at 50 V, and stained with SYBR Gold for 20 min.

of the other pairs also show a one-to-one structure, which seems to be a common trend in the design. As mentioned in 4.1.1, they can form closed shapes called γ in the simulation, but they are not critical for the bisector pattern formation shown in Chapter 4.

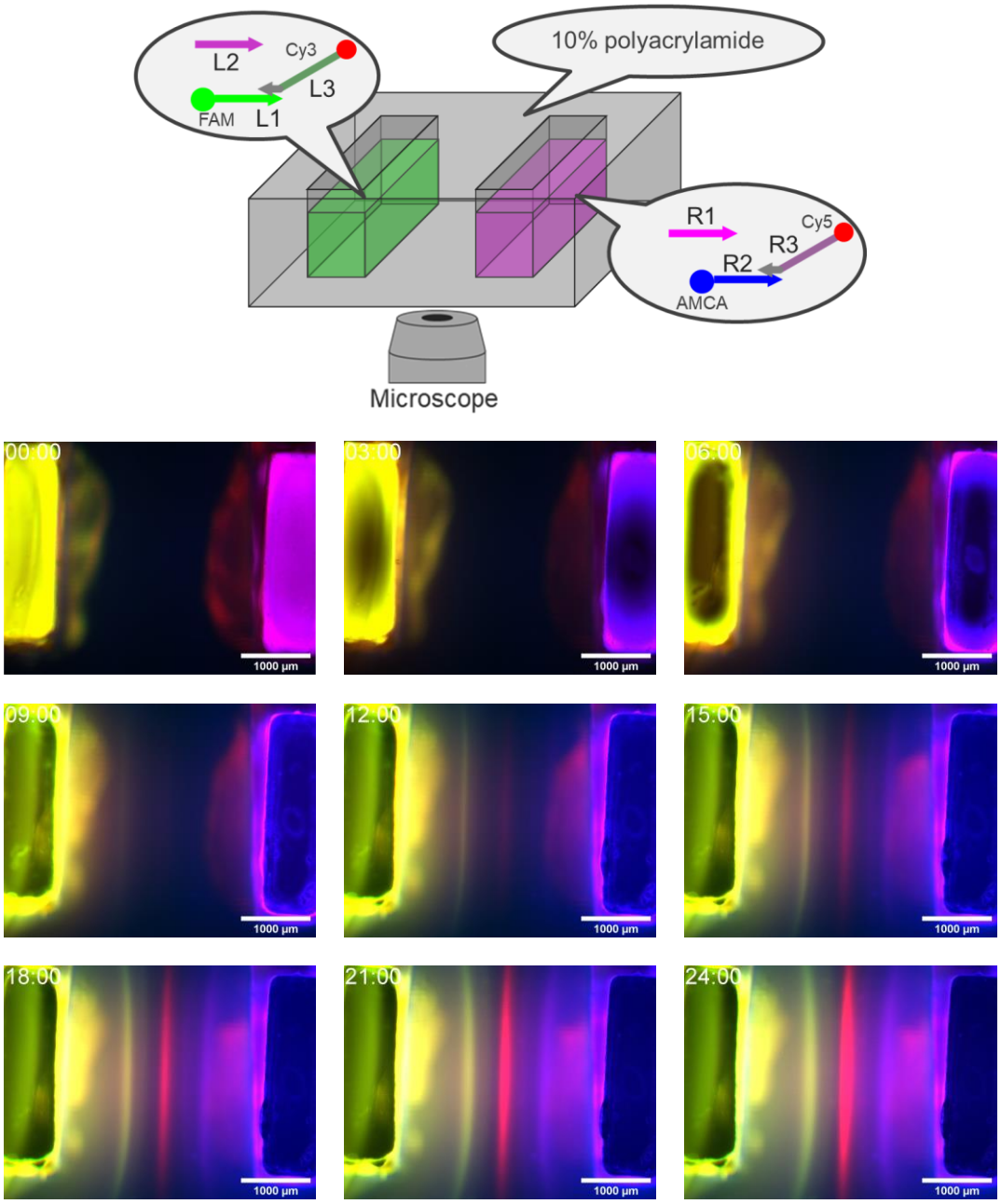

Figure 5.8 Cascaded pattern formation using two DNA pairs and A-pair3 as adjusters. The reaction–diffusion system was set up as shown above. The results show FAM, AMCA, Cy3, and Cy5 fluorescence images. The FAM and AMCA images are shown in green and blue channels, respectively. Cy3 and Cy5 images are merged using the “Multiply” function of Fiji (https://fiji.sc/), and the resultant image is shown in red.

Using these DNAs, we performed an experiment to make a pattern formation cascade. For fluorescence observation, L1, R1, L2, and R2 were modified with FAM, Cy5, Cy3, and AMCA, respectively as same as the 5.2.2, while AL1–L3 and AR2–R3 were modified with Cy3 and Cy5, respectively. The images of four fluorescent channels were converted to color images by assigning FAM, AMCA, and Cy3–Cy5 as green, blue, and red, respectively (Figure 5.8). After

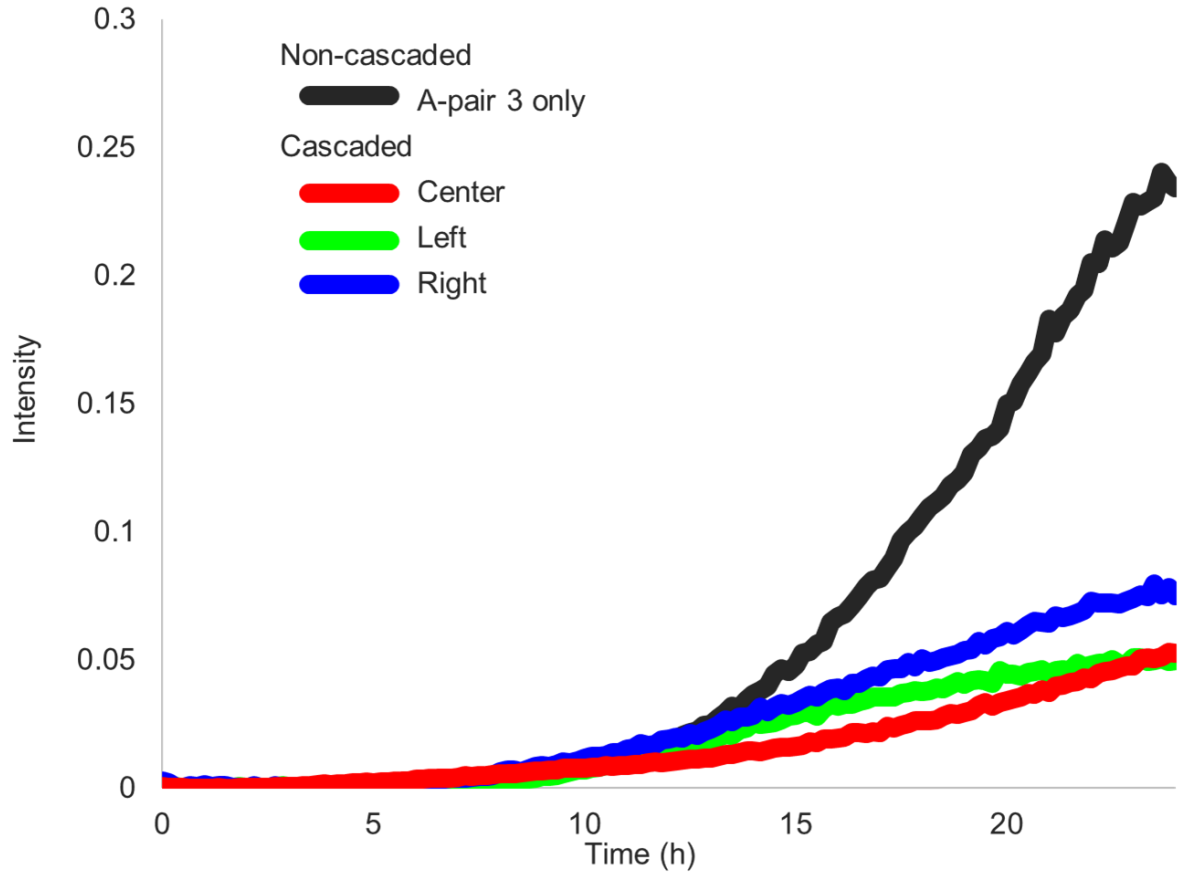

Figure 5.9 Peak intensity growth of each bisector. The bisector of A-pair 3 in the non-cascaded process appeared faster than pairs 1(Left) and 2(Right) in the cascaded process, whereas that in the cascaded process appeared slower than them. Note that the non-cascaded pattern formation was observed in a separate hydrogel from the others.

12 hours, yellow (green+red) and magenta (blue+red) bisectors appeared. Their intensity gradually increased, and an additional red bisector appeared between the two bisectors 15 hours later.

To compare the formation process, the temporal changes in fluorescence intensity were examined for each bisector peak position at 24 hours (Figure 5.9). Taking time on the horizontal axis and the geometric mean of the fluorescence intensity on the vertical axis, the center bisector pattern formed later and has less intensity than the bisector pattern with the A-pair 3 alone. This indicates that the bisector was not formed by the diffusion of free A-pair 3 strands. In addition, middle bisector formation is slower than the left and right bisectors formed in the same hydrogel. The intensity of left and right, and middle bisectors are 0.05 at 22.5, 18.5, and 23.5 hours, respectively. Therefore, this result indicates that the center bisector formed after the formation of the left and right bisectors; in other words, the cascaded pattern formation was realized.

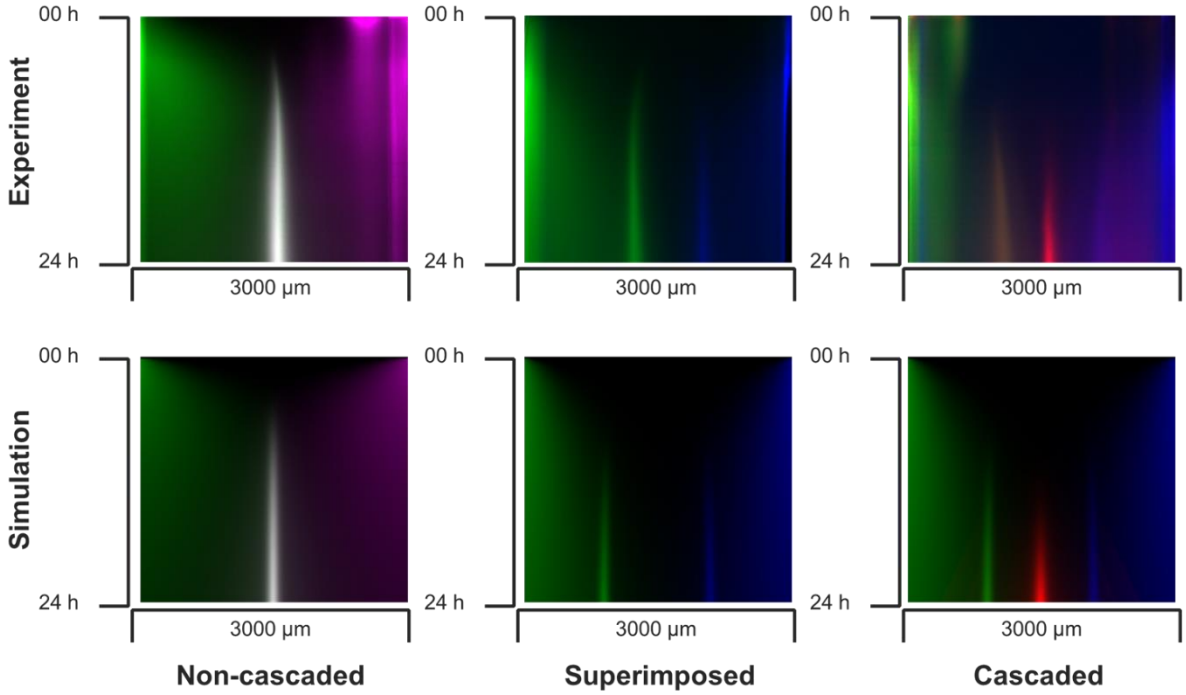

Figure 5.10 Kymographs of bisector (non-cascaded), superimposed, and cascaded pattern formation in experiment and simulation. Each process in the simulation agreed well with those in the experiment.

5.3 Reaction–diffusion simulation

The model in 4.4.2 was applied to simulate superimposed and cascaded patterns. The superimposition of the pattern can be simulated using the same model when using adjuster and introducing the chemical species corresponding to pair 2. The cascaded pattern can be further developed by introducing the A-pair 3 produced in the reaction shown in Figure 4.14. For example, since the pair 1 polymerization process produces AL1–L3, the following reaction terms were added:

$$f_{\alpha 3_1} = \sum_{i \le n-1} \sum_{j \le n-i-1} (k_s[\alpha 1_{2n-1}][\beta 1_{2i-1}] + k_s[\alpha 1_{2i-1}][\beta 1_{2_j}] + k_s[\beta 1_{2i-1}][\beta 1_{2_j}] + k_s[\beta 1_{2i}][\beta 1_{2_j}] + k_s[\beta 1_{2_j}][\beta 1_{2i}])$$

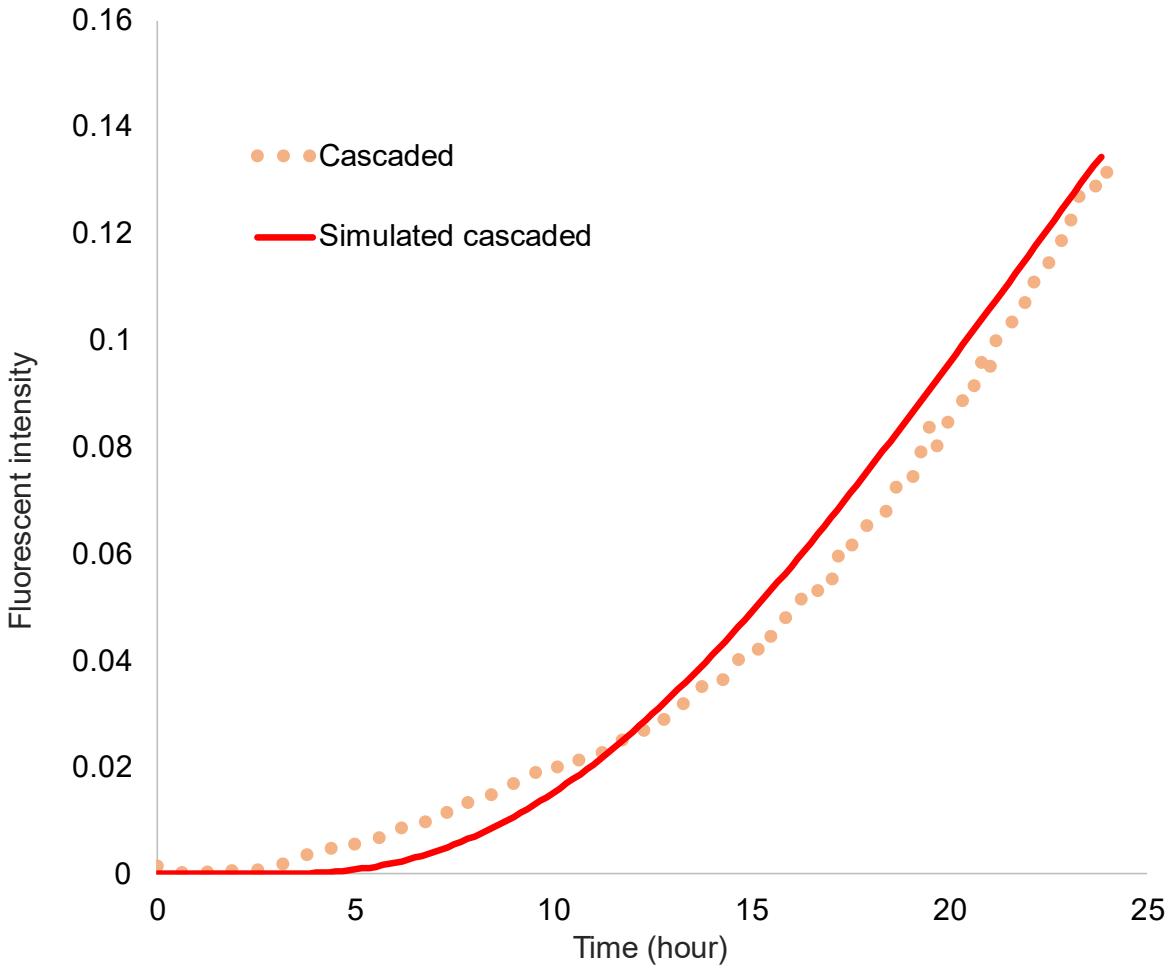

Figure 5.11 Peak intensity growth of cascaded bisector in experiment and simulation. The values of are corrected by the effect of FRET between the Cy5 (AL1–L3) and Cy3 (AR2–R3).

where $\alpha 1$ and $\beta 1$ are pair 1 monomers or polymers and $\alpha 3_1$is AL1–L3 monomer. The initial concentration was set at zero. Figure 5.10 shows the resulting kymograph from the simulation, which reproduces the pattern formations. In particular, the A-pair 3 consisting middle bisector formation process, for which additional reaction equation was introduced, was compared with the experiment.

The graph in Figure 5.11, with time on the horizontal axis and bisector peak fluorescence intensity on the vertical axis, shows that the cascaded pattern formation process is well reproduced by the simulation. According to the parameter fitting described in 4.4.1, E was 6.2×10^{-3}. The value under condition #15 in Table 4.2, which is in good agreement with bisector pattern formation the experiment, is 0.28. Due to the difference in the experimental values, we normalized them by the following equation:

$$E' = \frac{E}{\max\left(I_{\mathrm{experiment}}(t)\right)^2}$$

and obtained E' for condition #15 and this cascaded process are 0.52 and 0.36, respectively.

Overall, the simulations based on this model and the parameters of condition #15 are in good agreement with experimental results, even for the complicated system. Therefore, the model and the parameters reproduce the reaction–diffusion system constructed in this study.

5.4 Summary

In this chapter, I have described the superimposed pattern formation using multiple orthogonal DNA pairs. The experiments showed that at least four patterns can form in parallel. Furthermore, I have described a cascaded pattern formation by superimposing pattern formation and designing the released adjusters that react with each other. The bisectors appeared on the left and right sides, followed by a third bisector in the middle. The simulation model reported in the previous chapter well reproduced the pattern formation process.

6. Conclusions

6.1 Achievements in this thesis

In this thesis, I have reported the developme t of a method to program a reaction–diffusion system for pattern formation using synthetic DNA. A series of reaction–diffusion systems for pattern formation were developed to form various patterns.

In Chapter 1, I have described the advantages of using synthetic DNA as a material for the construction of artificial reaction–diffusion systems, and then, presented the following three issues:

1) To construct a reaction–diffusion system that switches the DNA diffusion state in the hydrogel to form static patterns.
2) To program the spatiotemporal DNA diffusion process by introducing a mechanism to inhibit diffusion and change the patterns formed.
3) To combine and link multiple pattern formation processes in a cascade.

In Chapter 2, I have discussed the development of a method of constructing DNA anchoring-based a reaction–diffusion system for static pattern formation. First, I fabricated anchor DNA bonded to polyacrylamide by acrydite-modification and verified that it inhibits diffusion, but not hybridization. Next, I combined an associative toehold activation-based DNA logic gate for bisector pattern formation. The performance of proposed method is evaluated through experiments and simulations.

In Chapter 3, I have discussed the diffusion modulation used to program diffusion. I verified the position shift of the bisector by the diffusion modulation. Furthermore, I showed that the degree of the shift can be adjusted by changing the competitor concentration. By applying diffusion modulation to a weighting of the sources, I implemented the weighted Voronoi diagrams as a demonstration.

In Chapter 4, I have discussed the problems of the methods described in Chapters 2 and 3 and proposed the polymerization approach to form a sharp pattern. I redesigned the system using polymerization by hybridization. Through experiments and simulations, I found that polymerization approach is effective in forming sharp patterns.

In Chapter 5, I have discussed superimposed and cascaded pattern formation based on polymerization approach. First, using DNA orthogonality, I prepared multiple independent DNA pairs for polymerization. I have experimentally proved that patterns by at least four DNA pairs can be superimposed in a single system. Furthermore, I realized cascaded pattern formation using the adjuster DNA released during polymerization for the next step of pattern formation.

Taken together, a reaction–diffusion system that can be programed in both reaction and diffusion was built in hydrogel.

In the next step, an artificial system that self-organizes by mapping the DNA concentration patterns should be developed to develop further physical properties, shape, and functionalities.

6.2 Future perspectives

Although the fundamental questions on using the reaction–diffusion system for DNA pattern formation were successfully, the obtained patterns are just a chemical gradient and have no function. We should be inspired from biological development and associate patterns with physical properties and location-specific functionalization. DNA nanotechnology can play a major role in realizing such a vision. For example, molecular motors are used for changing shapes. Synthetic DNA can be used to control the kinetic state of molecular motors. Vesicle deformation [80] and sheet structure contraction [81, 82] have been proposed so far. Moreover, the physical properties and volume of materials can be altered via several techniques. DNA hydrogel realizes such behavior, and various changes such as gel-sol transition [83, 84], swelling [85-87], and deformation [87, 88] can be induced via DNA.

Since DNA does not have chemical activities other than hybridization, it must be functionalized to interact with other chemicals. Modifications through fluorescence, functional peptide, and photoreactors, mentioned in Chapter 1 [42-46] are typical examples. The detection

of various chemicals using aptamers has also been reported [89-94] and may be used to functionalize DNA.

Integrating these techniques for DNA will materialize artificial self-assembly system inspired by biological development. Such technology is expected to contribute to the development of building non-biological tissues such as artificial organs. Furthermore, this technology may develop large-scale, higher-order systems. Progress in related areas such as large-scale DNA synthesis, artificial metabolism [95], and chemical AI technology [96] will pave the way to develop not only artificial tissues but also intelligent life-like systems in the future.

Funding

This work was supported by JPSP KAKENHI (Grants-in-Aid for Scientific Research) Grant Numbers JP15H01715, JP18K19830, JP19J20990, JP24104005, and JP20H00618, JP18K18144, JP19KK0261, JP20H05971, JP20K20979, JP20H05969.

Reference

[1] Wolpert, L., Tickle, C., & Arias, A. M. *Principles of development*. Oxford University Press, USA, (2015).

[2] Wolpert, L. *Developmental biology: A very short introduction*. OUP Oxford, (2011).

[3] Kondo, S., & Asai, R. A reaction–diffusion wave on the skin of the marine angelfish Pomacanthus. *Nature*, *376*(6543), 765. (1995).

[4] Meinhardt, H. *The algorithmic beauty of sea shells*. Springer Science & Business Media. (2009).

[5] Turing, A. M. The chemical theory of morphogenesis. *Phil. Trans. R. Soc.* B**237**, 37–72. (1952).

[6] Kondo, S., & Miura, T. Reaction-diffusion model as a framework for understanding biological pattern formation. *science*, *329*(5999), 1616-1620. (2010).

[7] A. Einstein, [AdP 17, 549 (1905)]. *Annalen der Physik*, 2005, **14.S1 1**, 182-193.

[8] Sutherland, W. (1905). LXXV. A dynamical theory of diffusion for non-electrolytes and the molecular mass of albumin. *The London, Edinburgh, and Dublin Philosophical Magazine and Journal of Science*, *9*(54), 781-785.

[9] Belousov, B. P. An oscillating reaction and its mechanism. *Sborn. referat. radiat. med.*, *145*. (1959).

[10] Zhabotinsky, A. M. Periodical oxidation of malonic acid in solution (a study of the Belousov reaction kinetics). *Biofizika*, 9, 306-311. (1964).

[11] Zaikin, A. N., & Zhabotinsky, A. M. Concentration wave propagation in two-dimensional liquid-phase self-oscillating system. *Nature*, *225*(5232), 535-537. (1970)

[12] Zhabotinsky, A. M., & Zaikin, A. N. Spatial effects in a self-oscillating chemical system. *Oscillatory processes in biological and chemical systems II*. (1971).

[13] Adamatzky, A., and Costello, B. L., On some limitations of reaction–diffusion chemical computers in relation to Voronoi diagram and its inversion. *Physics Letters A* 309.5-6 (2003): 397-406.

[14] Boekhoven, J., Poolman, J. M., Maity, C., Li, F., Van Der Mee, L., Minkenberg, C. B., ... & Eelkema, R. Catalytic control over supramolecular gel formation. *Nature chemistry*, *5*(5), 433. (2013).

[15] Lovrak, M., Hendriksen, W. E., Maity, C., Mytnyk, S., van Steijn, V., Eelkema, R., & van Esch, J. H. Free-standing supramolecular hydrogel objects by reaction-diffusion. *Nature communications*, *8*, 15317. (2017).

[16] Lovrak, M., Hendriksen, W. E., Kreutzer, M. T., van Steijn, V., Eelkema, R., & van Esch, J. H. Control over the formation of supramolecular material objects using reaction–diffusion. *Soft matter*. (2019).

[17] Sirimungkala, A., Försterling, H. D., Dlask, V., & Field, R. J. Bromination Reactions Important in the Mechanism of the Belousov− Zhabotinsky System. *The Journal of Physical Chemistry A*, 103(8), 1038-1043. (1999).

[18] Bánsági Jr, T., Leda, M., Toiya, M., Zhabotinsky, A. M., & Epstein, I. R. "High-frequency oscillations in the Belousov− Zhabotinsky reaction." *The Journal of Physical Chemistry A*, 113(19), 5644-5648. (2009).

[19] Seeman, Nadrian C. "DNA nanotechnology: novel DNA constructions." *Annual review of biophysics and biomolecular structure* 27, 225. (1998)

[20] Seeman, Nadrian C., and Hanadi F. Sleiman. "DNA nanotechnology." *Nature Reviews Materials* 3.11-23. (2017)

[21] Murata, S., Konagaya, A., Kobayashi, S., Saito, H., & Hagiya, M. "Molecular robotics: A new paradigm for artifacts." *New Generation Computing*, *31*(1), 27-45. (2013).

[22] Murata, S. (Ed.). *Molecular Robotics: An Introduction.* Springer, (2022)

[23] Watson, James D., and Francis HC Crick. "The structure of DNA." *Cold Spring Harbor symposia on quantitative biology*. Vol. 18. Cold Spring Harbor Laboratory Press, (1953).

[24] Dirks, R. M., & Pierce, N. A. "A partition function algorithm for nucleic acid secondary structure including pseudoknots". *Journal of computational chemistry*, 24(13), 1664-1677. (2003).

[25] SantaLucia, J., Allawi, H. T., & Seneviratne, P. A. “Improved nearest-neighbor parameters for predicting DNA duplex stability”. *Biochemistry*, 35(11), 3555-3562. (1996).

[26] SantaLucia, J. “A unified view of polymer, dumbbell, and oligonucleotide DNA nearest-neighbor thermodynamics”. *Proceedings of the National Academy of Sciences*, 95(4), 1460-1465. (1998).

[27] R. M. Dirks, J. S. Bois, J. M. Schaeffer, E. Winfree, and N. A. Pierce. “Thermodynamic analysis of interacting nucleic acid strands”. *SIAM Rev*, 49:65-88, (2007).

[28] R. M. Dirks and N. A. Pierce. A partition function algorithm for nucleic acid secondary structure including pseudoknots. J Comput Chem, 24:1664-1677, (2003).

[29] R. M. Dirks and N. A. Pierce. An algorithm for computing nucleic acid base-pairing probabilities including pseudoknots. *J Comput Chem*, 25:1295-1304, (2004).

[30] Antao, V. P., & Tinoco Jr, I. (1992). Thermodynamic parameters for loop formation in RNA and DNA hairpin tetraloops. *Nucleic acids research*, *20*(4), 819-824.

[31] Zhang, D. Y., & Winfree, E. “Control of DNA strand displacement kinetics using toehold exchange”. *Journal of the American Chemical Society*, 131(47), 17303-17314. (2009).

[32] Zhang, David Yu, and Georg Seelig. "Dynamic DNA nanotechnology using strand-displacement reactions." *Nature chemistry* 3.2, 103. (2011).

[33] Okamoto, A., Tanaka, K., & Saito, I. DNA logic gates. *Journal of the American Chemical Society*, 126(30), 9458-9463. (2004).

[34] Chen, X. Expanding the rule set of DNA circuitry with associative toehold activation. *Journal of the American Chemical Society*, *134*(1), 263-271. (2011).

[35] Srinivas, N., Parkin, J., Seelig, G., Winfree, E., & Soloveichik, D. Enzyme-free nucleic acid dynamical systems. *Science*, *358*(6369), eaal2052. (2017).

[36] Seelig, G., Soloveichik, D., Zhang, D. Y., & Winfree, E. "Enzyme-free nucleic acid logic circuits." *science*, *314*(5805), 1585-1588. (2006).

[37] D. Soloveichik, G. Seelig and E. Winfree, "DNA as a universal substrate for chemical kinetics." *Proc. Natl. Acad. Sci. U. S. A.,* 107(12), 5393 – 5398. (2010).

[38] Katz, E. (Ed.). *DNA-and RNA-based Computing Systems*. John Wiley & Sons. (2020).

[39] Markham, N. R., & Zuker, M. (2005). DINAMelt web server for nucleic acid melting prediction. *Nucleic acids research, 33*(suppl_2), W577-W581.

[40] Zadeh, J. N., Steenberg, C. D., Bois, J. S., Wolfe, B. R., Pierce, M. B., Khan, A. R., ... & Pierce, N. A. (2011). NUPACK: analysis and design of nucleic acid systems. *Journal of computational chemistry, 32*(1), 170-173.

[41] Lakin, M. R., Youssef, S., Polo, F., Emmott, S., & Phillips, A. Visual DSD: a design and analysis tool for DNA strand displacement systems. *Bioinformatics, 27*(22), 3211-3213. (2011).

[42] Madsen, M., & Gothelf, K. V. Chemistries for DNA nanotechnology. *Chemical reviews*, *119*(10), 6384-6458. (2019).

[43] El-Sagheer, A. H., & Brown, T. Click chemistry with DNA. *Chemical Society Reviews*, *39*(4), 1388-1405. (2010).

[44] Klabenkova, K., Fokina, A., & Stetsenko, D. (2021). Chemistry of peptide-oligonucleotide conjugates: A review. *Molecules*, *26*(17), 5420.

[45] Wang, K., Tang, Z., Yang, C. J., Kim, Y., Fang, X., Li, W., ... & Tan, W. Molecular engineering of DNA: molecular beacons. *Angewandte Chemie International Edition*, *48*(5), 856-870. (2009).

[46] Gogoi, K., Mane, M. V., Kunte, S. S., & Kumar, V. A. A versatile method for the preparation of conjugates of peptides with DNA/PNA/analog by employing chemo-selective click reaction in water. *Nucleic acids research*, *35*(21), e139-e139. (2007).

[47] Kamiya, Y., & Asanuma, H. Light-driven DNA nanomachine with a photoresponsive molecular engine. *Accounts of chemical research*, *47*(6), 1663-1672. (2014).

[48] Yoshimura, Y., & Fujimoto, K. Ultrafast reversible photo-cross-linking reaction: toward in situ DNA manipulation. *Organic letters*, *10*(15), 3227-3230. (2008).

[49] Fujimoto, K., Sasago, S., Mihara, J., & Nakamura, S. DNA photo-cross-linking using pyranocarbazole and visible light. *Organic letters*, *20*(10), 2802-2805. (2018).

[50] Ordoukhanian, P., & Taylor, J. S. Design and synthesis of a versatile photocleavable DNA building block. Application to phototriggered hybridization. *Journal of the American Chemical Society*, *117*(37), 9570-9571. (1995).

[51] Thoo, P. K., & Brown, D. M. Synthesis of oligodeoxyribonucleotides containing degenerate bases and their use as primers in the polymerase chain reaction. *Nucleic acids research*, *20*(19), 5149-5152. (1992).

[52] Hirao, I., Kimoto, M., Mitsui, T., Fujiwara, T., Kawai, R., Sato, A., ... & Yokoyama, S. An unnatural hydrophobic base pair system: site-specific incorporation of nucleotide analogs into DNA and RNA. *Nature Methods*, *3*(9), 729-735. (2006).

[53] Hirao, I., Mitsui, T., Kimoto, M., & Yokoyama, S. An efficient unnatural base pair for PCR amplification. *Journal of the American Chemical Society*, *129*(50), 15549-15555. (2007).

[54] Montagne, K., Plasson, R., Sakai, Y., Fujii, T., & Rondelez, Y. Programming an in vitro DNA oscillator using a molecular networking strategy. *Molecular systems biology*, *7*(1), 466. (2011).

[55] Padirac, A., Fujii, T., & Rondelez, Y. Quencher-free multiplexed monitoring of DNA reaction circuits. *Nucleic acids research*, *40*(15), e118-e118. (2012).

[56] Baccouche, A., Montagne, K., Padirac, A., Fujii, T., & Rondelez, Y. Dynamic DNA-toolbox reaction circuits: A walkthrough. *Methods*, *67*(2), 234-249. (2014).

[57] Fujii, T., & Rondelez, Y. Predator–prey molecular ecosystems. *ACS nano*, *7*(1), 27-34. (2013).

[58] Lotka, A. J. Undamped oscillations derived from the law of mass action. *Journal of the american chemical society*, *42*(8), 1595-1599. (1920).

[59] Volterra, V. Fluctuations in the abundance of a species considered mathematically. *Nature*, *119*(2983), 12-13. (1927).

[60] Padirac, A., Fujii, T., Estévez-Torres, A., & Rondelez, Y. Spatial waves in synthetic biochemical networks. *Journal of the American Chemical Society*, *135*(39), 14586-14592. (2013).

[61] Zadorin, A. S., Rondelez, Y., Gines, G., Dilhas, V., Urtel, G., Zambrano, A., ... & Estévez-Torres, A. Synthesis and materialization of a reaction–diffusion French flag pattern. *Nature chemistry*, 9(10), 990. (2017).

[62] Wolpert, Lewis. "Positional information and the spatial pattern of cellular differentiation." *Journal of theoretical biology* 25.1 1-47. (1969).

[63] Scalise, D., & Schulman, R. Designing modular reaction-diffusion programs for complex pattern formation. *Technology*, 2(01), 55-66. (2014).

[64] Qian, L., & Winfree, E. Scaling up digital circuit computation with DNA strand displacement cascades. *science*, *332*(6034), 1196-1201. (2011).

[65] Chen, Y. J., Dalchau, N., Srinivas, N., Phillips, A., Cardelli, L., Soloveichik, D., & Seelig, G. Programmable chemical controllers made from DNA. *Nature nanotechnology*, *8*(10), 755-762. (2013).

[66] Cherry, K. M., & Qian, L. Scaling up molecular pattern recognition with DNA-based winner-take-all neural networks. *Nature*, *559*(7714), 370-376. (2018).

[67] Eimer, W., & Pecora, R. J. Rotational and translational diffusion of short rodlike molecules in solution: oligonucleotides. *The Journal of chemical physics*, *94*(3), 2324-2329. (1991).

[68] Zenk, J., Scalise, D., Wang, K., Dorsey, P., Fern, J., Cruz, A., & Schulman, R. Stable DNA-based reaction–diffusion patterns. *RSC Advances*, *7*(29), 18032-18040. (2017).

[69] Dorsey, P. J., Scalise, D., & Schulman, R. DNA Reaction–Diffusion Attractor Patterns. *Angewandte Chemie*, *133*(1), 342-348. (2021).

[70] Chirieleison, S. M., Allen, P. B., Simpson, Z. B., Ellington, A. D., & Chen, X. Pattern transformation with DNA circuits. *Nature chemistry*, *5*(12), 1000-1005. (2013).

[71] Hosoya, T., Kawamata, I., Nomura, S. I. M., & Murata, S. Pattern formation on discrete gel matrix based on DNA computing. *New Generation Computing*, *37*(1), 97-111. (2019).

[72] Hagiya, M., Wang, S., Kawamata, I., Murata, S., Isokawa, T., Peper, F., Imai, K.: On DNA-based gellular automata. Lect. Notes Comput. Sci. 8553, 177. (2014).

[73] Takabatake, F., Kawamata, I., Sugawara, K., & Murata, S. Discretization of chemical reactions in a periodic cellular space. New Generation Computing, *35*(3), 213-223. (2017).

[74] Kawamata, I., Hosoya, T., Takabatake, F., Sugawara, K., Nomura, S.I., Isokawa, T., Peper, F., Hagiya, M., Murata, S.: Pattern formation and computation by autonomous chemical reaction diffusion model inspired by cellular automata. In: The Fourth International Symposium on Computing and Networking, pp. 215–221. (2016).

[75] Urtel, G., Estevez-Torres, A., & Galas, J. C. DNA-based long-lived reaction–diffusion patterning in a host hydrogel. *Soft matter*. (2019).

[76] Rodjanapanyakul, T., Takabatake, F., Abe, K., Kawamata, I., Nomura, S. M., & Murata, S. Diffusion modulation of DNA by toehold exchange. *Physical Review E, 97*(5), 052617. (2018).

[77] Tim Hutton, Robert Munafo, Andrew Trevorrow, Tom Rokicki, Dan Wills. "Ready, a cross-platform implementation of various reaction-diffusion systems."

[78] Tinland, B., Pluen, A., Sturm, J., & Weill, G. Persistence length of single-stranded DNA. *Macromolecules, 30*(19), 5763-5765. (1997).

[79] Kitajima, T., Takinoue, M., Shohda, K. I., & Suyama, A. Design of code words for DNA computers and nanostructures with consideration of hybridization kinetics. In *International Workshop on DNA-Based Computers* (pp. 119-129). Springer, Berlin, Heidelberg. (2007, June).

[80] Sato, Y., Hiratsuka, Y., Kawamata, I., Murata, S., & Nomura, S. I. M. Micrometer-sized molecular robot changes its shape in response to signal molecules. *Science Robotics*, *2*(4), eaal3735. (2017).

[81] Vyborna, Y., Galas, J. C., & Estevez-Torres, A. DNA-Controlled Spatiotemporal Patterning of a Cytoskeletal Active Gel. *Journal of the American Chemical Society*, *143*(48), 20022-20026. (2021).

[82] Senoussi, A., Galas, J. C., & Estévez-Torres, A. Programmed mechano-chemical coupling in reaction-diffusion active matter. *Science Advances*, *7*(51), eabi9865. (2021).

[83] Lin, D. C., Yurke, B., & Langrana, N. A. Mechanical properties of a reversible, DNA-crosslinked polyacrylamide hydrogel. *Journal of biomechanical engineering*, *126*(1), 104-110. (2004).

[84] Kandatsu, D., Cervantes-Salguero, K., Kawamata, I., Hamada, S., Nomura, S. I. M., Fujimoto, K., & Murata, S. Reversible Gel–Sol Transition of a Photo-Responsive DNA Gel. *ChemBioChem*, 17(12), 1118-1121. (2016).

[85] Murakami, Y., & Maeda, M. DNA-responsive hydrogels that can shrink or swell. *Biomacromolecules*, 6(6), 2927-2929. (2005).

[86] Karacan, P., Cakmak, H., & Okay, O. Swelling behavior of physical and chemical DNA hydrogels. *Journal of applied polymer science*, *128*(5), 3330-3337. (2013).

[87] Cangialosi, A., Yoon, C., Liu, J., Huang, Q., Guo, J., Nguyen, T. D., ... & Schulman, R. DNA sequence–directed shape change of photopatterned hydrogels via high-degree swelling. *Science*, *357*(6356), 1126-1130. (2017).

[88] Lee, J. B., Peng, S., Yang, D., Roh, Y. H., Funabashi, H., Park, N., ... & Luo, D. A mechanical metamaterial made from a DNA hydrogel. *Nature nanotechnology*, *7*(12), 816-820. (2012).

[89] Zhu, Z., Wu, C., Liu, H., Zou, Y., Zhang, X., Kang, H., ... & Tan, W. An aptamer cross-linked hydrogel as a colorimetric platform for visual detection. *Angewandte Chemie International Edition*, *49*(6), 1052-1056. (2010).

[90] Dirks, R. M., & Pierce, N. A. Triggered amplification by hybridization chain reaction. *Proceedings of the National Academy of Sciences*, *101*(43), 15275-15278. (2004).

[91] Simmel, F. C., Yurke, B., & Singh, H. R. Principles and applications of nucleic acid strand displacement reactions. *Chemical reviews*, *119*(10), 6326-6369. (2019).

[92] Song, W., Zhu, K., Cao, Z., Lau, C., & Lu, J. Hybridization chain reaction-based aptameric system for the highly selective and sensitive detection of protein. *Analyst*, *137*(6), 1396-1401. (2012).

[93] Zhao, J., Chen, C., Zhang, L., Jiang, J., & Yu, R. An electrochemical aptasensor based on hybridization chain reaction with enzyme-signal amplification for interferon-gamma detection. *Biosensors and Bioelectronics*, *36*(1), 129-134. (2012).

[94] Bai, L., Chai, Y., Yuan, R., Yuan, Y., Xie, S., & Jiang, L. Amperometric aptasensor for thrombin detection using enzyme-mediated direct electrochemistry and DNA-based signal amplification strategy. *Biosensors and Bioelectronics*, *50*, 325-330. (2013).

[95] Hamada, S., Yancey, K. G., Pardo, Y., Gan, M., Vanatta, M., An, D., ... & Luo, D. Dynamic DNA material with emergent locomotion behavior powered by artificial metabolism. *Science Robotics*, *4*(29), eaaw3512. (2019).

[96] Murata, S., Toyota, T., Nomura, S. I. M., Nakakuki, T., & Kuzuya, A. Molecular Cybernetics: Challenges toward Cellular Chemical Artificial Intelligence. *Advanced Functional Materials*, *32*(37), 2201866. (2022).

Appendix

A.1 DNAs used in Chapter 2 and 3

DNA strands expected to be acrydite-modified were purchased from Eurofins Genomics Japan, Tokyo, Japan. The acrydite-modified DNA was purchased from Integrated DNA Technologies, Coralville, IA, USA. The purification was HPLC for DNAs with modifications and OPC for others. The samples were hydrated with MilliQ water.

The base sequence is listed in Figure A1.1. There are reaction domain names under the sequences and unnamed parts are spacers for adjusting the lengths. The complementary domain of “x” is described as “$\overline{x}$”. The roles of domains are as follows.

Domain "a": Toehold for strand displacement in AND gate reactions

Domain "b": Binding the input A and B

Domain "c": Binding the input A to connector (see Figure S3-2)

Domain "d": Migrated domain for diffusion modulation

Domain "e": Toehold of input A for diffusion modulation

Domain "g": Connecting input B and AND gate

Domain "j": Binding strands and anchor

Domain "k": Toehold for starter (see Figure S3-2)

Domain "l": Toehold of competitor A for diffusion modulation

Domains "h," "I," "m": Domains of input B for diffusion modulation

input A (60 nt): [FAM] CTTGAGGAGAAACTTAGACCGTAACCACTCTGCGACCACTATGACGGTCTCATCAATAGC
a b c d e

input B (60 nt): : CTCAAGGTGGTTACGGTCTAAGTTTCTCTCCTGATGCCTACGAACACCAGTTTCCAGAGT [TAM]
ā b̄ g h i

Gate strand 1 (56 nt): GTTCGTAGGCATCAGCTCAAGTTTTTTTTTTCAAAGACACCACGGAATAAGTTTAT
ḡ ā j

Gate strand 2 (15 nt): CTGATGCCTACGAAC
g

Anchor (31 nt): [Acrydite]TTTTTATAAACTTATTCCGTGGTGTCTTTGC
j

Connector A (56 nt): GTCATAGTGGTCGCAGGACTCTTTTTTTTTTCAAAGACACCACGGAATAAGTTTAT
c̄ k̄ j

Connector B (56 nt): GTTCGTAGGCATCAGGGACTCTTTTTTTTTTCAAAGACACCACGGAATAAGTTTAT
ḡ k̄ j

Starter A (21 nt): GAGTCCTGCGACCACTATGAC
k c

Starter B (21 nt): GAGTCCCTGATGCCTACGAAC
k g

Competitor A (16 nt): TCTGTCGGTCTCATCA
l d

Trap A (25 nt): [Acrydite] TTGCTATTGATGAGACCGACAGACT
ē d l

Competitor B (16 nt): GCCATTACCAGTTTCC
m h

Trap B (25 nt): [Acrydite] TTACTCTGGAAACTGGTAATGGCTC
i h̄ m̄

Figure A.1 DNA sequences used in Chapter 2 and 3.

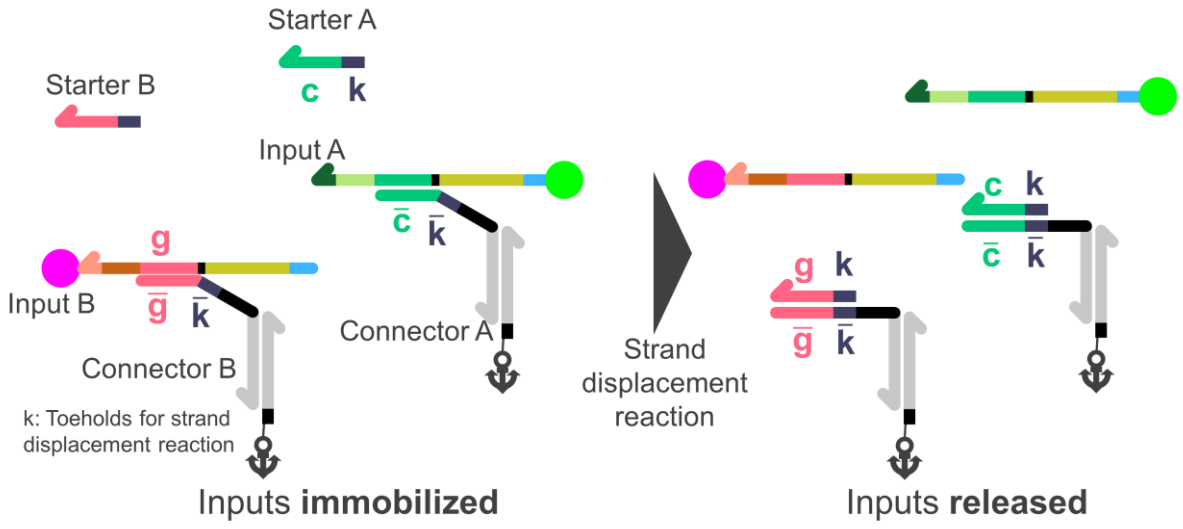

Figure A.2 Input releasing reaction initiated by starters.

A.2 Hybridization of anchoring DNA in hydrogel

To evaluate the reactivity of the anchored DNA, we measured the melting temperature (Tm) and folding temperature (Tf) in the hydrogel. The free single-stranded DNA was prepared in the solution and added to the hydrogel at the end because it diffuses into the $CaCl_2$ solution during alginate gel preparation. Therefore, the reaction in the surrounding solution affects the result for the no polymerization and in-gel conditions.

Figure A.3 shows the results of eight measurements. Tf is slightly lower than Tm both with and without polyacrylamide bonding (polymer and monomer) and the differences are higher after polymerization, indicating that the hybridization occurring in the presence of polyacrylamide is difficult to melt. This is because the polymer around the DNA inhibits double-stranded DNA dissociation.

Both Tm and Tf were slightly lower in the hydrogel than those in solution because the alginate polymers in the hydrogel inhibited the interaction with DNA. Although the maximum difference is approximately 7℃, it is still high compared to the temperature (25℃) at which the experiment was conducted; therefore, the effect on the pattern formation is small.

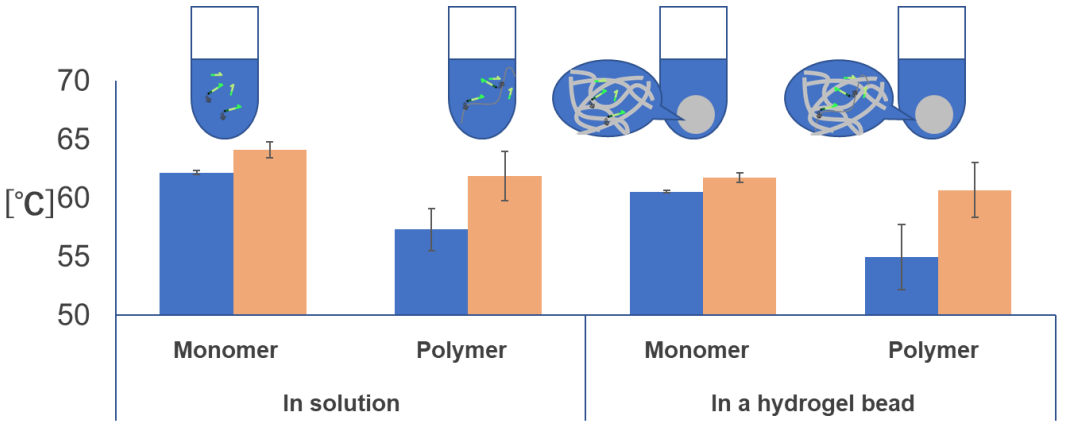

Tm	Average	SD	SE		Average	SD	SE		Average	SD	SE		Average	SD	SE	
	62.19	0.43	0.15		57.31	5.04	0.11		60.56	0.30	0.11		55.00	7.87	2.78	
	63	62	62.5	61.5	61.5	60.5	61.5	51	60.5	60.5	60.5	60.5	58	42	60.5	41
	62.5	62	62	62	61.5	50	61	51.5	61	60.5	61	60	60.5	58.5	61	58.5

Tf	Average	SD	SE		Average	SD	SE		Average	SD	SE		Average	SD	SE	
	64.13	1.98	0.70		61.88	5.97	2.11		61.75	1.21	0.43		60.69	6.62	2.34	
	64.5	64	64.5	64.5	64	64	65	55.5	61.5	62	62	61.5	61.5	60	62	52
	64	63.5	64.5	63.5	63.5	55	64	64	61.5	62	62	61.5	62.5	62.5	62.5	62.5

Figure. A.3 Melting temperature (Tm) and folding temperature (Tf) of the anchor DNA in solution and a hydrogel bead

A.3 Image processing for the results described in Chapter 2 and 3

The images in the experiment were obtained using a Nikon TE2000-U (Nikon, Tokyo, Japan) fluorescence microscope. The reaction–diffusion systems were built in 7×6×1 mm^3 and 5×5×5 mm^3 chambers made of silicon rubber sheet on glass for bisector patterns and weighted Voronoi diagrams, respectively. Image processing and analysis were performed using Fiji, an image-processing software (https://fiji.sc/).

A.3.1 Composition of images to visualize pattern formation process

The green and red fluorescence images were obtained separately and composited after normalizing the brightness for Figures 2.8, 2.9, 3.4, 3.5, and 3.7 (Figure A.4).

A.3.2 Kymographs

The kymographs show the temporal variation in the fluorescence intensity between sources indicating the pattern formation process. To obtain these, lines were drawn between the diffusion sources and the fluorescence intensity on the lines was measured for each time step in both channels. Intensity $\mathrm{F_{raw}}$ was normalized using the following equation:

$$\mathrm{F}(c,x,t) = 255 * \frac{\mathrm{F_{raw}}(c,x,t)}{\max\limits_{\mathrm{x}} \mathrm{F_{raw}}(c,x,t)},$$

where $c, x,$ and t represent the channel (green or red), position ($0 \leq x \leq 1$), and time ($0 \leq t \leq 360$ [min]), respectively. The $\max\limits_{\mathrm{x}} \mathrm{F_{raw}}(c,x,t)$ represents the maximum intensity at time step. The normalized values $\mathrm{F}(c,x,t)$ were plotted, composed, and resized to 512 ×512 pixels (Figure A.5).

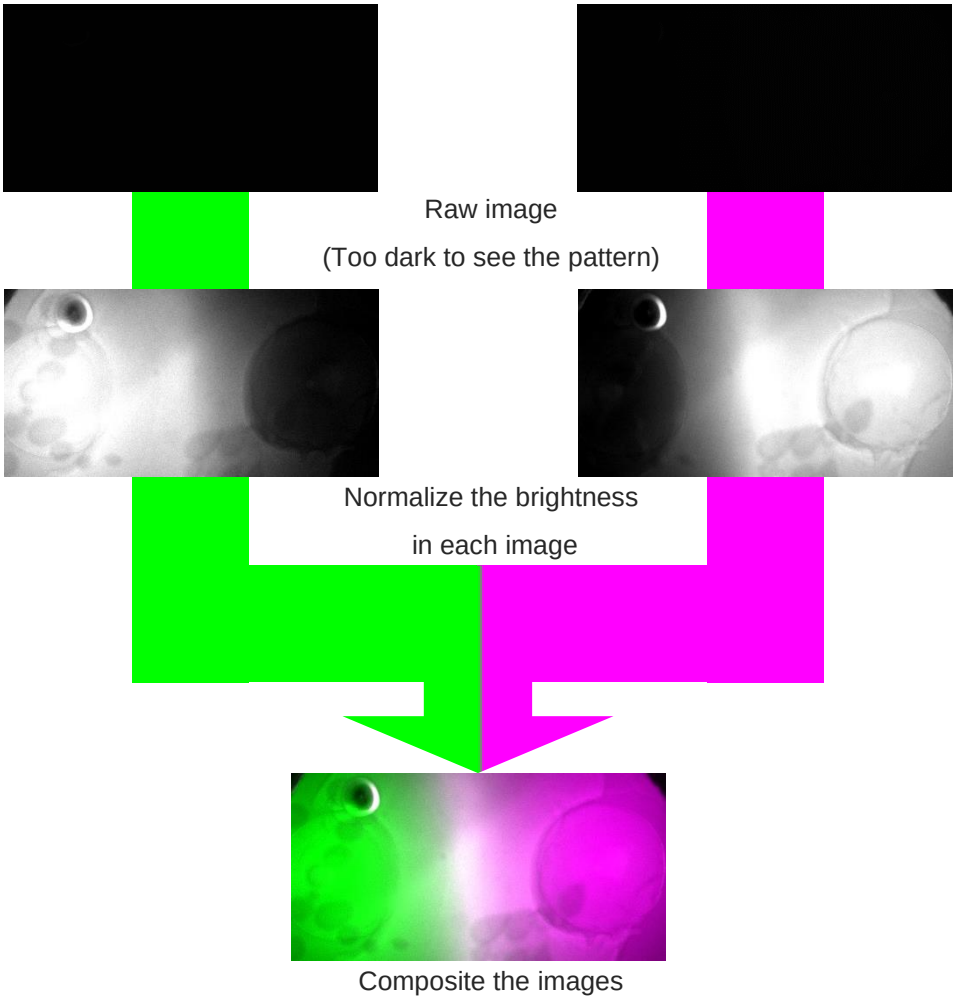

Figure A.4 Image-processing flow.

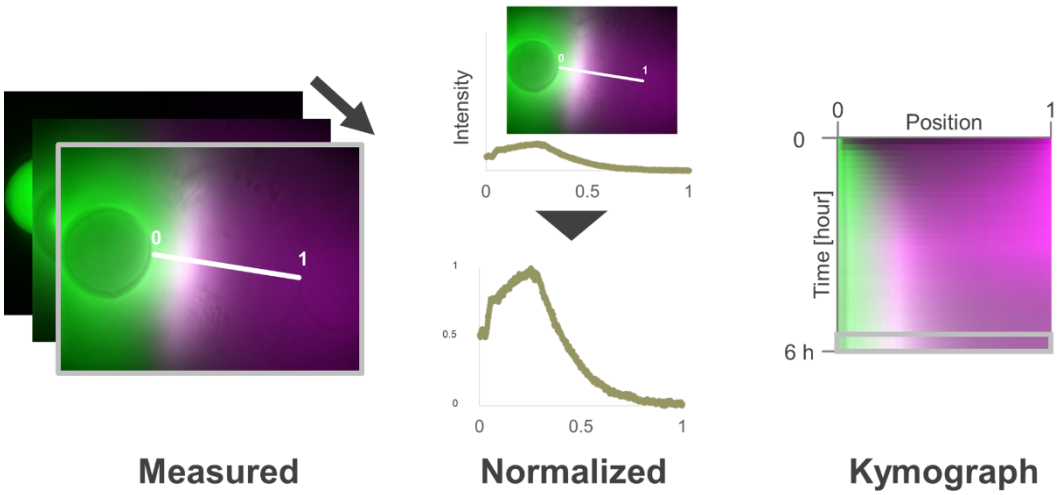

Figure A.5 Image processing for kymograph.

A.4 FRET caused by the input reaction

The FAM and TAMRA used for imaging inputs A and B undergo Förster resonance energy transfer (FRET); therefore the effect of FRET was evaluated. The effect of FRET on FAM due to the reaction between the inputs was confirmed by fluorescence spectral analysis using a spectrofluorometer (JASCO FP-6200). The fluorescence spectrum between 510 and 700 nm when a 945 nm emission irradiation was used. The intensities were normalized from 0 to 1 with respect to the maximum excitation radiation intensity.

Figure A.6 shows that FAM excited TAMRA and reduced the fluorescence intensity at 519 nm by 73.5%. FAM-tagged input A showed one peak around 519 nm, while input B showed no significant peak. In contrast, when the inputs reacted, two peaks appeared in the spectrum. The peak near 519 nm represents the fluorescence of FAM, which is weaker than that of input A. The peak near 580 nm represents the fluorescence of TAMRA.

Then, to investigate the FRET effect on the pattern, in Figure A.7, the spatial green fluorescence intensity in the pattern formation was corrected as follows:

$$\mathrm{F_{correct}}(\mathrm{green}, x, 360) = \begin{cases} \dfrac{\mathrm{F_{raw}}(\mathrm{red}, x, 360)}{Y} + \left(\mathrm{F_{raw}}(\mathrm{green}, x, 360) - \mathrm{F_{raw}}(\mathrm{red}, x, 360)\right) \\ \left(\mathrm{F_{raw}}(\mathrm{green}, x, 360) \geq \mathrm{F_{raw}}(\mathrm{red}, x, 360)\right), \\ \dfrac{\mathrm{F_{raw}}(\mathrm{green}, x, 360)}{Y} \\ \left(\mathrm{F_{raw}}(\mathrm{green}, x, 360) < \mathrm{F_{raw}}(\mathrm{red}, x, 360)\right), \end{cases}$$

where Y is the correction constant (0.265). However, it did not affect the position substantially. The uncorrected values are shown in Figure 3.6.

A.5 Effects of anchoring ratio to the pattern

Acrydite-modified DNA that fails to bind to polyacrylamide is not anchored. Assuming that such DNA remains in the hydrogel, we set the ratio of anchored DNA to 100%, 80%, and 50%, and investigated the effect of the anchoring ratio on bisector position by simulation. The diffusion coefficient was set such that the remaining DNA behaved as a single-stranded DNA.

Increasing anchoring ratio decrease the distance of the bisector to the midpoint between sources (Figure A.7). After matching, the parameter was set to 80% in the simulations.

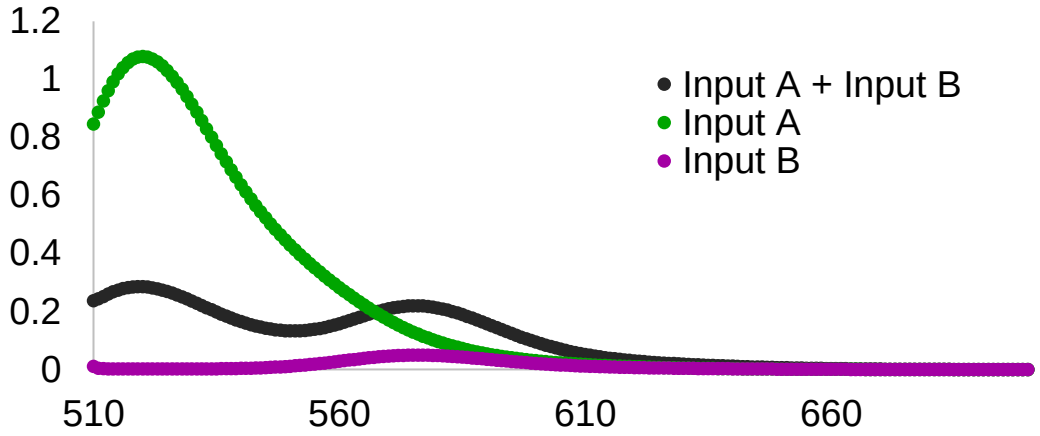

Figure A.6 Fluorescent spectrum of inputs.

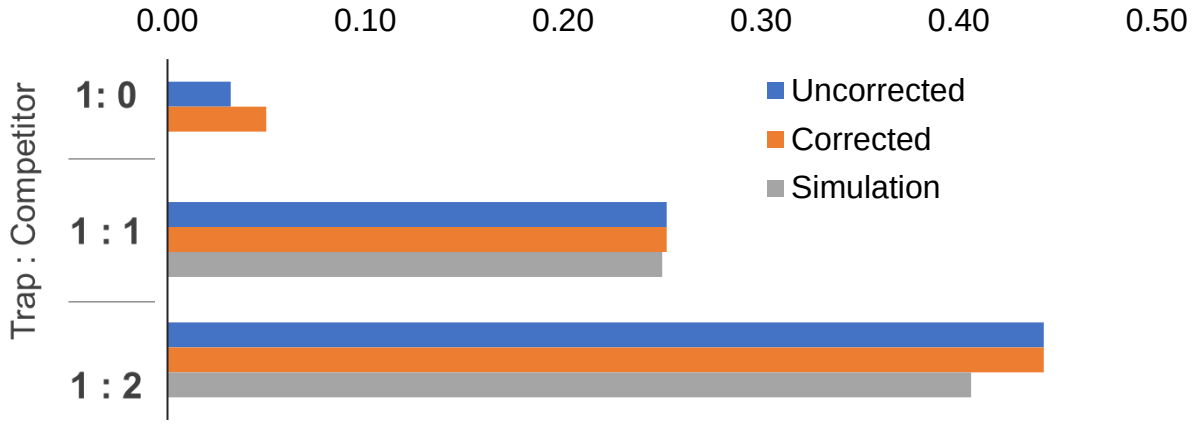

Figure A.7 Effects of FRET correction on bisector position.

Figure A.8 Effects of anchoring ratio on bisector position.

A.6 Polyaclylamide gel electrophoresis

The results of each electrophoresis were imaged using the Chemi Doc MP Imaging system (Bio-Rad, CA, USA). Blue Epi illumination and 530/38 filter, Green Epi illumination and 605/50 filter, and UV trans-illumination and standard filter were used for green, red and SYBR gold, respectively. When fluorescent-modified DNAs were used, the gel was imaged first, followed, by staining with SYBR gold for 20 min. The same protocol was used for electrophoresis in all chapters.

A.7 DNAs used in Chapter 4 and 5

The sequences are summarized in Table A.1. The DNA pairs were designed using the orthogonal sequences reported previously [79]. For the adjusters, the connector domains were complementary to the 15 bases from the 3' end of L1, R2, L3, or R4, and the domain not used in the reactions was filled with poly-T. Unmodified and FAM labeled DNA were purchased from Eurofins Genomics Japan (Tokyo, Japan) with an Oligonucleotide Purification Cartridge (OPC) and HPLC purification, respectively. Other fluorescence-modified DNAs were purchased from Sangon Biotech Co., Ltd. (Shanghai, China) using HPLC purification. All samples were diluted in Milli-Q water to 100 μM and stored at −30℃. In the pattern formation experiment, 4μL 10 μM DNAs were prepared in a reaction buffer, as described in A.8, and poured into the pockets of the hydrogel.

A.8 Reaction buffer and hydrogel used in Chapter 4 and 5

In the experiments, DNAs was dissolved in reaction buffer containing 50 mM HEPES, 20 mM $MgCl_2$, and 100 mM NaCl (pH 7.13). The reaction buffer, 40% polyacrylamide, and 2% N,N’-methylenebis (acrylamide) were mixed to prepare a pre-gel solution of 10% polyacrylamide gel (C%=5). To the pre-gel, 10% APS and 10% TEMED were added at a ratio of 98:1:1 and poured quickly into the mold to prevent air bubbles. The comb was set to prepare pockets and incubated at room temperature (25°C) for 1h. Then, the DNA solutions were injected into the pockets and sealed with liquid paraffin to prevent evaporation.

40% polyacrylamide and 2% N,N'- methylenebis (acrylamide) were purchased from Bio-Rad Laboratories, Inc. (CA, USA). NaCl was purchased from Sigma Life Science, and others were purchased from FUJIFILM Wako Pure Chemical Corporation, (Osaka, Japan). The mold and comb were designed to fit a 5.2-cm diameter Petri dish using Free CAD as shown in Figure A.X. They are printed by the 3D printers (Anycubic Photon-5, Anycubic Photon Mono X, or Anycubic photon M3 Plus) and the mold was placed in the Petri dish before pouring the pre-gel solution.

A.9 Fluorescence microscopy in Chapter 4 and 5

The pattern formation process was observed using a Nikon TE2000-U with four filter units for four-channel observations (FAM, Cy5, Cy3, and AMCA) at 10 min intervals over 24 h. An automated stage (Shiguma Koki, Japan) was used to observe five parallel reaction fields simultaneously. Figure A.9 shows the pre-composite images of the cascaded pattern formation shown in Figure 5.7. Figure 5.7 does not directly show the temporal changes in Cy3- or Cy5-labeled DNAs because their observations were not assigned to a color in the composite images.

Table A.1 DNA sequences used for polymerization approach described in Chapter 4 and 5

L1	[FAM]GCATCTACACTCAATACCCAGCCCGTCTATTGCTTGTCACTTCCCC
R1	[Cy5] GGCTGGGTATTGAGTGTAGATGCGGGGAAGTGACAAGCAATAGACG
A0	GGGGAAGTGACAAGC
A46	TTTTTTTTTTTTTTTTTTTTTTTTTTTTTTTTTTTTTTTTTTTTTTGGGGAAGTGACAAGC
A92	TTTTTTTTTTTTTTTTTTTTTTTTTTTTTTTTTTTTTTTTTTTTTTTTTTTTTTTTTTTTTTTTTTTTTTTTTT TTTTTTTTTTTTTTTTTTGGGGAAGTGACAAGC
L2	[Cy3] CGCGACGATTTTAACATTCCTTCAGACACGTTATCAAGCACTTCTC
R2	[AMCA] GAAGGAATGTTAAAATCGTCGCGGAGAAGTGCTTGATAACGTGTCT
L3	[Cy3] GAGTCCGCAAAAATATAGGAGGCTTCGGTTCTCTCCAAAAAAAGCA
R3	GCCTCCTATATTTTTGCGGACTCTGCTTTTTTTGGAGAGAACCGAA
L4	AGGGGTCTTTAATAACACGACGGTCTTCCGACAGCTATAAGTGCCA
R4	[Cy5] CCGTCGTGTTATTAAAGACCCCTTGGCACTTATAGCTGTCGGAAGA
A46 for R2	TTTTTTTTTTTTTTTTTTTTTTTTTTTTTTTTTTTTTTTTTTTTTTAGACACGTTATCAAG
A46 for L3	TTTTTTTTTTTTTTTTTTTTTTTTTTTTTTTTTTTTTTTTTTTTTTGCTTTTTTTGGAGA
A46 for R4	TTTTTTTTTTTTTTTTTTTTTTTTTTTTTTTTTTTTTTTTTTTTTTCTTCCGACAGCTAT
AL1-L3	[Cy3]GAGTCCGCAAAAATATAGGAGGCTTCGGTTCTCTCCAAAAAAAGCAGGGGAAGTGACAAGC
AR2-R3	[Cy5]GCCTCCTATATTTTTGCGGACTCTGCTTTTTTTGGAGAGAACCGAAAGACACGTTATCAAG

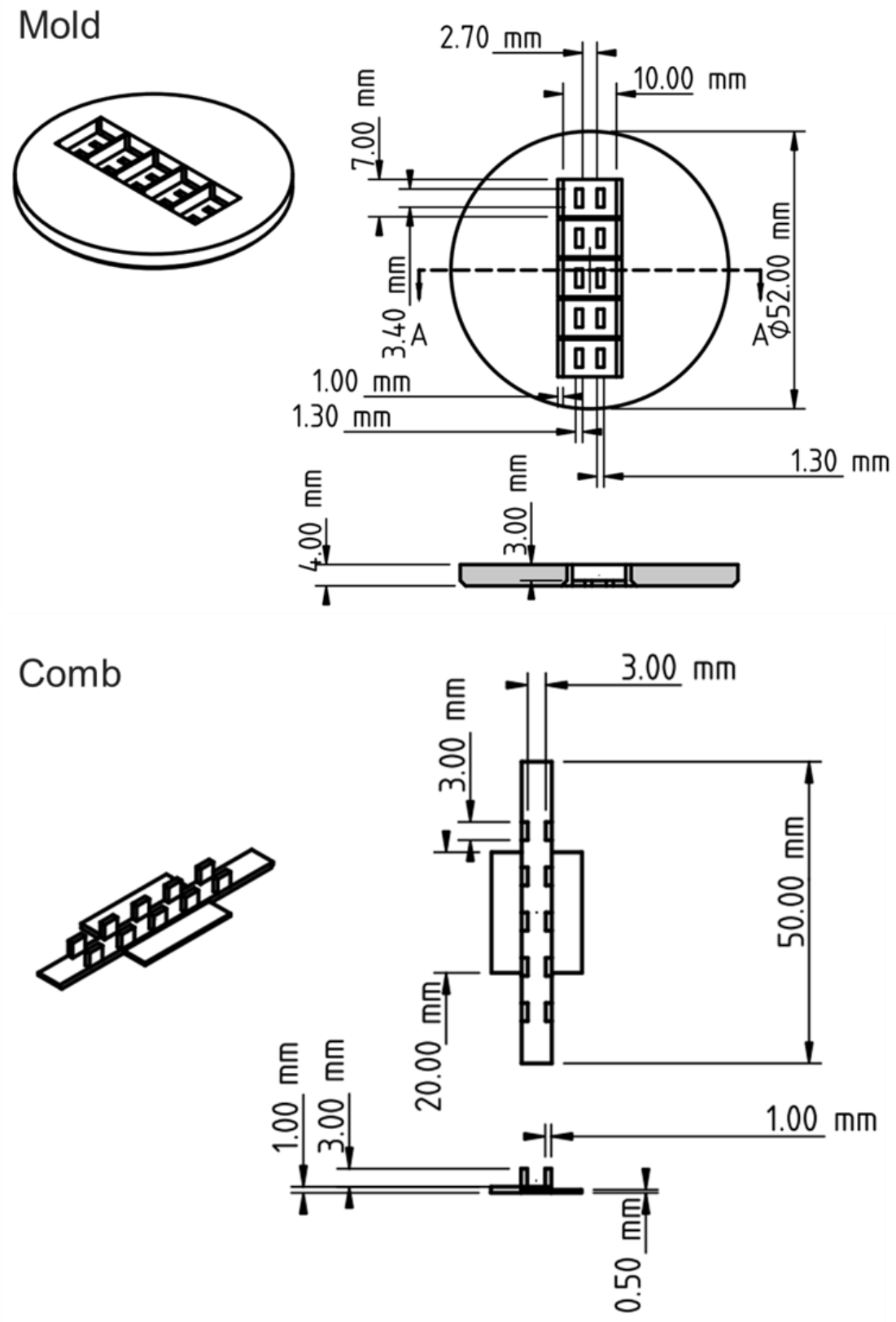

Figure A.8 Blueprint of a gel mold and comb for observation

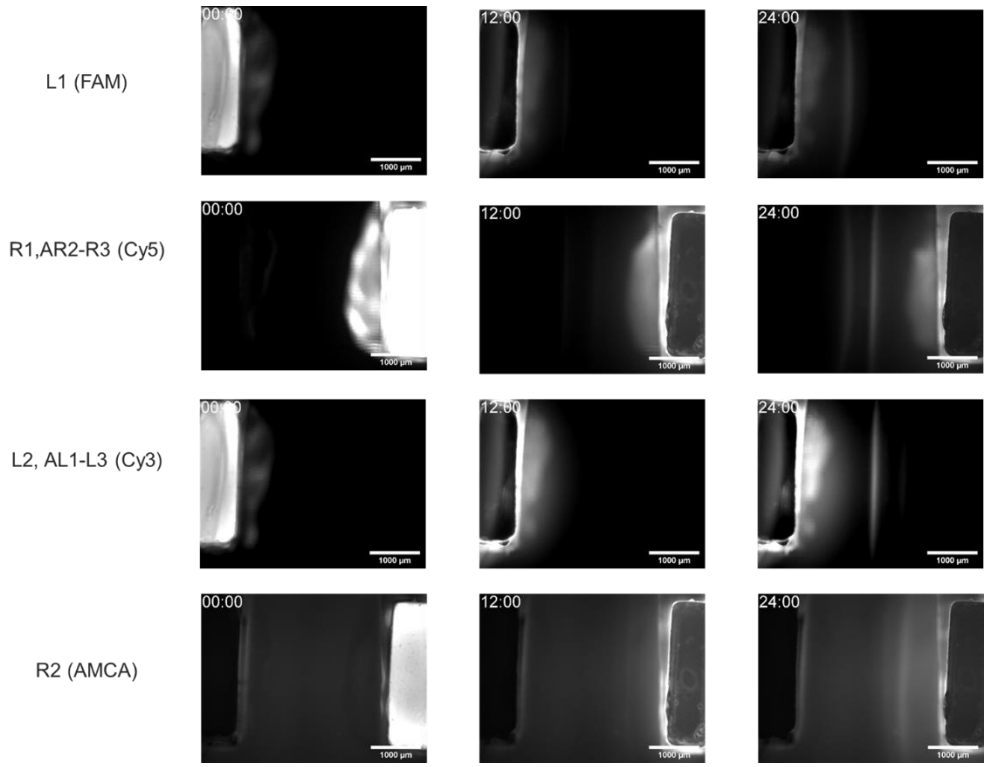

Figure A.9 Cascaded pattern in each channel

A.10 Analysis in FRAP experiment

In the FRAP procedure in 4.3.1, a solution of 9.5% acrylamide, 0.5% N,N'-methylenebis (acrylamide), and 5 µM DNA in a 10 µL volume was first prepared and incubated for 1 h at room temperature as the reaction time for the DNA. TEMED and APS were then added to 0.01% solution and incubated for 1 h at room temperature for gelation. The prepared gels were placed in a silicon chamber, covered with liquid paraffin to prevent evaporation, and optically stimulated with an Olympus FV3000 confocal unit attached to Olympus IX83 (Olympus, Tokyo, Japan) to measure the fluorescence recovery. The temporal change in the recovery was normalized as follows:

$$I_{norm}(t) = \frac{I_{\mathrm{bleach}}(t) - I_{\mathrm{bg}}(t)}{I_{\mathrm{pre}}(t) - I_{\mathrm{bg}}(t)},$$

where $I_{bleach}(t)$, $I_{pre}(t)$, and $I_{bg}(t)$ are the intensites of the bleached, unbleached, and background areas, respectively, as obtained from Figure A.10. As with pair 1, FRAP was also performed for pairs 2 and 3, which were used for cascaded pattern formation (Figure A.11).

The fluorescence recovery observed for each DNA was fitted as follows:

$$f(t) = \beta \exp\left(\frac{2\tau_D}{(t-\alpha)}\right)\left(I_0\left(\frac{2\tau_D}{(t-\alpha)}\right) + I_1\left(\frac{2\tau_D}{(t-\alpha)}\right)\right),$$

where $I_0(x)$ and $I_1(x)$ are modified Bessel functions, α is the time point at which fluorescence intensity becomes zero after light stimulation, β is the intensity at the plateau, and t is the time set to zero when the first image is obtained after stimulation. By incorporating τ_D, the characteristic time scale of diffusion, and ω, the radius of the bleaching zone can be expressed as

$$D = \frac{\omega^2}{4\tau_D}.$$

The obtained values are summarized in Table A.2. Interestingly, no fluorescence recovery was observed after mixing any of the three pairs, so the diffusion coefficient of the well-grown polymer in the hydrogel was assumed to be zero. The difference between the measured and fitted values in the simulation may be due to the inadequate FRAP setup. There were some issues, such as the homogeneity of the hydrogel and the fluorescence intensity did not reach zero due to photobleaching or did not fully recover to one.

A.11 DNA propagation in hydrogel medium

To prove that DNA strand propagation in the hydrogel was due to diffusion, L1 and R1 fluorescence was observed for 24 h (Figure A.12). The fluorescence intensity distribution at each time point was measured, and the position at which the fluorescence intensity exceeded the threshold was defined as the propagation front of the time point. The threshold values were set to 425, 200, and 20 for L1, R1, and simulation, respectively, based on the average intensity at each time point (Figure A.13).

A comparison with the simulation at each time point based on a graph plotting time on the horizontal axis and propagation front position on the vertical axis shows that the average difference was 96 and 88 μm for L1 and R1, respectively (Figure A.14). The resolution of the fluorescence microscopy images and simulation were 3.2 and 23 μm/pixel (4489 μm/1392

pixels and 3000 μm/128 pixels, respectively). This error was less than 5 pixels for the simulation. As only diffusion was computed in the simulation, this similarity suggests that L1 and R1 propagate through the hydrogel by diffusion.

A.12 Bisector pattern formation using A-pair 3

To compare the difference between pair 1 and A-pair 3, which has 46 nt and 61 nt, respectively, we observed bisector pattern formation using A-pair 3. The bisector pattern of A-pair 3 formed slower than that of pair 1 (the intensity of pair 1 and A-pair 3 reached 0.05 in 4.3 and 15 h, respectively; Figure A.15), but clearly faster than the cascaded process (Figure 5.9).

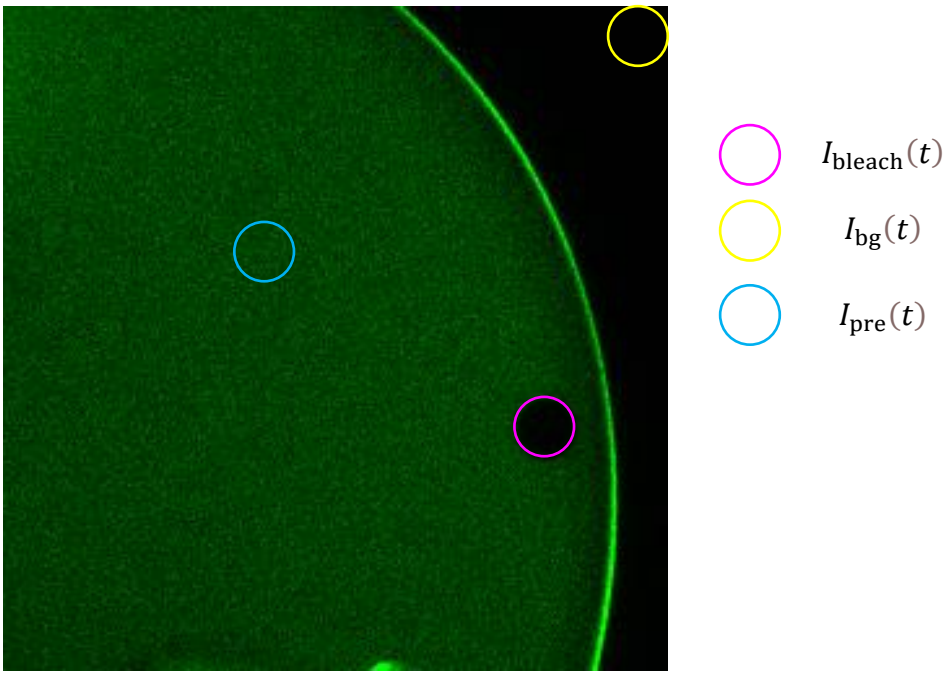

Figure A.10 Referring areas for FRAP analysis

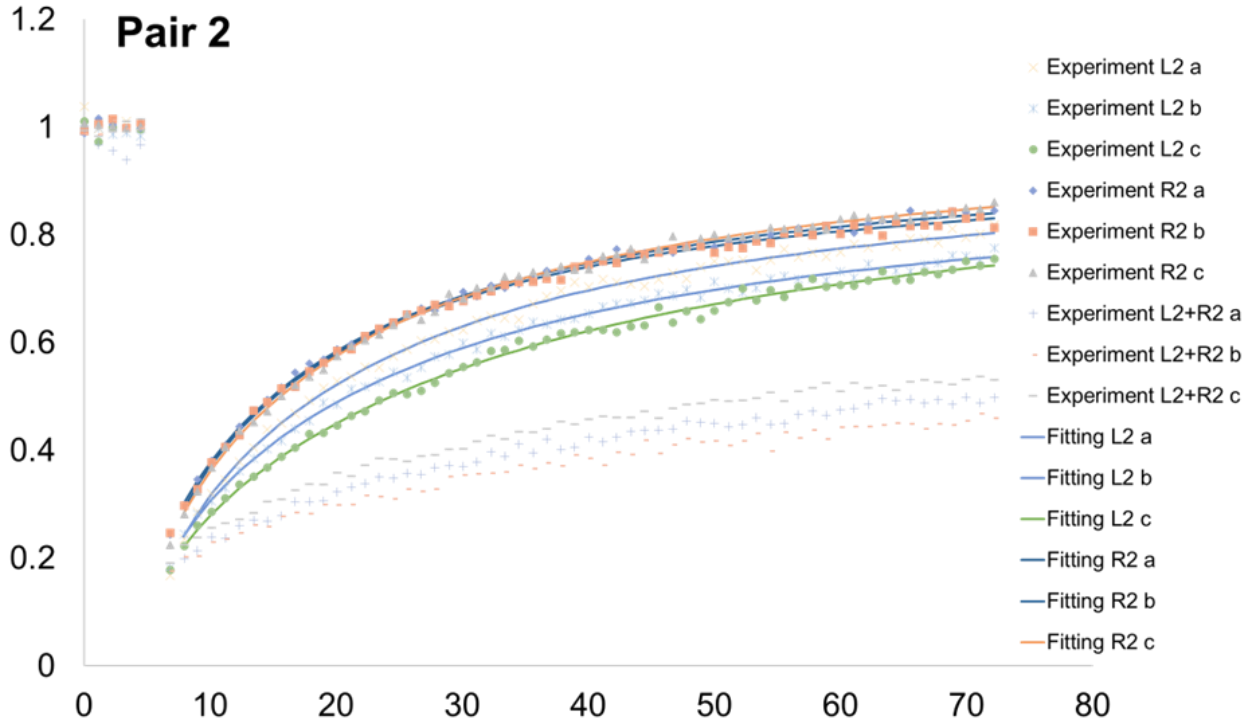

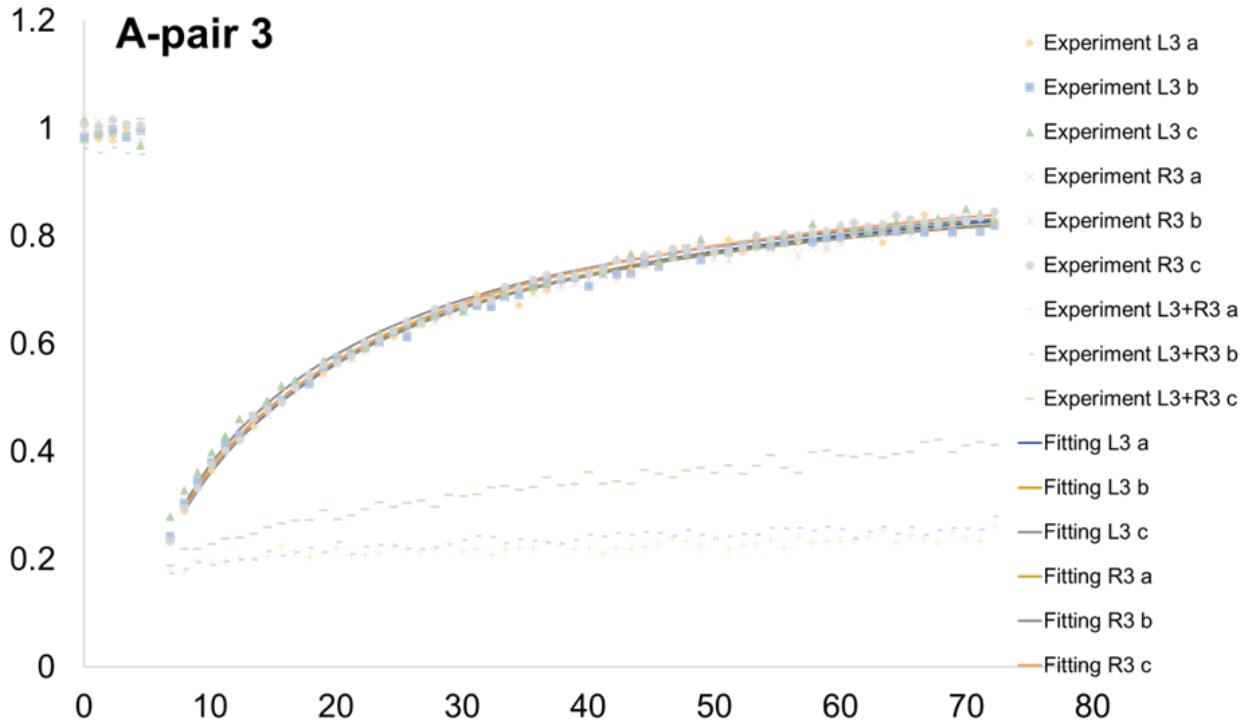

Figure A.11 Fluorescence recovery of pair 2 and A-pair 3

Table A.2 Diffusion coefficients of the DNA obtained from FRAP analysis

Condition	Components (Each DNA is 10 μM)	Diffusion coefficient [μm²/sec]
Experiment L1 a, b, c	L1	42.3
Experiment R1 a, b, c	R1	84.0
Experiment L1 + R1 a, b, c	L1 and R1	No recovery
Experiment L2 a, b, c	L2	46.4
Experiment R2 a, b, c	R2	66.4
Experiment L2 + R2 a, b, c	L2 and R2	No recovery
Experiment L3 a, b, c	L3	65.2
Experiment R3 a, b, c	R3	63.6
Experiment L3 + R3 a, b, c	L3 and R3	No recovery

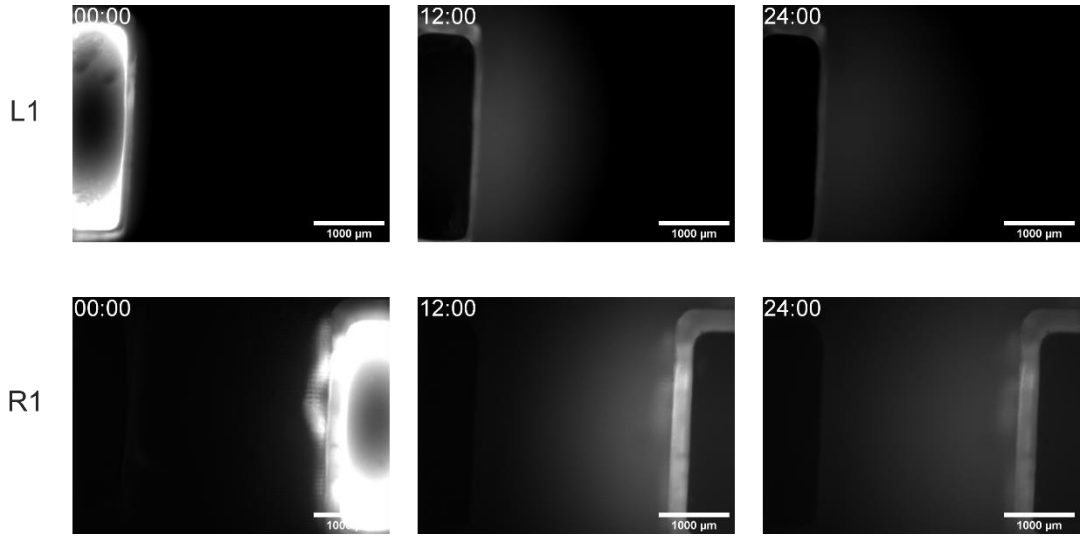

Figure A.12 Spatial propagation of L1 and R1 in hydrogel.

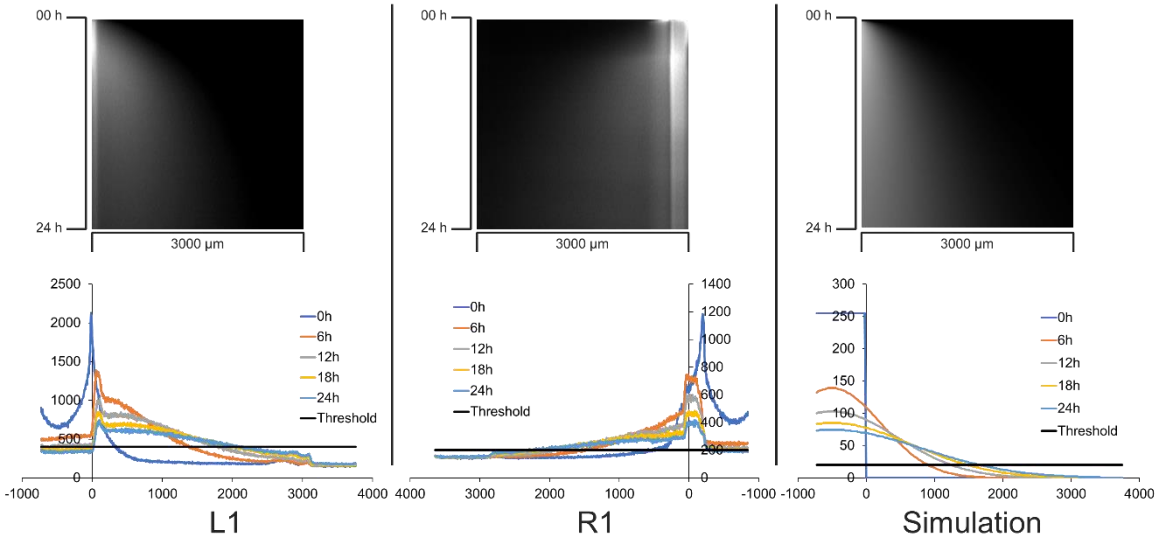

Figure A.13 Time change of the propagation front.

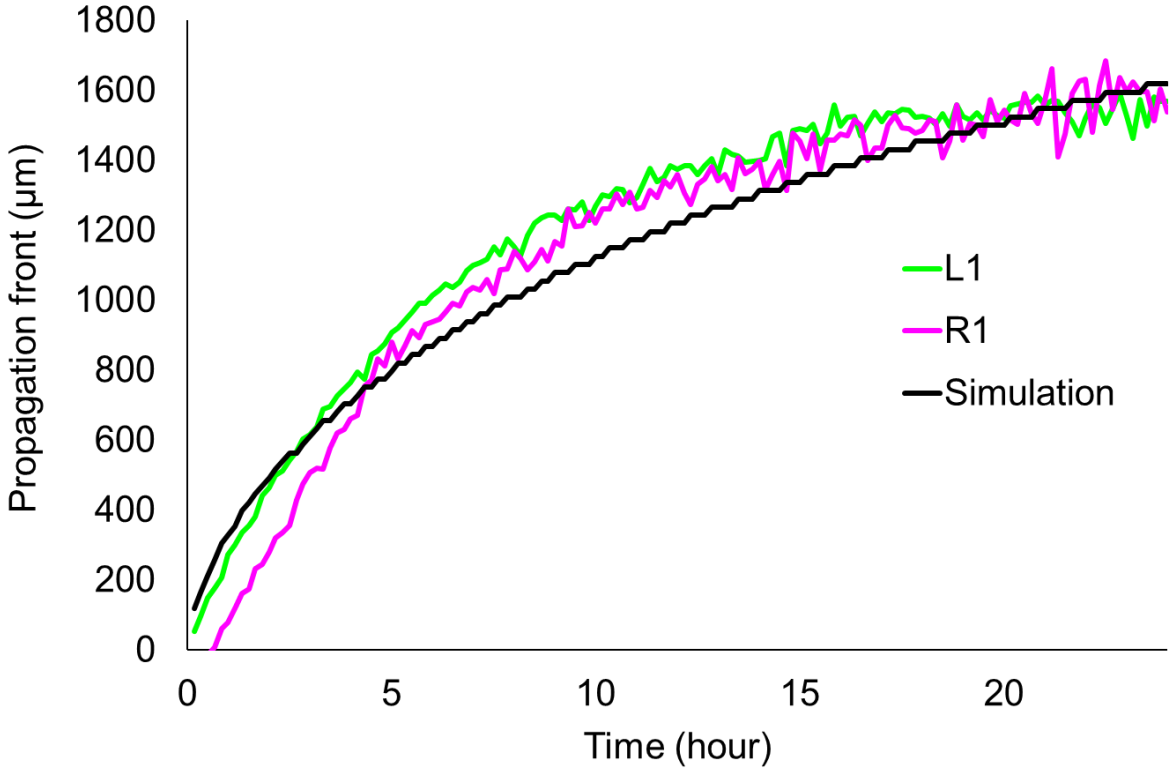

Figure A.14 Propagation of DNA in experiment and diffusion in simulation

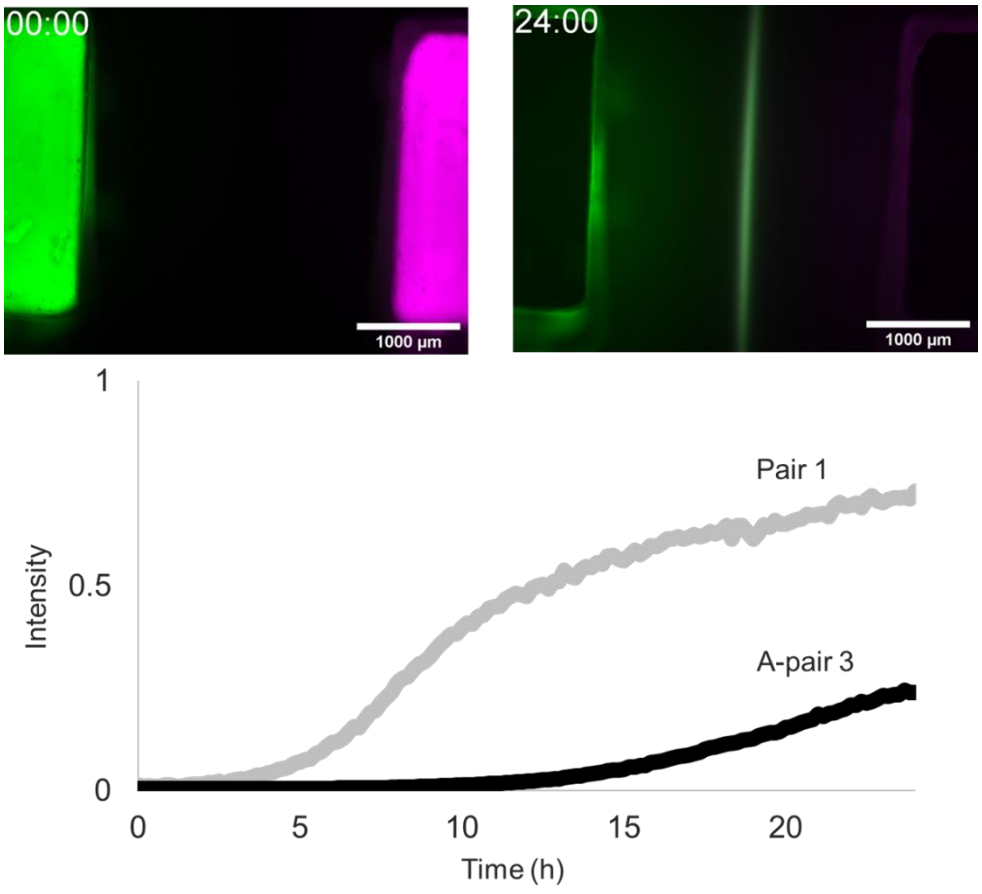

Figure A.15 Bisector pattern formed by A-pair 3

A.13 Reaction–diffusion simulation

The reaction–diffusion simulation was performed using the "Ready" simulator or its executable file "rdy.exe." Simulations based on the model for the polymerization approach involving many chemical species were performed on an Elite Desk800 G4 SFF (Hewlett-Packard) equipped with an NVIDIA FGeForce GTX 1650 for bisector patterns. For superimposed and cascaded pattern formation, a DAIV-DGX760H2-M2S5 (Mouse Computer) equipped with an NVIDIA GeForce RTX 2080 was used. The equations representing the models using logic gates and diffusion modulation (Chapters 2 and 3) were described directly in the Ready software, whereas those for the polymerization approach were generated using a Python program. When "rdy.exe" was used, a batch file was used to automate the simulation. The results were obtained in Visual Toolkit Image Data (vti) format, and numerical information such as spatial concentration distribution was obtained using Python's visual toolkit (vtk) library (https://vtk.org/).

Source code 1. Partial differential equation generator for polymerization approach

```
#!/usr/bin/env python
# coding: utf-8

# In[ ]:

pair = input('Input pair (1 or 2 or 3)')
categorySizeReference=8
diffusion_coefficient = input('Set diffusion coefficient(um^2/s)')
distance_um = 3000
distance_pixel = 128
diffusionMonomerReference =
round(int(diffusion_coefficient)*int(distance_pixel)**2/int(distance_um)**2,
6)
if pair == '3':
    categorySize = int(categorySizeReference*46/61)
    diffusionMonomer = diffusionMonomerReference*46/61
else:
    categorySize= categorySizeReference
    diffusionMonomer = diffusionMonomerReference
saveDirectory = ""


preserve=True
kineticsCirculization=0.0
reactionTypePairs=[
    [[],   [2,3],[0],[0],[]],
    [[2,3],[],   [1],[1],[]],
    [[0],  [1],  [2],[], []],
    [[0],  [1],  [], [3],[]],
    [[],   [],   [], [], []]
]


# In[ ]:

import string
species=categorySize*5
file=open(saveDirectory+'/ODE'+str(species)+'_cascaded_pair3_ver20221112_' +
str(pair) + '.txt', 'w')


# In[ ]:

def writeParameter(parameterName,index,kinetics):
    file.write('      <param name="' + str(parameterName) + '_' + str(index)
+ '">\n')
    file.write('         ' + '{:.6f}'.format(kinetics) + '\n')
    file.write('      </param>\n')
```

```
# In[ ]:
writeParameter("K","h",kineticsCirculization)#ハイブリダイゼーション
writeParameter("K","c",kineticsCirculization)#環状化
writeParameter("K","r",kineticsCirculization)#ディネイチャー
writeParameter("K","s",kineticsCirculization)#鎖置換
writeParameter("K","sr",kineticsCirculization)#鎖置換の逆反応
# In[ ]:

for i in range (1, categorySize*2):
    writeParameter("D"+str(pair),i, diffusionMonomer/i)
writeParameter("D"+str(pair),categorySize*2, 0.)


# In[ ]:

#ord('a')=97
def getVariableName0(index):
    rightMost=chr(ord('a')+index%26)
    if index<26:
        return rightMost
    else:
        return getVariableName0(index//26-1)+rightMost

def getVariableName(index):
    return getVariableName0(index+((int(pair)-
1)*(categorySizeReference*5+2)))

# In[ ]:

odes=[""]*species
odes3=[""]

# In[ ]:


def addUnimolecularReaction(dna1,dna2,kineticsVariable):
    odes[dna1]+="-"+kineticsVariable+"*"+getVariableName(dna1)
    odes[dna2]+="+"+kineticsVariable+"*"+getVariableName(dna1)
    if kineticsVariable=="K_c" and (dna1-3) % 5 ==0:
        odes3[0]+="+"+kineticsVariable+"*"+getVariableName(dna1)

def
addBimolecularReaction(dna1,dna2,dna3,kineticsVariable,kineticsVariableRever
se):
    odes[dna1]+="-
"+kineticsVariable+"*"+getVariableName(dna1)+"*"+getVariableName(dna2)+"+"+k
ineticsVariableReverse+"*"+getVariableName(dna3)
```

```
    odes[dna2]+="-
"+kineticsVariable+"*"+getVariableName(dna1)+"*"+getVariableName(dna2)+"+"+k
ineticsVariableReverse+"*"+getVariableName(dna3)
    odes[dna3]+="+"+kineticsVariable+"*"+getVariableName(dna1)+"*"+getVariab
leName(dna2)+"-"+kineticsVariableReverse+"*"+getVariableName(dna3)
    if kineticsVariable=="K_s":
        odes3[0]+="+"+kineticsVariable+"*"+getVariableName(dna1)+"*"+getVari
ableName(dna2)+"-"+kineticsVariableReverse+"*"+getVariableName(dna3)


def getIndex(category,type):
    if category>=categorySize:
        if(preserve) : return -1
        category=categorySize-1
    return category*5+type

def chemIniPattern(Name):
    file.write("      <overlay chemical=\""+ str(Name) +"\">\n")
    file.write("        <overwrite/>\n")
    file.write("        <constant value=\"0\"/>\n")
    file.write("        <everywhere/>\n")
    file.write("      </overlay>\n")
def chemIniPattern2(Name2,cat):
    if (cat==0):
        file.write("      <DataArray type=\"Float32\" Name=\""+ str(Name2)
+"\" format=\"binary\" RangeMin=\"0\" RangeMax=\"0\">\n")
        file.write("        AQAAAACAAAAACAAAFwAAAA==eJxjYBgFo2AUjIJRMApGwUgD
AAgAAAE=\n")
    elif (cat==1):
        file.write("      <DataArray type=\"Float32\" Name=\""+ str(Name2)
+"\" format=\"binary\" RangeMin=\"0\" RangeMax=\"10\">\n")
        file.write("        AQAAAACAAAAACAAAHAAAAA==eJxjYBgFo4DaQMFxaOBRMApG
wSgYuQAADMEP6w==\n")
    elif (cat==2):
        file.write("      <DataArray type=\"Float32\" Name=\""+ str(Name2)
+"\" format=\"binary\" RangeMin=\"0\" RangeMax=\"10\">\n")
        file.write("        AQAAAACAAAAACAAAHAAAAA==eJxjYBgFo2AUjIKRChQchwYe
BaOA+gAAhQQP6w==\n")
    file.write("      </DataArray>\n")

# In[ ]:

for category in range(categorySize):
    for type in range(5):
        dna=getIndex(category,type)
        variable=getVariableName(dna)
        odes[dna]+="        delta_"+variable+"=D" + str(pair) +
"_"+str(2*category+(1 if type<2 else 2))+"*laplacian_"+variable
```

```
# In[ ]:

for category1 in range(categorySize):
    dna1=getIndex(category1,2)
    dna2=getIndex(category1,4)
    if(dna1>=0 and dna2>=0): addUnimolecularReaction(dna1,dna2,"K_c")
    dna1=getIndex(category1,3)
    dna2=getIndex(category1,4)
    if(dna1>=0 and dna2>=0): addUnimolecularReaction(dna1,dna2,"K_c")

    for type1 in range(5):
        dna1=getIndex(category1,type1)
        if(dna1<0):
            continue


        for category2 in range(category1,categorySize):
            for type2 in range(0 if category2>category1 else type1,5):
                dna2=getIndex(category2,type2)
                if(dna2<0):
                    continue
                for type3 in reactionTypePairs[type1][type2]:
                    dna3=getIndex(category1+category2+(0 if type1==0 and
type2==1 or type1==1 and type2==0 else 1),type3)
                    if(dna3<0):
                        continue
                    #addBimolecularReaction(dna1,dna2,dna3,"K_h","K_r")
                    #!=は not equal
                    if (pair != '3' and type3==2 and type1 !=2):
                        addBimolecularReaction(dna1,dna2,dna3,"K_s","K_sr")
                    elif (type1==0 and type2==3):
                        addBimolecularReaction(dna1,dna2,dna3,"K_s","K_sr")
                    elif (type1==1 and type2==3):
                        addBimolecularReaction(dna1,dna2,dna3,"K_s","K_sr")
                    elif (type1==3 and type2==3):
                        addBimolecularReaction(dna1,dna2,dna3,"K_s","K_sr")
                    else:
                        addBimolecularReaction(dna1,dna2,dna3,"K_h","K_r")

# In[ ]:

for ode in odes:
    file.write(ode+";\n")
green=categorySize*5
red=categorySize*5+1
sums=[getVariableName(green)+"=",getVariableName(red)+"=","for sum of
pair3="]
```

```
for category in range(categorySize):
    variable0=getVariableName(getIndex(category,0))
    variable1=getVariableName(getIndex(category,1))
    variable2=getVariableName(getIndex(category,2))
    variable3=getVariableName(getIndex(category,3))
    variable4=getVariableName(getIndex(category,4))
    sums[0]+="+"+str(category+1)+"*("+variable0+"+"+variable2+"+"+variable3+
"+"+variable4+")"
    sums[1]+="+"+str(category+1)+"*("+variable1+"+"+variable2+"+"+variable3+
"+"+variable4+")"
    if (pair != '3'):
        sums[2]+="+("+variable0+"+"+variable3+")"
for sum in sums:
    file.write("        "+sum+";\n")
if (pair != '3'):
    for ode in odes3:
        file.write("        prodution of pair3 =" + ode + ";\n")

for category in range(categorySize):
    for type in range(5):
        variable=getVariableName(getIndex(category,type))
        chemIniPattern(variable)
chemIniPattern(getVariableName(green))
chemIniPattern(getVariableName(red))

for category in range(categorySize):
    for type in range(5):
        variable=getVariableName(getIndex(category,type))
        if (pair == '1' and category==0 and type==0) or (pair == '2' and
category==0 and type==1):
            chemIniPattern2(variable,1)
        elif (pair == '1' and category==0 and type==1) or (pair == '2' and
category==0 and type==0):
            chemIniPattern2(variable,2)
        else:
            chemIniPattern2(variable,0)

if (pair =='1' or pair =='3'):
    chemIniPattern2(getVariableName(green),1)
    chemIniPattern2(getVariableName(red),2)
elif (pair =='2'):
    chemIniPattern2(getVariableName(green),2)
    chemIniPattern2(getVariableName(red),1)

file.close()
```

Source code 2. Batch file for automate the simulation using “rdy.exe”

```
@echo off
rem

rem
setlocal ENABLEDELAYEDEXPANSION

FOR /L %%X IN (0, 6000,864000) DO (
    rem set
    set /a next= %%X + 6000
    .\rdy.exe -n 6000 -i output_%%X.vti -o output_!next!.vti
)
python vtk_output6.py
```

Source code 3. Numerical information acquisition program using visual toolkit library

```
import vtk
import numpy as np
from vtk.util import numpy_support
from PIL import Image

def loadFile(FileName):
    reader.SetFileName(FileName+".vti")
    reader.Update()

reader = vtk.vtkXMLImageDataReader()

kymograph_1 = []
kymograph_2 = []
img_kymograph_1 = []
img_kymograph_2 = []

def normalize(x, amin=0, amax=4095):
    xmax=x.max()
    xmin=x.min()

    if xmin==xmax:
        return npones_like(x)
    return (amax - amin)*(x-xmin)/(xmax-xmin)+amin

def normalize2(x, amin=0, amax=255):
    xmax=x.max()
    xmin=x.min()

    return (amax - amin)*(x-xmin)/(10-xmin)+amin

for num in range(0, 864000, 6000):
    loadFile("output" + "_" + str(num))
```

```
    distribution_1 =
numpy_support.vtk_to_numpy(reader.GetOutput().GetPointData().GetAbstractArra
y(40))
    nomlist_1 = [int(x) for x in normalize2(distribution_1)]
    kymograph_1.insert(len(kymograph_1), distribution_1)
    img_kymograph_1.insert(len(img_kymograph_1), nomlist_1)

    distribution_2 =
numpy_support.vtk_to_numpy(reader.GetOutput().GetPointData().GetAbstractArra
y(41))
    nomlist_2 = [int(x) for x in normalize2(distribution_2)]
    kymograph_2.insert(len(kymograph_2), distribution_2)
    img_kymograph_2.insert(len(img_kymograph_2), nomlist_2)

np.savetxt('output_kymograph_1.csv', kymograph_1, delimiter=',')
np.savetxt('output_kymograph_2.csv', kymograph_2, delimiter=',')
pil_img1 = Image.fromarray(np.uint8(np.array(img_kymograph_1)[:, 192:320]))
pil_img1.save('kymograph_1.png')

pil_img2 = Image.fromarray(np.uint8(np.array(img_kymograph_2)[:, 192:320]))
pil_img2.save('kymograph_2.png')

pil_img3 = Image.merge("RGB", (pil_img2.convert("L"),pil_img1.convert("L"),
pil_img2.convert("L")))
pil_img3.save('kymograph_color.png')
```

Acknowledgements

I express my sincere gratitude to my supervisor, Professor Satoshi Murata, for his great guidance and advice on the research and during writing the thesis. I also solved many problems facing during research with the help and cooperation of Assistant Professor Ibuki Kawamata, my research adviser. I am grateful to Associate Professor Shin-ichiro M. Nomura, Specially Appointed Lecturer Shogo Hamada, Assistant Professor Hideaki Matsubayashi at Frontier Research Institute for Interdisciplinary Sciences, and Yuki Suzuki at Mie University, who used to belong to Frontier Research Institute for Interdisciplinary Science, for their fruitful discussion and worthful comments. I also thank Professor Matsuhiko Nishizawa and Professor Takuji Ishikawa for the discussion and their advice in reviewing this study.

The design of the experimental system described in Chapters 2 and 3 is largely based on the work of Dr. Fumi Takabatake, Satoru Yoshizawa, Takuto Hosoya, and Thanapop Rodjanapanyakul, former members of Molecular Robotics Laboratory.

I received financial support from Japan Society for the Promotion of Science (JSPS), Japan Student Service Organization (JSSO), and Interdisciplinary Advanced Research and Education at Tohoku University Advanced Graduate School.

All past and present members of Molecular Robotics Laboratory have been important colleagues throughout my student life. I could advance my research with the support of senior students including Yusuke Sato, present Associate Professor at Kyushu Institute of Technology, who taught me the norms as a student. I was also supported by staff, Sumiyo Abe, who support my financial management, Kaori Tanabe, Yuka Minegishi, Tomoko Kondo, Ayaka Nakaoka, and Makiko Sumii who prepared the research environment in the past and present, and excellent students who gave me various insights. Especially, Yuto Otaki, Shosei Ichiseki, Takeo Uchida, Yuma Endo, and Shiyun Liu (Hikari Yukawa) Satoru Akita, who were my collegues, have been a great help to me in my laboratory life.

I also note that I received the generous and understanding support of Professor Satoshi Murata during a personal predicament. I also thank Assistant Professor Ibuki Kawamata, and

staff, especially Sumiyo Abe, and Ayaka Nakaoka, who I have already mentioned by name, my juniors Sho Aradachi, Hiroki Sawada, and Kotaro Watanabe, and present students, especially Hiroshi Ogata and Riku Yoshino, for their grateful kindness and assistance. Thanks to them for giving me some time, I have summarized this thesis.

My gratitude to them is beyond description and my vocabulary is not adequate to express it, but I would like to show my utmost appreciation. Finally, I thank my family from bottom of my heart for their mental and financial support in my everyday life.

論　　文　　目　　録

氏　　名	安部桂太

博士論文

Programming DNA-based Reaction–Diffusion system
(DNA を利用した反応拡散システムのプログラミング)

（　1　冊）

題名	公表の方法	公表の年月日
Programmable reactions and diffusion using DNA for pattern formation in hydrogel medium	Molecular Systems Design & Engineering, 4(3), 639-643.	平成 31 年 3 月 26 日
Programming Methods for DNA-Based Reaction–Diffusion Systems	New Generation Computing, 38(2).	令和 2 年 5 月 11 日
Cascaded pattern formation in hydrogel medium using the polymerisation approach	Soft Matter. 17(25), 6160-6167.	令和 3 年 6 月 4 日

参考論文 題　　名	公表の方法	公表年月日	冊数

1　論文題名（博士論文,参考論文）が外国語の場合は,活字体で記入し,日本語の訳文を括弧書きすること。

If the title of the thesis is in English, please provide a Japanese translation.

2　論文（博士論文,参考論文）が未公表の場合は，公表予定の方法及び時期を記入すること。

If the thesis has not yet been published, indicate how and when it will be published.

3　参考論文については,提出する論文についてのみその題名及び冊数を記入すること。

For reference thesis, enter only those related to the doctoral thesis.